ABSTRACT

ELECTRO HYDRODYNAMIC MANIPULATION OF THE PROCESS OF SELF-ASSEMBLY OF PARTICLES AT FLUID-FLUID INTERFACES

by

Muhammad Mansoor Janjua

This dissertation is divided into two parts, first deals with the numerical study of motion of dielectric particles subjected to nonuniform electric fields and second deals with the process of self-assembly of particles at fluid-fluid interfaces and subjected to uniform electric field normal to the interface. In the numerical study, the particles are moved using a direct simulation scheme (DNS) in which the fundamental equations of motion of fluid and solid particles are solved without the use of models. The motion of particles is tracked using a distributed Lagrange multiplier method (DLM) and the electric force acting on the particles is calculated by integrating the Maxwell stress tensor (MST) over the particle surfaces. One of the key features of the DLM method is that the fluid-particle system is treated implicitly by using a combined weak formulation where the forces and moments between the particles and fluid cancel, as they are internal to the combined system. The MST is obtained from the electric potential, which, in turn, is obtained by solving the electrostatic problem. A comparison of the DNS results with those from the point-dipole approximation shows that the accuracy of the latter diminishes when the distance between the particles becomes comparable to the particle diameter, the domain size is comparable to the diameter, and also when the dielectric mismatch between the fluid and particles is relatively large.

The second part of the dissertation deals with the process of self assembly of particles at fluid fluid interface. One of the most popular techniques for two-dimensional assembly (self-assembled monolayers) is based on capillary forces acting on particles placed at a liquid interface. Capillarity-induced clustering, however, has several limitations: it applies to relatively large (radius greater than ~10 um) particles only, the clustering is usually non-defect free and lacks long range order, and the lattice spacing cannot be adjusted. The goal of this thesis is to show that these shortcomings can be addressed by utilizing an external electric field normal to the interface. The resulting self-assembly is capable of controlling the lattice spacing statically or dynamically, forming virtually defect-free monolayers, and manipulating a broad range of particle sizes and types including nano-particles and electrically neutral particles. It is also demonstrated that technique also works for rod-like, ellipsoidal and cubical particles floating on fluid-fluid interfaces. The method consists of sprinkling particles at a liquid interface and applying an electric field normal to the interface, thus resulting in a combination of hydrodynamic (capillary) and electrostatic forces acting on the particles. It is shown that the relative orientation of two rod-like particles can be controlled by applying an electric field normal to the interface. The spacing between monolayer of ellipsoids is also controlled. The spacing between two cubes, as well as the spacing of a monolayer of cubes, can be adjusted by controlling the electric field strength. Similarly, the lattice spacing of the self-assembled monolayer of rods increases with increasing the electric field strength. Furthermore, there is a tendency for the rods to align so that they are parallel to each other.

ELECTRO HYDRODYNAMIC MANIPULATION OF THE PROCESS OF SELF-ASSEMBLY OF PARTICLES AT FLUID-FLUID INTERFACES

by

Muhammad Mansoor Janjua

A Dissertation
Submitted to the Faculty of
New Jersey Institute of Technology
in Partial Fulfillment of the Requirements for the Degree of
Doctor of Philosophy in Mechanical Engineering

Department of Mechanical Engineering

January 2009

APPROVAL PAGE

ELECTRO HYDRODYNAMIC MANIPULATION OF THE PROCESS OF SELF-ASSEMBLY OF PARTICLES AT FLUID-FLUID INTERFACES

Muhammad Mansoor Janjua

Dr. Ian S. Fischer, Dissertation Co-Advisor — Date
Professor, Department of Mechanical Engineering, NJIT

Dr. Pushpendra Singh, Dissertation Co-Advisor — Date
Professor, Department of Mechanical Engineering, NJIT

Dr. Nadine Aubry, Committee Member — Date
Professor, Department of Mechanical Engineering, Carnegie Mellon University

Dr. David Horntrop, Committee Member — Date
Associate Professor, Department of Mathematics, NJIT

Dr. I. Joga Rao, Committee Member — Date
Associate Professor, Department of Mechanical Engineering, NJIT

Dr. Anthony Rosato, Committee Member — Date
Professor, Department of Mechanical Engineering, NJIT

BIOGRAPHICAL SKETCH

Author: Muhammad Mansoor Janjua

Degree: Doctor of Philosophy

Date: January 2009

Undergraduate and Graduate Education:

- Doctor of Philosophy in Mechanical Engineering,
  New Jersey Institute of Technology, Newark, NJ, 2009

- Master of Engineering in Mechanical Engineering,
  City College of City University of New York, NY, 2003

- Bachelor of Science in Mechanical Engineering,
  Ghulam Ishaq Khan Institute of Engineering Sciences and Technology, Pakistan, 2000

Major: Mechanical Engineering

Presentations and Publications:

N. Aubry, P. Singh, M. Janjua, and S. Nudurupati,
"Micro- and nano-particles self-assembly for virtually defect-free, adjustable monolayers,"
Proceeding of National Academy of Sciences 105 (2007) 3711-3714.

M. Janjua, S. Nudurupati, I. Fischer, P. Singh, and N. Aubry,
"Electric field induced alignment and self-assembly of rods on fluid-fluid interfaces,"
To appear in Mechanics Research Communications.

S. Nudurupati, M. Janjua, N. Aubry, and P. Singh,
"Concentrating particles on drop surfaces using external electric fields,"
Electrophoresis 29 (2008) 1164-1172.

S. Nudurupati, M. Janjua, N. Aubry, and P. Singh,
"Removal of particle distributed on the surface of a drop,"
Submitted to Physical Review Letters.

N. Aubry, P. Singh, M. Janjua, and S. Nudurupati,
"Self-assembly of Particles into 2D Lattices with Adaptable Spacing,"
Proceedings of FEDSM2008-55248 2008 ASME Fluids Engineering Division Summer Meeting and Exhibition, August 10-14 (2008) Jacksonville, FL, USA.

N. Aubry, P. Singh, M. Janjua, and S. Nudurupati,
"Removal of Particles from the Surface of a Droplet,"
Proceedings of FEDSM2008-55247 2008 ASME Fluids Engineering Division Summer Meeting and Exhibition, August 10-14 (2008) Jacksonville, FL, USA.

M. Janjua, S. Nudurupati, P. Singh, and N. Aubry,
"Direct Numerical Simulation (DNS) of suspensions in spatially varying electric fields," ASME annual meeting (2007) Seattle, WA, USA.

M. Janjua, S. Nudurupati, I. Fischer, P. Singh, and N. Aubry,
"Self-assembly of Rod-like Particles into 2D Lattices,"
ASME annual meeting (2008) Boston, MA, USA.

M. Janjua, S. Nudurupati, I. Fischer, P. Singh, and N. Aubry,
"Micro- and Nano-Particles Self-Assembly for Virtually Defect-Free, Adjustable Monolayers,"
Frontiers in Applied and Computational Mathematics, May 19-21 (2008) Newark, NJ, USA.

S. Nudurupati, M. Janjua, P. Singh, and N. Aubry,
"Transport and Deformation of Droplets in a Micro-Device using Dielectrophoresis," Frontiers in Applied and Computational Mathematics, May 19-21 (2008) Newark, NJ, USA.

M. Janjua, S. Nudurupati, P. Singh, and N. Aubry,
"Direct Numerical Simulation (DNS) of Suspensions in Spatially Varying Electric Fields,"
American Physical Society-Division of Fluid Dynamics Annual Meeting (2007) Salt Lake City, UT, USA.

M. Janjua, S. Nudurupati, I. Fischer, P. Singh, and N. Aubry,
"Electric Field Induced Alignment and Self-Assembly of Rods and Ellipsoids on Fluid-Fluid Interfaces,"
American Physical Society-Division of Fluid Dynamics Annual Meeting (2008) San Antonio, TX, USA.

To

My Parents, Family and Everyone I learnt from

ACKNOWLEDGMENT

I would like to thank Almighty Allah for all the blessings in my life. I would also like to extend my appreciation for people who have made such a huge contribution in my life. With utmost respect, I thank Dr. Ian Fischer for his guidance and encouragement for making me not only a better researcher but also a better person.

Special thanks to Dr. Pushpendra Singh, who I truly admire. Dr. Singh gave me the opportunity to excel, and taught me valuable lessons by living up to the values of commitment and hard work as keys to success.

I also extend my thanks to Dr. Anthony Rosato, Dr. Joga Rao, Dr. David Horntrop and Dr. Nadine Aubry for taking interest in my research. I have a learnt a lot from these professors during my stay at NJIT. I appreciate the sense of humor of Dr. Rosato, as it had always been uplifting. I liked the calm nature of Dr. Rao, and I was also inspired by the enthusiasm of Dr. Horntrop. I truly am honored to know them all.

I would also like to thank my group members, Sai, Satish and Bhavin. Without Sai, my stay at NJIT would not have been as productive and without Satish it would not have been as motivating.

I would also like to thank Jaskirat, Mahesh and Bharath, without them life at NJIT would not have been as dynamic.

In the end, I would like to thank my family, Abbu, Ammi, Munawar, Mudassar and Mustafa for their unconditional love and support.

This research was supported by National Science Foundation, the New Jeresey Commission on Science and Technology through the New Jersey Center for Mirco-Flow Control.

TABLE OF CONTENTS

Chapter		Page
1	INTRODUCTION	1
	1.1 Theory	2
	1.2 Literature Review	8
2	DIRECT NUMERICAL SIMULATION OF SUSPENSIONS SUBJECTED TO ELECTRIC FIELDS	17
	2.1 Overview	17
	2.2 Governing Equations	19
	2.2.1 Point-Dipole and Maxwell Stress Tensor Approaches	21
	2.2.2 Dimensionless Equations and Parameters	22
	2.3 Finite Element Method	25
	2.4 Results	30
	2.4.1 Convergence Study	34
	2.4.2 Motion of Single Particle	35
	2.4.3 Motion of Two Particles	38
	2.5 Discussion	45
3	MICRO AND NANO PARTICLES ASSEMBLY FOR VIRTUALLY DEFECT FREE MONOLAYERS	46
	3.1 Overview	46
	3.2 Governing Equations	49
	3.2.1 Vertical Force Balance in Equilibrium	52
	3.2.2 Interfacial Deformation and Lateral Capillary Force	54

TABLE OF CONTENTS
(Continued)

Chapter	Page
3.3 Results	57
3.3.1 Spheres at a Liquid-Air Interface	57
3.3.2 Spheres at a Liquid-Liquid Interface	62
3.4 Discussion	65
4 ELECTRIC FIELD INDUCED ALIGNMENT AND SELF ASSEMBLY OF RODS AND ELLIPSOIDS ON FLUID-FLUID INTERFACES	67
4.1 Overview	67
4.2 Results	68
4.2.1 Alignment of Two Rods in the Absence of an Electric Field	69
4.2.2 Alignment of Two Rods in the Presence of an Electric Field	74
4.2.3 Monolayers of Rods	81
4.2.3 Alignment of Two Ellipsoids in the Absence of an Electric Field	84
4.2.3 Alignment of Two Ellipsoids in the Presence of an Electric Field	86
4.2.3 Monolayers of Ellipsoids	88
4.3 Discussion	89
5 DEFECT FREE SELF ASSEMBLY OF PRISMATIC PARTICLES	92
5.1 Overview	92
5.2 Results	93
5.3 Discussion	96
6 CONCLUSION	98
7 REFERENCES	103

CHAPTER 1

INTRODUCTION

The study of particles subjected to uniform and non uniform electric fields deserves special attention because of its enormous potential and unique effects. A few applications associated with this idea are pumping of fluids, removal of particulate matter from liquid suspensions, classification and separation of minerals, classification of micro organisms, and self assembly of micro and nano particles.

This research is divided into two parts. First part is to numerically study the motion of electrically-neutral particles suspended in a liquid and subjected to varying electric fields. The particles experience a net force due to the non-uniformity of the electric-field. This force is called the dielectrophoretic (DEP) force and the phenomenon is called dielectrophoresis. The magnitude and direction of the force experienced by a particle depends on the strength and spatial variation of the applied electric-field. The second part of the research is to experimentally study the process of self-assembly of particles at a fluid-fluid interface. By utilizing an external electric field normal to the interface, self-assembly is capable of controlling the lattice spacing statically or dynamically, forming virtually defect free monolayers. A salient feature of these processes is that there are no moving parts involved, and the particles can be moved without touching them. This makes the force suitable for manipulating biological particles in various applications such as cell lysing, cell sorting, cell fusion, etc.

Before moving into the details of the numerical simulations and the results of simulations and experiments, the basic theory of dielectrophoresis along with the process

of self assembly of particles at fluid-fluid interface will be discussed. In the following section, a review of the literature that talks about the immense research that has been done and also ongoing in the area of dielectrophoresis and self-assembly of particles at fluid-fluid interface is presented. The rest of the thesis is organized as follows. In the second chapter, a numerical study has been performed to study the motion of particles under the influence of a varying electric field. In the third chapter, the self-assembly process of spheres at a fluid-fluid interface subjected to a uniform electric field normal to the interface is discussed. In the fourth chapter, the self-assembly process for rods and ellipsoids is analyzed with and without the presence of a uniform electric field normal to the interface. In the fifth chapter, the self-assembly of particles with sharp edges under the influence of an electric field is considered as they float differently compared to spheres, rods and ellipsoids. The conclusions derived from numerical and experimental research are presented in the last chapter.

1.1 Theory

An uncharged particle subjected to an electric field develops an induced dipole if the dielectric constant of particle is different from that of the suspending fluid. The dielectric constant is a relative measure of polarity, and more polarisable substances have a dielectric constant much greater than 1. The induced dipole on the particle due to the electric field is further enhanced if there are other particles in the vicinity as they intensify the local electric-field experienced by any single particle. A dipole can be thought of a concentration of positive charge on one side of the particle and negative on

the other side (shown in Figure 1.1). Why Electrorheological (ER) fluids form chains of particles aligned with the electric field can be qualitatively explained [1].

Two particles are subjected to a uniform electric field in a fluid that has a different dielectric constant than that of the particles (see Figure 1.1). The particles are polarized. There will be attraction between the positive and negative charges on the particle surfaces and there will repulsion between charges of same sign. When the applied electric field is parallel to the line joining the centers of particles, they move toward each other. Similarly if the applied electric field is perpendicular to the line joining their centers, they experience a net repulsion and move away from each other. For particles whose line of centers are neither parallel nor perpendicular, they experience both attraction and repulsion causing the particles to eventually translate and rotate into alignment with the electric field [2]. This result in formation of particle chains aligned with the electric field. The microstructure of a suspension is related to its bulk rheological properties, so by increasing the dielectric mismatch between the particle and fluid and increasing the electric-field intensity, stronger chains are formed and that affect the viscosity of an ER fluid.

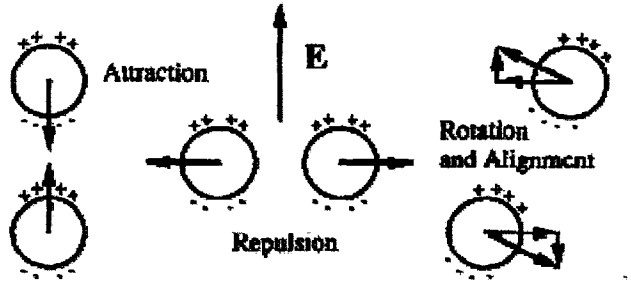

Figure 1.1 Due to the dielectric mismatch between the particles and the fluid, the particles have an induced dielectric as illustrated. The interaction of these dipoles cause attraction, repulsion, rotation and alignment of particles, creating chains that are aligned with the applied electric field.
The above picture is taken from Ref. [2].

Another interesting phenomenon occurs when dielectric particles suspended in a fluid are subjected to non-uniform electric fields. The particles go to regions of either high or low electric-field intensity depending on their dielectric mismatch with the suspended fluid (as shown in Figure 1.2). This phenomenon is called dielectrophoresis [3, 4]. The force which the particles experience is called Dielectrophoretic (DEP) force. The Dielectrophoretic (DEP) force also acts in an AC electric-field. The magnitude of the force depends on the Root-Mean-Square (RMS) value of the AC electric-field. The electrostatic forces exerted by a non-uniform field on the particles of the suspension can be utilized in many biological and engineering applications such as manipulation of biological cells, filtration of dirty fluids, etc.

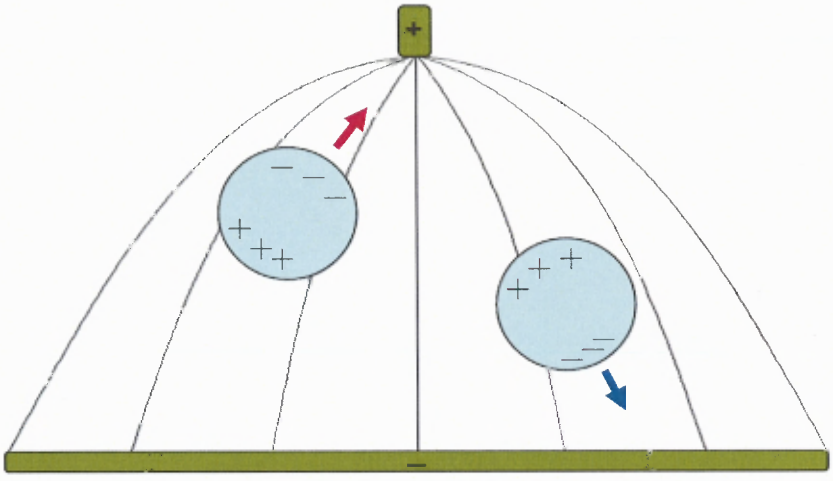

Figure 1.2 Two different particles in a non-uniform electric field. The particle on the left is more polarisable than the surrounding medium and is attracted towards the strong field at the pin electrode. The particle on the right has low polarisability compared to the surrounding medium and is directed away from the strong electric field region.

The DEP force arises because a dielectric sphere placed in a spatially varying electric field becomes polarized and experiences a net force:

$$\mathbf{F}_{DEP} = 4\pi a^3 \varepsilon_0 \varepsilon_c \beta \mathbf{E} \cdot \nabla \mathbf{E}$$

where a is the particle radius, , ε_0 = 8.8542x10^{-12} F/m is the permittivity of free space, ε_c the permittivity of the fluid and **E** is the electric field, β is the real part of the complex frequency dependent Clausius-Mossotti factor $\frac{\varepsilon_p^* - \varepsilon_c^*}{\varepsilon_p^* + 2\varepsilon_c^*}$, i.e., $\beta(f) = \mathrm{Re}\left(\frac{\varepsilon_p^* - \varepsilon_c^*}{\varepsilon_p^* + 2\varepsilon_c^*}\right)$, ε_p^* and ε_c^* being the complex permittivities of the particles and the fluid, and $\varepsilon^* = \varepsilon - j\frac{\sigma}{f}$, where σ is the conductivity, ε is the permittivity and f is the angular frequency of the applied electric field.

The value of β is limited within the range -0.5 to 1.0 (shown in Figure 1.3), and it has negative values when the dielectric constant of the suspending fluid is greater than that of the particles, and assumes positive values when the dielectric constant of the suspending fluid is less than that of the particles. Since β is frequency dependent, it is possible, at least in theory, for every fluid particle system to have a frequency at which β goes to zero. This frequency at which the Clausius-Mossotti factor is zero is called the crossover frequency. At frequencies above and below the crossover frequency β will have opposite signs.

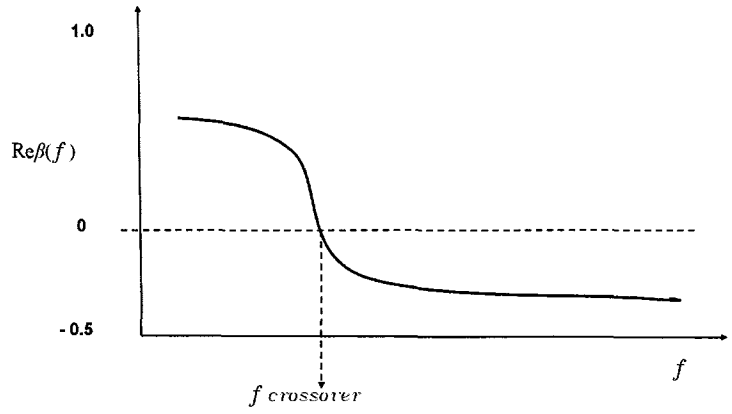

Figure 1.3 A typical curve for Clausius-Mossotti factor, showing the crossover frequency.

From the expression for the Clausius-Mossotti factor, notice that when β is positive the direction of the dielectrophoretic force is along the gradient of the electric-field magnitude and when β is negative, the force acts in the opposite direction. In these simulations, it is assumed that both fluid and suspended particles are nonconductive or ideal dielectrics. Notice that in this case the Clausius-Mossotti factor is real as the conductivities of both mediums are zero. However, the equations used here are applicable even for lossy dielectrics, provided the frequency of the applied AC electric field is sufficiently large such that $\varepsilon >> \frac{\sigma}{f}$.

It follows that the direction of the dielectrophoretic force determines the regions in which the particles collect. For example, when β is positive, the dielectrophoretic force moves the particles into the regions where the electric field strength is locally maximum which is normally on the electrode surfaces, while when β is negative, it moves the particles into the regions where the electric field strength is locally minimum. The dielectrophoretic force, therefore, makes the particle distribution less uniform and

thus, as mentioned above, can have a dramatic impact on the particle suspension structure. Such a force can also be used for removing particles from a suspending liquid, as well as for separating particles for which the sign of β is different. For a given particle, the sign of β depends on the dielectric constant of the fluid, as well as the frequency of the applied AC field. Therefore, at least in principle, any two sets of particles with different dielectric constants can be separated, provided a suitable fluid is used, such that the sign of β is different for each set. Particles also experience an electrostatic particle-particle interaction force, known as mutual dielectrophoresis [4]. So the total electrostatic force acting on a particle will have two contributions, one arising from DEP force and other from mutual dielectrophoresis.

Particles float on the surface of a liquid due to surface tension. While surface tension is a macroscopic effect, its origin lies in the micro scale. The molecules in a fluid exert a variety of forces on each other, both attractive and repulsive. The magnitude of attractive forces is not strong enough to bind molecules together, but these forces do affect the behavior of the fluid. A molecule, interior in the fluid will experience an equal average force from all directions. This however, is not the case for a molecule near the surface of liquid. A molecule at the surface of a liquid experiences less force from the gaseous region above it and more force from molecules in the bulk liquid. The net force resulting on a molecule at the surface pulls it into the bulk liquid. At macroscopic scale, it appears that the surface is behaving like an elastic membrane. The surface exerts a force and tries to minimize its area, and this phenomenon is called surface tension.

Mathematically, the concept of surface tension is given by the Laplace Young Law.

$$\Delta p = \sigma H$$

Here Δp deonotes the jump in pressure across a fluid surface, σ is the surface tension, and H is the mean curvature of the surface.

When two heavy hydrophobic spheres are close to each other, the deformed interface is not symmetric around the spheres. The interface is lowered in between the two spheres and this result in a net lateral capillary force that tend to cluster the particles (shown in Figure 1.4). The same is true for hydrophilic particles, in which case the interface between two particles is elevated, resulting in a lateral force between the two spheres. This force is attractive and that result in clustering of particles (shown in Figure 1.4).

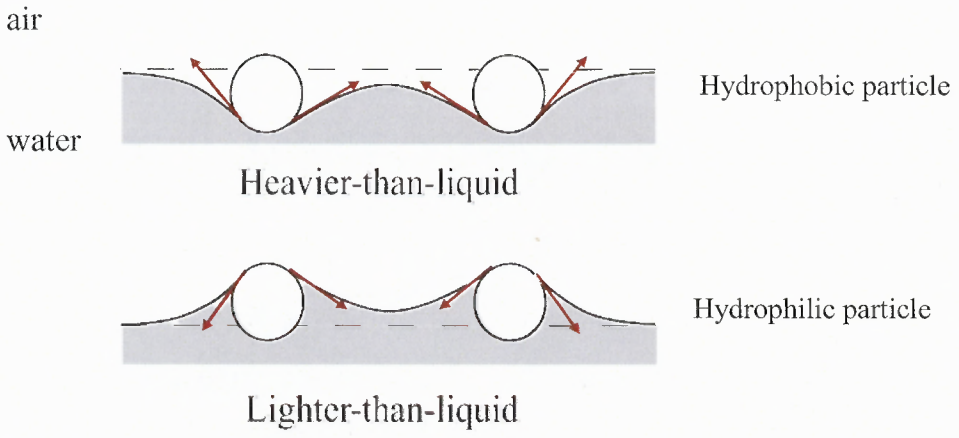

Figure 1.4 A schematic diagram that shows that particles deform the interface. There is a net lateral capillary force because in the case of hydrophobic particles, the interface is depressed in between the particles. For hydrophilic case the interface is elevated and that resulted in net lateral capillary force.
The above picture is taken from Ref. [95].

1.2 Literature Review

Winslow, observed in 1930 [1] that when he applied a uniform electric field to dielectric particles suspended in oil that the electrically-induced particles formed chains in the direction of the applied electric field. One salient feature Winslow discovered was that the effective viscosity of the liquid could be controlled by changing the electric field strength. The Electrorehelogical (ER) response noted by Winslow was the induced electrostatic polarization forces on particles due to dielectric mismatch between particle and fluid.

Pohl [4], did extensive experiments related to dielectrophoresis and its applications and discussed about the topic in detail in one of his classic books on the subject, *Dielectrophoresis*, 1978. This book also covers extensively the various mechanisms of polarization in neutral matter. It also mentions that the conductivity of matter has to be taken into consideration along with permittivity for dielectrophoresis in real dielectrics. Pohl performed extensive experiments with electrorheological fluids and biological particles, and listed the various factors that influence particle separation or "yield" during dielectrophoresis.

Most of the research done in this area before 1980's is predominantly on manipulation of biological cells. Chen, C.S and Pohl H.A analyzed the behavior of single cells under dielectrophoresis [5]. Gvozdiak, P.I., and Chekhovckaia, T.P., used dielectrophoresis to separate microorganisms from water [6]. They concluded from their experiments that separation efficiency increases with increase in voltage and also from decrease in the flow rate of the suspending fluid. Dielectrophoresis was again used as a cell separation technique by Glaser, Pescheck, and Krause [7], where the coaxial wire

electrode was moved with a constant rate, and cells were collected on the wire and were removed in a filtration chamber. In addition, Jone et al. [8, 9], examined the behavior of biological cells, and the dielectrophoresis of bubbles, spheres and shells.

In early 1980's, the emphasis of research in dielectrophorsis continued to concern biological applications. However, the focus was on more-sophisticated applications such as cell sorting, cell lysing, cell fusion etc. [10, 11]. Also to be mentioned is the work by Zimmermann et al. [12]. It deals with the electro-rotation of particles which depends on the imaginary part of Clausius-Mossotti factor. He used the method of electro rotation to extract the dielectric properties of the particles. The work done by Gherardi et al. [13] and Mognashci et al. [14] considered particles as lossy. In this approach, instead of considering the particles to be pure dielectrics, their conductivity was also taken into account (which is true for a real particle) before analyzing the experimental results.

A few computational studies were also reported during this period, such as Goossens et al. [15] and Henry et al. [16]. In the later, numerical investigations were performed on the particle collection efficiency of a fibrous filter. Their model considered the effect of various forces like dielectrophoresis, electrophoresis, Brownian motion, and particle inertia, and predicted the collection efficiency of the filter under the influence of these forces.

Hitherto, electrodes built for dielectrophoresis were made using conventional manufacturing processes. For example, Pohl used the pin-plate or the wire-wire arrangements in his experiments, and Adamson and Kaler [17] used a more sophisticated "isomotive" electrode geometry manufactured by numerically-controlled milling machines. Washizu et al. [18, 19 and 20] revolutionized the dielectrophoretic processes

by introducing a novel device called the "fluid integrated circuit, (FIC)", in which photolithographic techniques were used to integrate all components of the device in a single substrate. These were the first dielectrophoretic devices manufactured using Microelectro-mechanical systems (MEMS) manufacturing processes. FIC enabled accurate control of the electrostatic and hydrodynamic forces, and therefore, the manipulation of single cells. The width of flow channels were slightly larger than the diameter of cells which allowed only single cells to pass through.

As already discussed, Pohl was the leading researcher in this area. However, his experimental apparatus was not capable of handling submicron and nano particles, as manipulation of small-size particles require strongly-divergent electric fields which he was not able to create in his devices. With the development of micro-fabrication techniques and MEMS devices, a renewed interest arose in dielectrophoretic manipulation of particles. These small devices could produce high-gradient electric fields which were of large magnitude, capable of manipulating submicron and nanoscale particles by applying voltages of order 1 volt.

Pethig, who was doing research in biological dielectrophoresis [21, 22] built on the idea of microelectrodes for dielectrophoresis and designed a new microelectrode structure for biological dielectrophoresis [23, 24]. He investigated the dielectrophoresis of live yeast suspensions [25, 26] using a device featuring integrated castellated microelectrode design. Yeast cells experienced positive dielectrophoresis for frequencies above 10 kHz and negative dielectrophoresis below 500 kHz. Pethig, made another important contribution with unified studies of dielectrophoresis and electrorotation [27, 28 and 29]. He derived a new theoretical relationship linking the dielectric properties of a

colloidal suspension to both dielectrophoresis and electrorotation. Until this point, these two phenomena were treated separately, even though they are closely related by the fact that they depend on real and imaginary parts of the induced dipole moment respectively.

Another important phenomenon observed by Batchelder in 1983 was traveling wave dielectrophoresis [30]. For producing a traveling wave, microelectrodes were arranged linearly with each electrode 90^{o} phase advanced than the previous. An electric field produced by this moves with the electrodes, and the polarized particles will also move along with the field. This phenomenon also depends on the imaginary part of the induced dipole moment. Fuhr et al. developed practical applications like micropumps using traveling wave dielectrophoresis.

Jones, gave insight into various theoretical aspects of dielectrophoresis in his classic book *Electromagnetics of Particles* [3]. The conventional theory of dielectrophoresis was based on dipole approximation which doesn't explain the dielectrophoretic phenomenon in the regions of highly-divergent electric fields and in microchannels where the domain size is comparable to that of particle size. Jones along with Washizu developed a theory which included multipole terms to calculate the dielectrophoretic force [31,32 and 33]. Lab-on-a-chip was another idea which was later introduced. These systems rely on various electrostatic forces to move around small volumes of fluid samples. Gunji, Washiz and Jones used dielectrophoresis to control the movement of water in such devices [34]. The high conductivity of water and associated joule heat made it impossible in the past to use dielectrophoreis for manipulation of water. However, the governing equations scale in such a way in microelectrode structures that the dielectrophoretic manipulation of water is impossible. The scaling laws for the

various electrostatic forces in lab-on-a-chip, which is a microdevice described in [35, 36]. He demonstrated high-speed dielectrophoretic actuators including "wall-less" flow structures, siphons and nanodroplet dispensers that operate with water [37, 38].

The breakfast food cheerios scattered randomly on the surface of milk in a bowl will cluster under the action of capillary force [39]. A similar experiment first proposed by Campell et al. [40], used ordinary soda straws to demonstrate capillary driven self-assembly. This clustering of particles on interfaces changes the interfacial properties of a two-phase system and is used in many flotation based extraction and separation processes [41]. This effect has been used for the self assembly of submicron particles on two liquid interfaces [42]. However, if one particle is hydrophobic and one is hydrophilic, the net lateral capillary force between these two particles is repulsive and the particles move away from each other. Kraclchevsky & Nagayama [43] and Saif [44] discussed these forces in detail. Even when particles experience attractive forces, the resulting structure obtained by this has several deficiencies: i) the resulting particle structure is usually not defect free and the defects take place because the particles physically block one another and the clustering lacks long range order, ii) the lateral capillary forces become insignificant when the particle size is small (nanoparticle) (more precisely, when the dimensionless Bond number, which accounts for the particle and fluid densities, is much smaller than one), thus restricting particle assembly using this method to the manipulation of mesoscale particles (larger than ~10 μm); and (iii) for a given particle and fluid system, and the lattice spacing is not adjustable.

To obtain a uniform structure, charged spherical particles were used at an air-water interface [45], dipolar electric fields induce surface charges that distort the

interface. This deformation of the interface causes attractive capillary forces while the dipolar interaction causes repulsion. Particles arrange themselves in a nice hexagonal structure while keeping a distance from each other because of induced charge upon them. The lattice spacing can not be altered for this system by external means. A similar study was done for charged mono-dispersed polymer particles that were adsorbed at an oil-water interface [46], the particles exhibited a long range repulsive force and an attractive capillary force. They also arranged in nice hexagonal structures at a distance from each other.

Hosokawa et al. [47] used differently-shaped particles for self-assembly. If the edges of particle are different, the deformation of interface around the particle is different and hence, particles approach each other in the orientation where they experience maximum attractive force. This allows them to assemble in nice structure. Bowden et al. [81], developed a strategy for the directed self-assembly of small objects. The idea is that ordered aggregates are energetically more stable than the individual particles or disordered aggregates, hydrophobic sides are attracted to one another over large distances resulting in rapid assembly, and particles can also move laterally from side to side, lubricated by intervening film of $C_{10}F_{18}$, thus maximizing the amount of hydrophobic area in contact.

Golosovsky et al. [48] used magnetic particles for self-assembly at a fluid-fluid interface to create uniform structures. The particles self assembled into ordered two-dimensional and three-dimensional structures whose symmetry and lattice parameters can be controlled by an external magnetic field. The structures achieved were used in the

design and construction of tunable and non-tunable photonic bandgap devices in the microwave and mm-wave range.

An ingenious method to move particles on a fluid-fluid interface was created by the Whitesides group [49], where they manufactured a particle composed of different materials. One edge of the particle was created with a material that when in contact with liquid caused small gas bubbles. The ejection of these bubbles provide a locomotive force for the particle.

Magnetic and hydrodynamic forces collaborate and contend in the formation of dynamic self-assembly of particles. Whitesides, Grzybowski and various collaborators [50, 51, 52 and 53] studied disks floating over a rotating bar magnet. When the magnet was not moving the particles in the fluid did feel a magnetic force and clustered in the region of fluid above the poles. Once the magnetic bar was set in motion the system came alive. Along with the magnetic force, the rotation of particles set the surrounding liquid in motion and created a repulsive hydrodynamic force between the particles. By changing the number of particles in the system, it was able to create a variety of dynamic structures.

In equilibrium, the vertical position of a floating particle within a two-fluid interface is such that the sum of the forces acting on the particle in the direction normal to the interface is zero. A particle denser than the liquid below can float on its surface because the vertical component of the capillary force acting upwards, which arises due to the deformation of the interface, balances the particle's buoyant weight which is acting downwards. For a small particle of radius a, the buoyant weight, which scales as a^3, becomes negligible, and therefore only a small interfacial deformation is needed in this

case for the vertical capillary force to balance the buoyant weight. Consequently, the lateral capillary forces due to this small deformation of the interface are too small to move micron and nano-sized particles, and thus, small particles, in general, do not self-assemble. It is known that for particles floating on the air-water interface the attractive capillary forces are significant only when the particle radius is larger than ~10 μm. This restriction, however, does not apply to particles trapped in thin films with a thickness smaller than the particle diameter. In fact, particles ranging from protein macromolecules to millimeter-sized particles can self-assemble in such thin films. Moreover, small particles can self-assemble if they are charged or if they have irregular contact lines.

All these techniques were intended to eliminate any defects in the structures obtained by self-assembly of particles. A novel technique is discussed in the later sections which allow us to produce defect free lattices and adjust the monolayers of particles. This idea can be applied along with dielectrophoresis on particles trapped at the drop interface.

CHAPTER 2

DIRECT NUMERICAL SIMULATION OF SUSPENSIONS SUBJECTED TO ELECTRIC FIELDS

2.1 Overview

Over the last two decades considerable effort has been directed at developing efficient techniques for segregating and trapping micro to nano scale biological and other particles suspended in fluids. These techniques are important for a variety of applications, such as in devices being developed for classifying DNA and protein molecules in which the first step is to concentrate them [54], and also in devices being developed for detecting cells, and for removing particulates from fluids [55-60].

It is well known that a particle in a spatially non-uniform electric field is subjected to an electrostatic force, called the dielectrophoretic (DEP) force, as well as interacts electrostatically with other particles. The latter is usually modeled as dipole-dipole interactions which are present even when the electric field is uniform. The DEP force arises because the particle becomes polarized and a polarized particle (or dipole) placed in a spatially varying electric field experiences a net force. This phenomenon itself is referred to as dielectropherosis [4].

Dielectrophoresis is a powerful technique because particles with different dielectric constants respond differently as the force depends on their dielectric constant relative to that of the fluid in which they are suspended. Therefore, in principle, dielectropherosis can be used to selectively manipulate and separate particles [54]. For example, it has been demonstrated that cancer cells can be removed from human blood since their dielectric constant is different from that of normal cells [61, 62].

Numerical simulations are essential for understanding the behavior of particles under various physical conditions, as well as for developing better designs for such devices. A direct numerical simulation method is developed to study the phenomena of dielectrophoresis in which the exact governing equations are solved to obtain the time dependent motion of a fluid-particle system. Direct numerical simulation (DNS) scheme based on the distributed Lagrange multiplier (DLM) method is used [74], to study the problem numerically.

In most numerical studies to date, the electric force acting on a particle is computed using the point dipole (PD) approximation [3, 4]. In this approximation, the particle is considered small compared to the characteristic length over which the electric field varies, and the distance between particles is assumed to be much larger than the diameter. In the PD model, the electric force a particle experiences has two components, one due to dielectrophoresis, and other due to particle-particle interaction. An energy based method was used in [65] to compute the electrostatic energy of the system subjected to an electrical field. This method allows one to include particle-particle interaction in both far and near fields. As mentioned before, the accuracy of PD approximation diminishes as non uniformity of electric field increases or the distance between the particles is reduced. Some of these limitations can be improved by involving higher order multipole moment terms [66]. Even though the multipole technique is more accurate than the PD model, it still lacks the completeness of the Maxwell Stress Tensor (MST), in which the force is computed in terms of the electric field that is obtained by accounting for the presence of particles [67]. The MST method, however, requires

calculation of the updated electric potential at each time step and thus is computationally more demanding [68, 69 and 70].

This research is performed to numerically study the movement of particles subjected to non uniform electric field by PD approximation and the MST method. The DEP force acting on the particles is computed numerically by solving Laplace's equation for the dielectric continuous medium, with appropriate boundary conditions. Key features of the method are discussed in later sections. The code used for the numerical analysis was written by Singh [75].

2.2 Governing Equations

The governing mass and momentum conservation equations for the motion of fluid and particles are given below. Then these equations are nondimensionalized and the governing dimensionless parameters are obtained. Let us denote the domain containing a Newtonian fluid and N solid particles by Ω, the interior of the i^{th} particle by $P_i(t)$, and the domain boundary by Γ. The governing equations for the fluid-particle system are:

$$\rho_L\left(\frac{\partial \mathbf{u}}{\partial t}+\mathbf{u}\cdot\nabla\mathbf{u}\right)=-\nabla p+\nabla\cdot(2\eta\mathbf{D}) \qquad \text{in } \Omega\backslash\overline{P(t)} \tag{2.1}$$

$$\nabla\cdot\mathbf{u}=0 \text{ in } \Omega\backslash\overline{P(t)} \tag{2.2}$$

$$\mathbf{u}=\mathbf{u}_L \text{ on } \Gamma \tag{2.3}$$

$$\mathbf{u}=\mathbf{U}_i+\boldsymbol{\omega}_i\times\mathbf{r}_i \text{ on, } \Gamma_{Pi} \; i=1,\ldots,N \tag{2.4}$$

Here $\mathbf{u}$ is the fluid velocity, p is the pressure, η is the dynamic viscosity of the fluid, ρ_L is the density of the fluid, $\mathbf{D}$ is the symmetric part of the velocity gradient tensor and $\mathbf{U}_i$ and $\boldsymbol{\omega}_i$ are the linear and angular velocities of the i^{th} particle and $\Gamma_{Pi} = \partial P_i(t)$ is the boundary

of the ith particle. The above equations are solved using the initial condition $\mathbf{u}|_{t=0} = \mathbf{u}_0$, where $\mathbf{u}_0$ is the known initial value of the velocity.

The linear velocity $\mathbf{U}_i$ and the angular velocity $\boldsymbol{\omega}_i$ of the i^{th} particle are governed by

$$m_i \frac{d\mathbf{U}_i}{dt} = \mathbf{F}_i + \mathbf{F}_{E,i} \tag{2.5}$$

$$I_i \frac{d\boldsymbol{\omega}_i}{dt} = \mathbf{T}_i + \mathbf{T}_{E,i} \tag{2.6}$$

$$\mathbf{U}_i|_{t=0} = \mathbf{U}_{i,0} \tag{2.7}$$

$$\boldsymbol{\omega}_i|_{t=0} = \boldsymbol{\omega}_{i,0} \tag{2.8}$$

where m_i and I_i are the mass and moment of inertia of the i^{th} particle, $\mathbf{F}_i$ and $\mathbf{T}_i$ are the hydrodynamic force and torque acting on the i^{th} particle, $\mathbf{F}_{E,i}$ is the electrostatic force acting on the i^{th} particle and $\mathbf{T}_{E,i}$ is the electrostatic torque acting on the i^{th} particle. In this work, there is no need to keep track of the particle orientation because, only spherical particles are considered. The particle positions are obtained from

$$\frac{d\mathbf{X}_i}{dt} = \mathbf{U}_i \tag{2.9}$$

$$\mathbf{X}_i|_{t=0} = \mathbf{X}_{i,0} \tag{2.10}$$

where $\mathbf{X}_{i,0}$ is the position of the i^{th} particle at time $t = 0$. Here, the assumption is that all particles have the same density ρ_p, and since they have the same radius, they also have the same mass m.

2.2.1 Point-Dipole and Maxwell Stress Tensor Approaches

According to the point dipole (PD) model, which assumes that the gradient of the electric field is constant, the time averaged dielectrophoretic (DEP) force acting on a particle in an AC electric field is given by [3, 4]

$$\mathbf{F}_{DEP} = 2\pi a^3 \varepsilon_0 \varepsilon_c \beta \nabla \mathbf{E}^2 \tag{2.11}$$

where a is the particle radius, ε_c is the dielectric constant of the fluid, $\varepsilon_0 = 8.8542\text{x}10^{-12}$ F/m is the permittivity of free space and **E** is the RMS value of the electric field. Expression (1) is also valid for a DC electric field where **E** is simply the electric field intensity. The coefficient $\beta(\omega)$ is the real part of the frequency dependent Clausius-Mossotti factor given by $\beta(\omega) = \mathrm{Re}\left(\frac{\varepsilon_p^* - \varepsilon_c^*}{\varepsilon_p^* + 2\varepsilon_c^*}\right)$, where ε_p^* and ε_c^* are the frequency dependent complex permittivity of the particle and fluid, respectively. The complex permittivity $\varepsilon^* = \varepsilon - j\sigma/\omega$, where ε is the permittivity, σ is the conductivity and $j = \sqrt{-1}$. The frequency dependence can be included in simulations by selecting an appropriate value of β. The Clausius-Mossotti factor can take values between -0.5 and 1.0.

According to the PD model, the particle-particle interaction force on the i^{th} particle due to the j^{th} particle in a non uniform electric field is [64-66]

$$\mathbf{F}_D = \frac{12\pi\varepsilon_0\varepsilon_c\beta^2 a^6}{r^4}\begin{pmatrix}\mathbf{r}_{ij}(\mathbf{E}_i\cdot\mathbf{E}_j)+(\mathbf{r}_{ij}\cdot\mathbf{E}_i)\mathbf{E}_j+(\mathbf{r}_{ij}\cdot\mathbf{E}_j)\mathbf{E}_i \\ -5\mathbf{r}_{ij}(\mathbf{E}_i\cdot\mathbf{r}_{ij})(\mathbf{E}_j\cdot\mathbf{r}_{ij})\end{pmatrix} \tag{2.12}$$

where $\mathbf{r}_{ij}$ is the unit vector in the direction from the center of i^{th} particle to the center of j^{th} particle. This force is present even if the applied electric field is uniform.

To calculate the electric field **E**, first solve the electric potential ϕ problem

$$\nabla \cdot (\varepsilon \nabla \phi) = 0 \tag{2.13}$$

with the boundary conditions on the particle surface given by

$$\phi_1 = \phi_2, \ \varepsilon_c \frac{\partial \phi_1}{\partial n} = \varepsilon_p \frac{\partial \phi_2}{\partial n} \tag{2.14}$$

where ϕ_1 and ϕ_2 are the electric potential in the liquid and particles, respectively, and the electric field $\mathbf{E} = -\nabla\phi$. The Maxwell stress tensor is given by

$$\boldsymbol{\sigma}_M = \varepsilon \mathbf{E}\mathbf{E} - \frac{1}{2}\varepsilon(\mathbf{E} \bullet \mathbf{E})\mathbf{I} \tag{2.15}$$

The electrostatic force and torque on the i^{th} particle are given by

$$\mathbf{F}_{E,i} = \int_{\Gamma_{Pi}} \boldsymbol{\sigma}_M \cdot \mathbf{n}_i \, d\mathbf{s} \tag{2.16}$$

$$\mathbf{T}_{E,i} = \int_{\Gamma_{Pi}} (\mathbf{x} - \mathbf{x}_i) \times \boldsymbol{\sigma}_M \cdot \mathbf{n}_i \, d\mathbf{s} \tag{2.17}$$

were $\mathbf{n_i}$ is the unit outer normal on the surface of the i^{th} particles and $\mathbf{x_i}$ is the center of the i^{th} particle.

2.2.2 Dimensionless Equations and Parameters

Equations (2.1) and (2.2) are nondimensionalized by assuming that the characteristic length, velocity, time, stress, angular velocity and electric field scales are a, U, a/U, $\eta U/a$, U/a and E_0, respectively. The gradient of the electric field is assumed to scale as E_0/L, where L is the distance between the electrodes which is taken to be the same as the domain width. The nondimensional equations for the liquid, after using the same symbols for the dimensionless variables, are:

$$Re\left(\frac{\partial \mathbf{u}}{\partial t}+\mathbf{u}\cdot\nabla\mathbf{u}\right)=-\nabla p+\nabla\cdot\boldsymbol{\sigma} \text{ in } \Omega\backslash\overline{P(t)} \tag{2.18}$$

$$\nabla\cdot\mathbf{u}=0 \text{ in } \Omega\backslash\overline{P(t)} \tag{2.19}$$

If the point dipole approximation is used for evaluating the electrostatic force, the dimensionless equations for the particles become

$$I_i\frac{d\boldsymbol{\omega}_i}{dt}=\oint(\mathbf{x}-\mathbf{x}_i)\times[(-p\mathbf{I}+\boldsymbol{\sigma}).n]\,dA+\mathbf{T}_{E,i} \tag{2.20}$$

$$\frac{d\mathbf{U}}{dt}=\frac{6\pi\eta a^2}{mU}\int\left(\frac{-pI+\sigma}{6\pi}\right)n\,ds+\frac{4\pi a^4\varepsilon_0\varepsilon_c\beta|E_0|^2}{mU^2L}\mathbf{E}.\nabla\mathbf{E}+\frac{3\pi\varepsilon_0\varepsilon_c a^3\beta^2|E_0|^2}{4mU^2|r_{ij}|^4}\mathbf{F}_D \tag{2.21}$$

and in terms of the Maxwell stress tensor they are

$$\frac{d\mathbf{U}}{dt}=\frac{6\pi\eta a^2}{mU}\int\boldsymbol{\sigma}.\mathbf{n}ds\quad+\frac{\varepsilon E_0^2a^3}{mU^2}\int\boldsymbol{\sigma}_M.\mathbf{n}ds \tag{2.22}$$

$$\frac{d\boldsymbol{\omega}}{dt}=\frac{5\eta a^2}{2mU}\int(\mathbf{x}-\mathbf{x}_i)\times\boldsymbol{\sigma}.\mathbf{n}ds\quad+\frac{\varepsilon E_0^2a^3}{mU^2}\int(\mathbf{x}-\mathbf{x}_i)\times\boldsymbol{\sigma}_M.\mathbf{n}ds \tag{2.23}$$

If the point dipole approximation is used, the above equations contain the following dimensionless parameters:

$$Re=\frac{\rho_L U a}{\eta} \tag{2.24}$$

$$P_1=\frac{6\pi\eta a^2}{mU} \tag{2.25}$$

$$P_2=\frac{3\pi\varepsilon_0\varepsilon_c\beta^2a^3\,|E_0|^2}{4mU^2} \tag{2.26}$$

$$P_3=\frac{4\pi\varepsilon_0\varepsilon_c\beta a^4\,|E_0|^2}{mU^2L} \tag{2.27}$$

$$h'=\frac{L}{a} \tag{2.28}$$

Here *Re* is the Reynolds number, which determines the relative importance of the fluid inertia and viscous forces, P_1 is the ratio of the viscous and inertia forces, P_2 is the ratio of the electrostatic particle-particle interaction and inertia forces and P_3 is the ratio of the dielectrophoretic and inertia forces. Another important parameter, which does not appear directly in the above equations, is the solids fraction of the particles; the rheological properties of ER suspensions depend strongly on the solids fraction. Now, define another Reynolds number $Re_L = \frac{\rho_L L U}{\eta}$ based on the channel width *L*.

If the Maxwell stress tensor approach is used, an alternative parameter $P_E = \frac{\varepsilon E_0^2 a^3}{mU^2}$ is obtained, which is a measure of the electrostatic forces, in place of P_2 and P_3. This parameter is less informative than parameters P_2 and P_3, as it does not contain any information about the extent of polarization or the shape of the particle. In flows for which the applied pressure gradient or the imposed flow velocity is zero, assume that the characteristic velocity $U = \frac{2\varepsilon_0 \varepsilon_c \beta a^2 |E_0|^2}{3\eta L}$, which is obtained by assuming that the dielectrophoretic force and the viscous drag terms balance each other.

In order to investigate the relative importance of the electrostatic particle-particle and dielectrophoretic forces, we define another parameter

$$P_4 = \frac{P_2}{P_3} = \frac{3\beta L}{16a} \tag{2.29}$$

Expression (2.18) implies that if β=O(1) and $L>>a$, and thus $P_4 > 1$, the particle-particle interaction forces will dominate, which is the case in most applications of

dielectrophoresis. On the other hand, if β<<O(1) and $\frac{L}{a} \sim$ O(1), and thus $P_4 < 1$, then the dielectrophoretic force dominates.

2.3 Finite Element Method

The computational scheme used here is a generalization of the DLM finite-element scheme described in [67, 68]. In this scheme, the fluid flow equations are solved on the combined fluid-solid domain, and the motion inside the particle boundaries is forced to be rigid-body motion using a distributed Lagrange multiplier. The fluid and particle equations of motion are combined into a single combined weak equation of motion, eliminating the hydrodynamic forces and torques, which helps ensure the stability of the time integration. For the sake of simplicity, in this section, assume that there is only one particle. The extension to the multi-particle case is straightforward.

The solution and variation are required to satisfy the strong form of the constraint of rigid body motion throughout *P(t)*. In the distributed Lagrange multiplier method, this constraint is removed from the velocity space and enforced weakly as a side constraint using a distributed Lagrange multiplier term. It was shown in [76, 77] that the following weak formulation of the problem holds in the extended domain:

For a.e. $t > 0$, find $\mathbf{u} \in \overline{W}_{u\Gamma}$, $p \in L_0^2(\Omega)$, $\boldsymbol{\lambda} \in \Lambda(t)$, $\mathbf{U} \in \mathbf{R}^3$ and $\boldsymbol{\omega} \in \mathbf{R}^3$, satisfying

$$\int_\Omega \rho_L \left(\frac{d\mathbf{u}}{dt} - \mathbf{g} \right) \cdot \mathbf{v} d\mathbf{x} - \int_\Omega p \nabla . \mathbf{v} \, d\mathbf{x} + \int_\Omega 2\eta \mathbf{D}[\mathbf{u}] : \mathbf{D}[\mathbf{v}] d\mathbf{x}$$
$$+ \left(1 - \frac{\rho_L}{\rho_d} \right) \left(M \left(\frac{d\mathbf{U}}{dt} - \mathbf{g} \right) \cdot \mathbf{V} + I \frac{d\omega}{dt} \xi \right) - \mathbf{F}' . \mathbf{V} = \left\langle \boldsymbol{\lambda}, \mathbf{v} - (\mathbf{V} + \xi \times \mathbf{r}) \right\rangle_{P(t)} \qquad (2.30)$$

for all $\mathbf{v} \in \overline{W}_0$, $\mathbf{V} \in \mathbf{R}^3$, and $\xi \in \mathbf{R}^3$

$$\int_{\Omega} q \nabla . u \, dx = 0 \qquad \text{for all } q \in L^2(\Omega), \tag{2.31}$$

$$\langle \boldsymbol{\mu}, \mathbf{u} - (\mathbf{U} + \omega \times \mathbf{r}) \rangle_{P(t)} = 0 \qquad \text{for all } \boldsymbol{\mu} \in \Lambda(t), \tag{2.32}$$

$$\mathbf{u}|_{t=0} = \mathbf{u}_o \qquad \text{in } \Omega, \tag{2.33}$$

as well as the kinematic equations and the initial conditions for the particle linear and angular velocities. Here $\mathbf{F}'$ is the additional body force applied to the particles to limit the extent of overlap and $\boldsymbol{\lambda}$ is the distributed Lagrange multiplier

$$\overline{W}_{u\Gamma} = \{\mathbf{v} \in H^1(\Omega)^3 \mid \mathbf{v} = \mathbf{u}_\Gamma(t) \quad \text{on} \quad \Gamma\}, \tag{2.34}$$

$$\overline{W}_0 = H_0^1(\Omega)^3, \tag{2.35}$$

$$L_0^2(\Omega) = \{q \in L^2(\Omega) \mid \int_{\Omega} q \, d\mathbf{x} = 0\} \tag{2.36}$$

and $\Lambda(t)$ is $L^2(P(t))^3$, with $\langle .,. \rangle_{P(t)}$ denoting the L^2 inner product over the particle, where Γ^- is the upstream part of Γ. In simulations, since the velocity and $\boldsymbol{\mu}$ are in L^2, the following inner product is used

$$\langle \boldsymbol{\mu}, \mathbf{v} \rangle_{P(t)} = \int_{P(t)} (\boldsymbol{\mu} . \mathbf{v}) \, d\mathbf{x} \tag{2.37}$$

In order to solve the above problem numerically, discretize the domain using a regular tetrahedral mesh T_h for the velocity, where h is the mesh size, and a regular tetrahedral mesh T_{2h} for the pressure. The following finite dimensional spaces are defined for approximating $\overline{W}_{u\Gamma}$, $\overline{W}_0$, $L^2(\Omega)$ and $L_0^2(\Omega)$:

$$W_{u\Gamma,h} = \{\mathbf{v}_h \in C^0(\overline{\Omega})^3 \mid \mathbf{v}_h|_T \in P_1 \times P_1 \times P_1 \text{ for all } T \in T_h, \mathbf{v}_h = \mathbf{u}_{\Gamma,h} \text{ on } \Gamma\} \tag{2.38}$$

$$W_{0,h} = \{\mathbf{v}_h \in C^0(\overline{\Omega})^3 \mid \mathbf{v}_h|_T \in P_1 \times P_1 \times P_1 \text{ for all } T \in T_h, \mathbf{v}_h = 0 \text{ on } \Gamma\} \tag{2.39}$$

$$L_h^2 = \{q_h \in C^0(\overline{\Omega}) \mid q_h|_T \in P_1 \text{ for all } T \in T_{2h}\} \tag{2.40}$$

$$L^2_{0,h} = \{q_h \in L^2_h \mid \int_\Omega q_h \, d\mathbf{x} = 0\} \tag{2.41}$$

The particle inner product terms in (2.30) and (2.32) are obtained using the discrete L^2 inner product defined in Glowinski, et al. [74]. Specifically, choose M points, $\mathbf{x}_1,\ldots,\mathbf{x}_M$ that uniformly cover $\overline{P}(t)$, and define

$$\Lambda_h(t) = \left\{ \boldsymbol{\mu}_h \;\middle|\; \boldsymbol{\mu} = \sum_{i=1}^{M} \boldsymbol{\mu}_{h,i}\, \delta(\mathbf{x}-\mathbf{x}_i), \quad \boldsymbol{\mu}_{h,1},\ldots,\boldsymbol{\mu}_{h,M} \in \mathbf{R}^3 \right\} \tag{2.42}$$

Using these finite dimensional spaces, it is straightforward to discretize equations (2.30-2.33).

Time Discretization Using the Marchuk-Yanenko Operator Splitting Scheme

The initial value problem (Equations 2.30-2.33) is solved by using the Marchuk-Yanenko operator-splitting scheme, which allows us to decouple its three primary difficulties:

1. The incompressibility condition, and the related unknown pressure p_h,
2. The nonlinear advection term,
3. The constraint of rigid-body motion in $P_h(t)$, and the related distributed Lagrange multiplier λ_h.

The Marchuk-Yanenko operator-splitting scheme can be applied to an initial value problem of the form

$$\frac{d\phi}{dt} + A_1(\phi) + A_2(\phi) + A_3(\phi) = f \tag{2.43}$$

where the operators A_1, A_2 and A_3 can be multi-valued. Let Δt be the time step. Now, use the following version of the Marchuk-Yanenko operator splitting scheme to simulate the motion of particles in an ER fluid:

Set $\mathbf{u}^0 = \mathbf{u}_{0,h}$, $\mathbf{U}^0 = \mathbf{U}_0$, $\mathbf{X}^0 = \mathbf{X}_0$ and $\boldsymbol{\omega}^0 = \boldsymbol{\omega}_0$, and calculate $\mathbf{E}$ by solving $\nabla^2\varphi = 0$, subjected to the electric potential boundary conditions, and then calculating $\mathbf{E} = \nabla\varphi$.

For n = 0, 1, 2,... assuming $\mathbf{u}^n$, $\mathbf{U}^n$, $\mathbf{X}^n$, and $\boldsymbol{\omega}^n$ are known, find the values for the $(n+1)^{th}$ time step using the following steps:

STEP 1:

Find $\mathbf{u}^{n+1/4} \in W^{n+1}_{u\Gamma,h}$ and $p^{n+1/4} \in L^2_{0,h}$, by solving

$$\int_\Omega \rho_L \frac{\mathbf{u}^{n+1/4} - \mathbf{u}^n}{\Delta t}.\mathbf{v}\,dx - \int_\Omega p^{n+1/4}\nabla.\mathbf{v}\,dx + \alpha\int_\Omega 2\eta_s \mathbf{D}[\mathbf{u}^{n+1/4}]:\mathbf{D}[\mathbf{v}]dx = \mathbf{0} \tag{2.44}$$

$$\text{for all } \mathbf{v} \in W_{0,h},$$

$$\int_\Omega q\nabla.\mathbf{u}^{n+1/4}\,dx = 0 \qquad \text{for all } q \in L^2_h, \tag{2.45}$$

STEP 2:

Find $\mathbf{u}^{n+2/4} \in W^{n+1}_{u\Gamma,h}$, by solving

$$\int_\Omega \rho_L \frac{\mathbf{u}^{n+2/4} - \mathbf{u}^{n+1/4}}{\Delta t}.\mathbf{v}dx + \int_\Omega \rho_L(\mathbf{u}^{n+2/4}.\nabla\mathbf{u}^{n+2/4}).\mathbf{v}\,dx + \beta\int_\Omega 2\eta_s \mathbf{D}[\mathbf{u}^{n+2/4}]:\mathbf{D}[\mathbf{v}]dx = 0 \tag{2.46}$$

$$\text{for all } \mathbf{v} \in W_{0,h}$$

STEP 3:

Compute $\mathbf{U}^{n+2/4}$ and $\mathbf{X}^{n+2/4}$ using the prediction procedure

Set $\mathbf{U}^{n,0} = \mathbf{U}^n$, $\mathbf{X}^{n,0} = \mathbf{X}^n$.

Do k = 1,K

Calculate $\mathbf{F}_E\left(X^{n,k-1}\right)$

$$\mathbf{U}^{*n,k} = \mathbf{U}^{n,k-1} + \left(\mathbf{g} + \left(1 - \frac{\rho_L}{\rho_d}\right)^{-1} M^{-1}\left[\mathbf{F}'(X^{n,k-1}) + \mathbf{F}_E\left(X^{n,k-1}\right)\right]\right)\frac{\Delta t}{K}$$

$$\mathbf{X}^{*n,k} = \mathbf{X}^{n,k-1} + \left(\frac{\mathbf{U}^{n,k-1} + \mathbf{U}^{*n,k}}{2}\right)\frac{\Delta t}{K}$$

$$\mathbf{U}^{n,k} = \mathbf{U}^{n,k-}$$

$$^{1} + \left(\mathbf{g} + \left(1 - \frac{\rho_L}{\rho_d}\right)^{-1} M^{-1} \frac{\mathbf{F}'(X^{n,k-1}) + \mathbf{F}'(X^{*n,k-1}) + \mathbf{F}_E(X^{n,k-1}) + \mathbf{F}_E(X^{*n,k-1})}{2}\right)\frac{\Delta t}{K}$$

$$\mathbf{X}^{n,k} = \mathbf{X}^{n,k-1} + \left(\frac{\mathbf{U}^{n,k-1} + \mathbf{U}^{n,k}}{2}\right)\frac{\Delta t}{K}$$

end do

$$\text{Then set } \mathbf{U}^{n+2/4} = \mathbf{U}^{n,K},\ \mathbf{X}^{n+2/4} = \mathbf{X}^{n,K}. \tag{2.47}$$

The next step consists of finding $\mathbf{u}^{n+1} \in W^{n+1}_{u\Gamma,h}$, $\lambda^{n+1} \in \Lambda_h((n+2/4)\Delta t)$, $\mathbf{U}^{n+1} \in \mathbf{R}^3$, and $\omega^{n+1} \in \mathbf{R}^3$, satisfying

$$\int_\Omega \rho_L \frac{\mathbf{u}^{n+1} - \mathbf{u}^{n+2/4}}{\Delta t}.\mathbf{v}\,dx + \left(1 - \frac{\rho_L}{\rho_d}\right)\left(M\frac{\mathbf{U}^{n+1} - \mathbf{U}^{n+2/4}}{\Delta t}.\mathbf{V} + I\frac{\boldsymbol{\omega}^{n+1} - \boldsymbol{\omega}^{n+2/4}}{\Delta t}\xi\right) +$$
$$= \left\langle \lambda^{n+1}, \mathbf{v} - (\mathbf{V} + \xi \times \mathbf{r}^{n+2/4})\right\rangle_{P((n+2/4)\Delta t)} \tag{2.48}$$

$$\text{for all } \mathbf{v} \in W_{0,h},\ \mathbf{V} \in \mathbf{R}^2, \text{ and } \xi \in \mathbf{R}$$

where the center of the particle $P((n+2/4)\Delta t)$ is at the location $X^{n+2/4}$.

Then set $\mathbf{X}^{n+1,0} = \mathbf{X}^n$.

For k = 1, K, follow the do-loop

$$\mathbf{X}^{*n+1,k} = \mathbf{X}^{n+1,k-1} + \left(\frac{\mathbf{U}^n + \mathbf{U}^{n+1}}{2}\right)\frac{\Delta t}{K}$$

$$\mathbf{X}^{n,k} = \mathbf{X}^{*n,k-1} + \left(1 - \frac{\rho_L}{\rho_d}\right)^{-1} M^{-1}\left(\frac{F'(X^{n+1,k-1}) + F'(X^{*n+1,k})}{2}\right)\frac{(\Delta t)^2}{2K}$$

end do

$$\text{Then set } \mathbf{X}^{n+1} = \mathbf{X}^{n+1,K}. \tag{2.49}$$

Then set $p^{n+1} = p^{n+1/4}$, and go back to the first step.

Remarks:

1. The problems arising in the first and second steps are solved using the conjugate gradient algorithm described in [74].
2. α_1 and α_2 are assumed to be the same and its value is 0.5.
3. The third step is used to obtain the distributed Lagrange multiplier that enforces rigid body motion inside the particles. This problem is solved by using the conjugate gradient method described in [74, 75]. In this step, electrostatic forces are accounted that arise due to the dielectrophoretic effect and the particle-particle interactions.

2.4 Results

Results are obtained using finite element code by performing direct numerical simulations of the transient motion of particles in a three dimensional dielectrophoretic cage. The cage is formed by embedding four electrodes in the four side walls parallel to the *yz*- and xy-coordinate planes of a square shaped channel (see Figure 2.1). The electrodes are placed at the center of the side walls and their width is one half the length of the sides. The voltage applied to the electrodes is selected such that the electric field magnitude is locally minimal at the center of the domain where one wishes to attract and hold particles. This device is of practical interest as it provides a way to trap one or more particles at the center of the cage in a contact less fashion.

The fluid density ρ_L = 1.0 g/cm^3, and the particles are assumed to be neutrally buoyant. The viscosity of the fluid is 0.01 g/(cm.s). Both particles and fluid are assumed

to be nonconducting. The normalized dielectric constant of particles is varied and that of the fluid is assumed to be one. The voltage applied to the electrodes is 1000 volts. All dimensional lengths reported in this paper are expressed in mm and the time is reported in seconds. The initial fluid and particle velocities are set to zero. The fluid velocity is assumed to be zero on the domain side walls. The domain is discretized using a pseudo P2-P1 tetrahedral mesh.

The domain dimensions are L, $L/2$ and L, along the x, y and z directions, respectively, (as shown in Figure 2.1). All lengths are nondimensionalized using L. Also note that there are two other characteristic length scales in this problem: the particle radius and the distance between the particles. The latter in general is related to the concentration of particles in the device which is not important since for most cases considered in this paper there are only 1-2 particles in the domain.

The magnitude of the electric field **E** in the xz-plane is shown (in Figure 2.1). Notice that the magnitude is locally minimum at the center of the domain and increases with increasing distance from the center. The figure also shows that the electric field inside the cage is nonuniform, and its gradient near the domain center is non zero, except at the center itself where it is zero. Figure 2.1b shows that the gradient of the electric field magnitude points radially outward from the center and towards the edges of the electrodes. Therefore, if a particle is placed in this domain and its dielectric constant is smaller than that of the liquid, it will experience an electric force towards the center of the domain, i.e., in the direction opposite to the lines of the gradient of the electric field magnitude. If the dielectric constant of the particle is greater than that of the liquid, the direction of the electric force is away from the center.

Figures 2.2 and 2.3 show the modified electric field distribution when two particles are present in the domain. Notice that the electric field is changed in the vicinity of the particles and that this change is especially significant (in Figure 2.3) where particle diameters are larger and comparable to the cage size. Therefore, as discussed below, under these conditions the error in the electric force given by the PD model is relatively larger as it does not account for the fact that the electric field changes when particles are present in the domain. This is also the case, i.e., the electric field changes substantially, when the distance between particles is comparable to their diameter. It is therefore important that for such cases the electric force be computed by first solving the Laplace's equation for the dielectric medium, and then this computed electric potential is used to compute the MST which is integrated over the particle's surface to obtain the force.

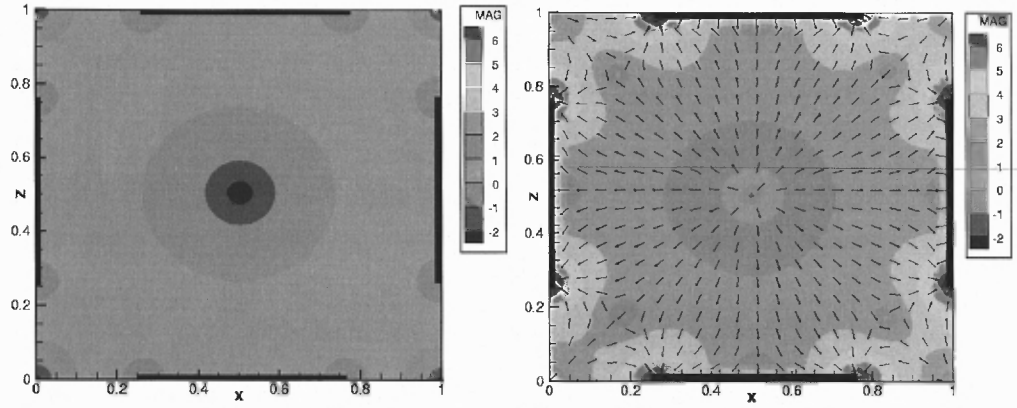

(a) (b)

Figure 2.1 Electric field distribution. (a) Isovalues of log|**E**| at y = 0.25, i.e., the domain mid plane. Electric field does not vary with y. The magnitude is maximum near the electrode edges and decreases with increasing distance. The minimum is at the center. (b) Magnitude and direction of ∇E^2 to which the dielectrophoretic force is proportional. Arrows indicate the direction of positive DEP force (for negative DEP, the direction is the opposite).

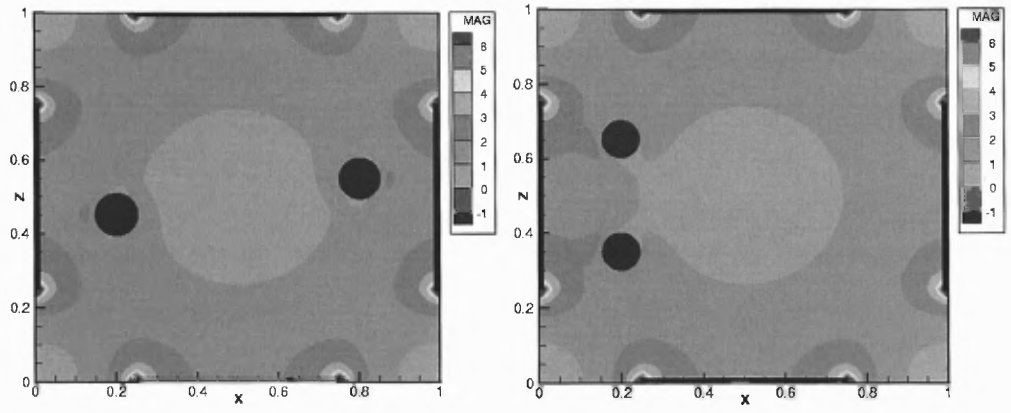

(a) (b)

Figure 2.2 Isovalues of log|**E**| are shown when two particles with radii 0.05 are present. The particles coordinates are (a) (0.2, 0.25, 0.45) and (0.8, 0.25, 0.55), (b) (0.2, 0.25, 0.35) and (0.2, 0.25, 0.65).

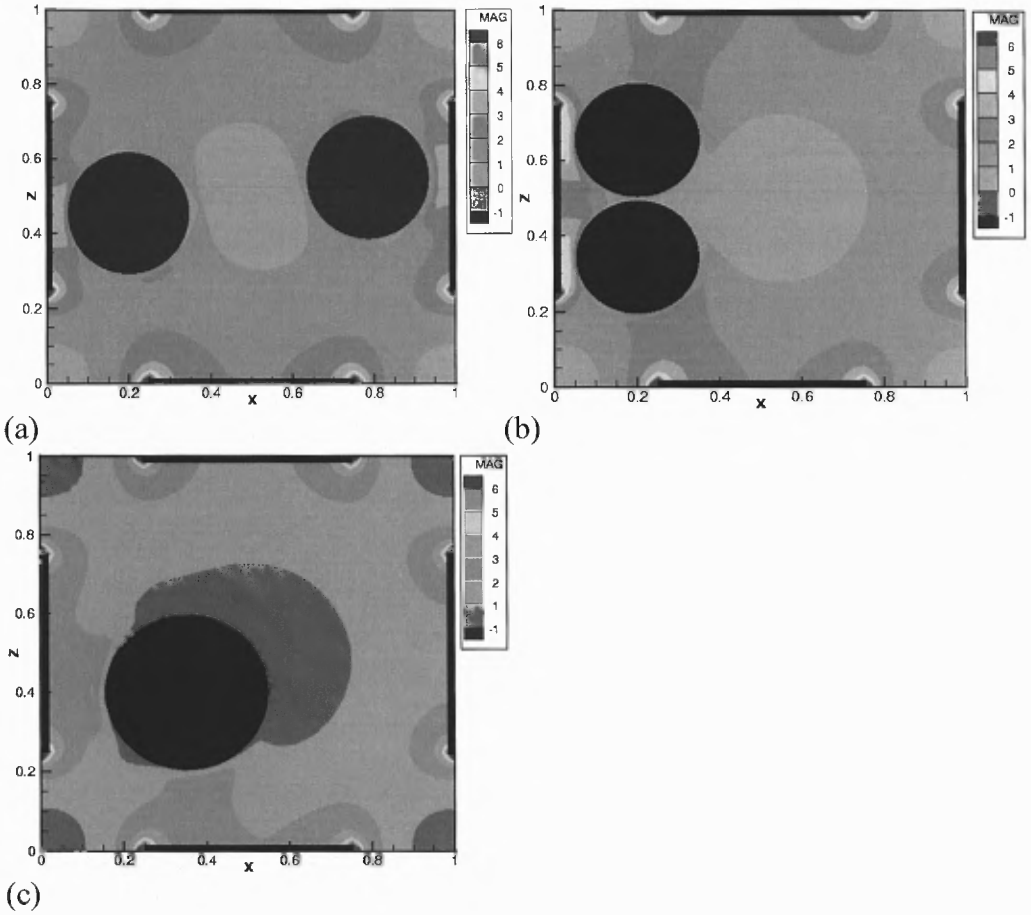

(a) (b)

(c)

Figure 2.3 Isovalues of log|**E**| are modified when size of particles are bigger. The particles coordinates are (a) (0.2, 0.25, 0.45) and (0.8, 0.25, 0.55) with radius 0.15. (b) (0.2, 0.25, 0.34) and (0.2, 0.25, 0.66) with radius 0.15. (c) (0.35,0.25,0.4) with radius 0.20.

2.4.1 Convergence Study

To show that the numerical results obtained using the MST method converge when the time step is reduced or the mesh resolution is increased, the domain is discretized using two meshes, one with 139425 nodes and second with 269001 nodes. The time step used was 2.5×10^{-4} s or 5×10^{-4} s. The trajectories of two particles released close to each other were studied. The initial positions of the two particles were (0.2, 0.25, 0.45) and (0.8, 0.25, 0.55) and the diameter is 0.05. Since the particles are initially close to each other, the electric force contains contribution both from the electrostatic particle-particle interactions and the spatial non uniformity of the electric field.

The dimensionless parameters for the case shown in Figure 2.4 are: $\varepsilon_p = 0.2$, Re $= -2.67 \times 10^{-8}$, Pe $= 7.36 \times 10^{8}$. $\varepsilon_p = 1.1$ Re $= 2.37 \times 10^{-9}$, Pe $= 9.36 \times 10^{10}$. Figure 2.4 shows the z-position of the first particle for two different mesh resolutions and time steps, and for $\varepsilon_p = 0.2$ and 1.1. From (Figure 2.4) note that the particles trajectories remain virtually unchanged when the mesh is refined and also when the time step is reduced. Therefore, the conclusion is that the results have converged for all two values of dielectric constant.

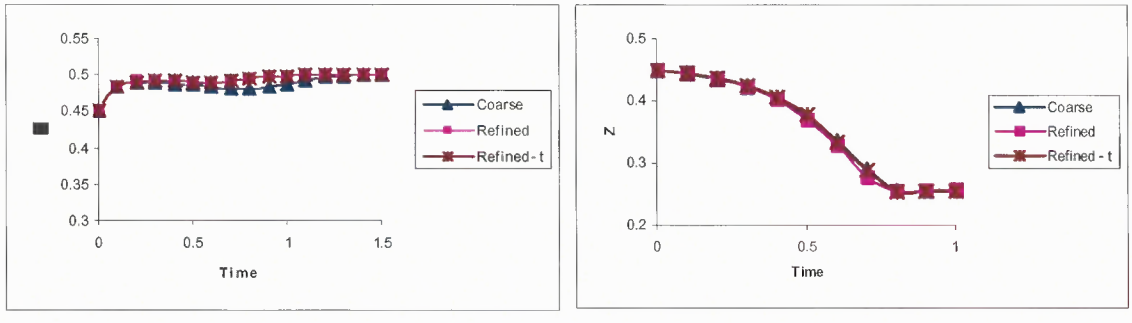

Figure 2.4 The z-component of the first particle is shown as a function of time. There are two particles in the domain and their initial positions were (0.2, 0.25, 0.45) and (0.8, 0.25, 0.55). For "Coarse" there are 139425 nodes and the time step is 5×10^{-4}, for "Refined" there are 269001 nodes and the time step is 5×10^{-4}, and for "Refined - t" there are 269001 nodes and the time step is 2.5×10^{-4}. (a) $\varepsilon_p = 0.2$ (b) $\varepsilon_p = 1.1$.

2.4.2 Motion of a Single Particle:

(a) Variation with ε_p

A single particle with a = 0.05 is released from (0.35, 0.25, 0.40) at t = 0. The transient motion of the particle is studied, and four values of ε_p used in this study are 0.2, 0.5, 1.5 and 5. When the value of $\varepsilon_p < \varepsilon_c = 1$, particles go to regions of minimum electric field due to negative dielectrophoresis. The final position and velocity obtained by particle for PD and MST method is similar (shown in Figures 2.5 and 2.6) for different dielectric mismatch. There is only one particle in the domain so there is no particle particle interaction force.

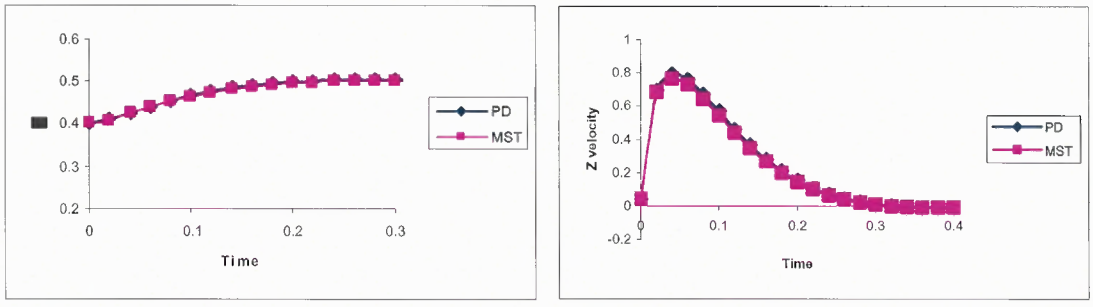

Figure 2.5 The z-component of particle position computed using the PD and MST methods for a = 0.05 and ε_p=0.2. The initial particle position is (0.35, 0.25, 0.40). (a) z-coordinate, (b) z-velocity

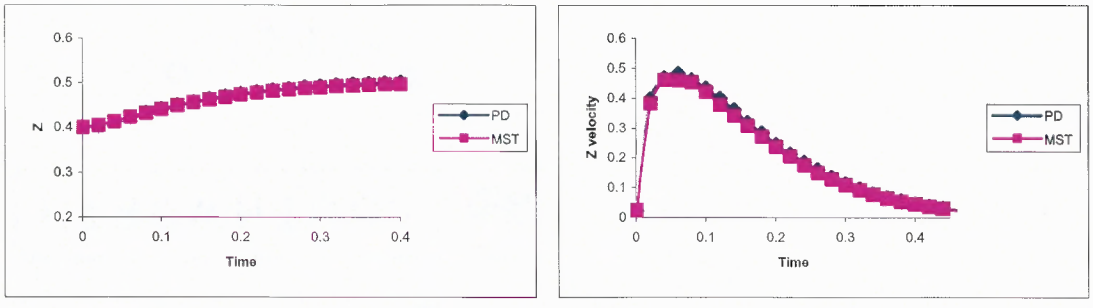

Figure 2.6 The z-component of particle position computed using the PD and MST methods for a = 0.05 and ε_p=0.5. The initial particle position is (0.35, 0.25, 0.40). (a) z-coordinate, (b) z-velocity

This however, is not the case when the value of $\varepsilon_p > \varepsilon_c = 1$ and particle experiences positive dielectrophoresis, and moves toward the regions of high electric field. Velocity obtained by particle for two methods is similar when dielectric mismatch between particle and liquid is less (as shown in Figure 2.7), but particle achieve much higher velocity for MST method when dielectric mismatch between particle and fluid is high (as shown in Figure 2.8).

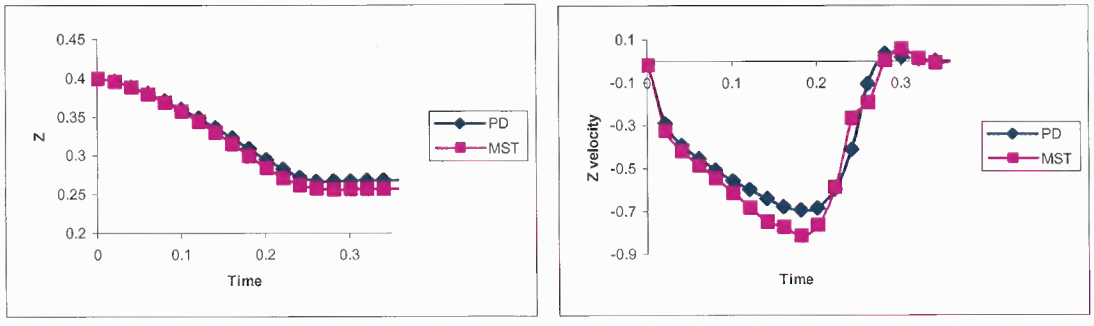

Figure 2.7 The z-component of particle position computed using the PD and MST methods for a = 0.05 and ε_p=1.5. The initial particle position is (0.35, 0.25, 0.40). (a) z-coordinate, (b) z-velocity

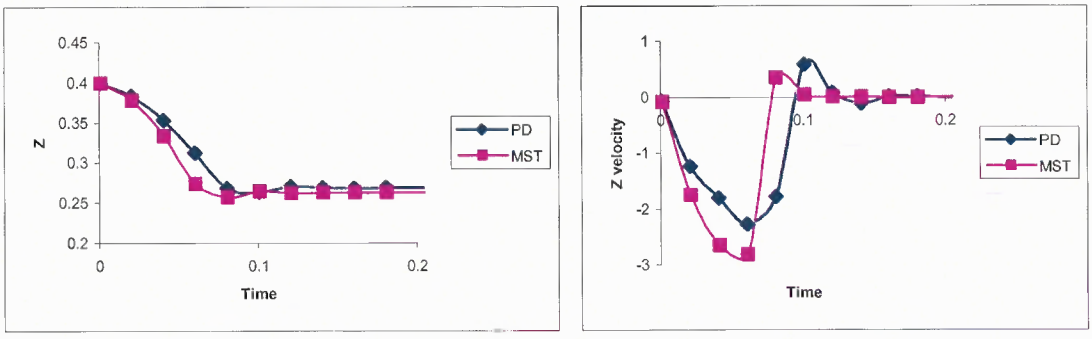

Figure 2.8 The z-component of particle position computed using the PD and MST methods for a = 0.05 and ε_p=5.0. The initial particle position is (0.35, 0.25, 0.40). (a) z-coordinate, (b) z-velocity

(b) Variation with a

(i) Negative Dielectrophoresis

Now, discussion is about the influence of particle radius on trajectory and velocity of a single particle for same dielectric constant. For ε_p = 0.2, particle experiences negative

dielectrophoresis. The particle radius a is varied for two values 0.05 and 0.2. For both a's, the velocities and trajectories obtained by particle remains similar for both PD and MST method (as shown in Figures 2.9 and 2.10).

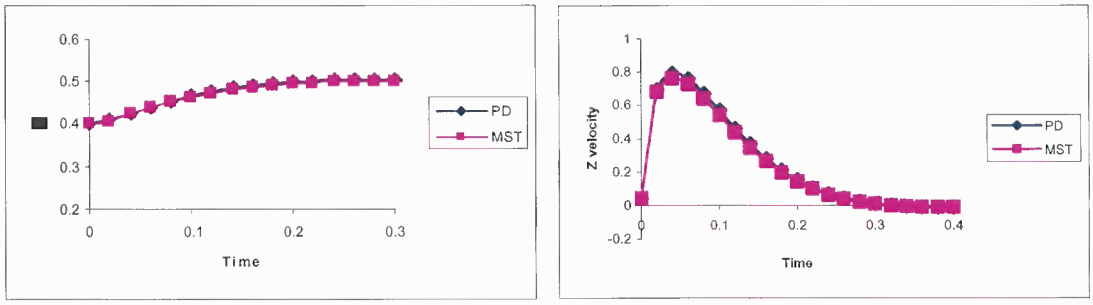

Figure 2.9 The z-component of particle position computed using the PD and MST methods for a = 0.05 and ε_p=0.2. The initial particle position is (0.35, 0.25, 0.40). (a) z-coordinate, (b) z-velocity

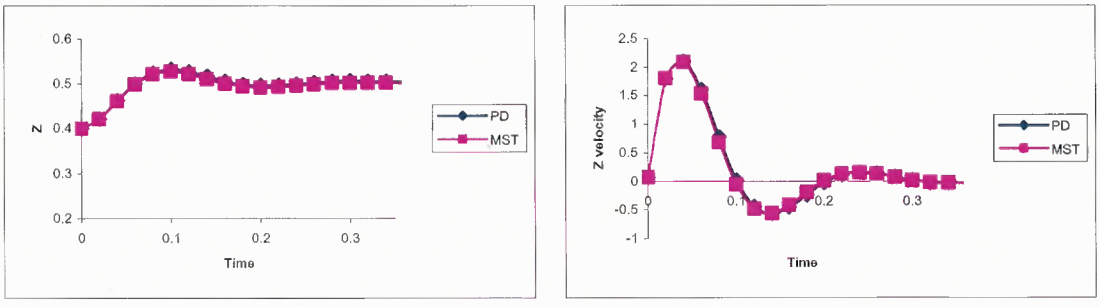

Figure 2.10 The z-component of particle position computed using the PD and MST methods for a = 0.2 and ε_p=0.2. The initial particle position is (0.35, 0.25, 0.40). (a) z-coordinate, (b) z-velocity

(ii) Positive Dielectrophoresis

Particles experience positive dielectrophoresis when the values of $\varepsilon_p > \varepsilon_c = 1$. A bigger particle with higher dielectric mismatch will modify more electric field, thus the trajectories and velocities obtained by MST method is significantly different from PD approximation (Figures 2.11 and 2.12).

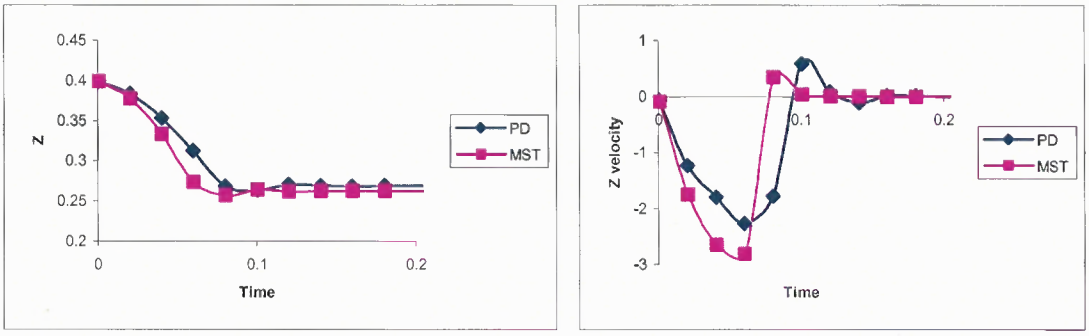

Figure 2.11 The z-component of particle position computed using the PD and MST methods for a = 0.05 and ε_p=5.0. The initial particle position is (0.35, 0.25, 0.40). (a) z-coordinate, (b) z-velocity

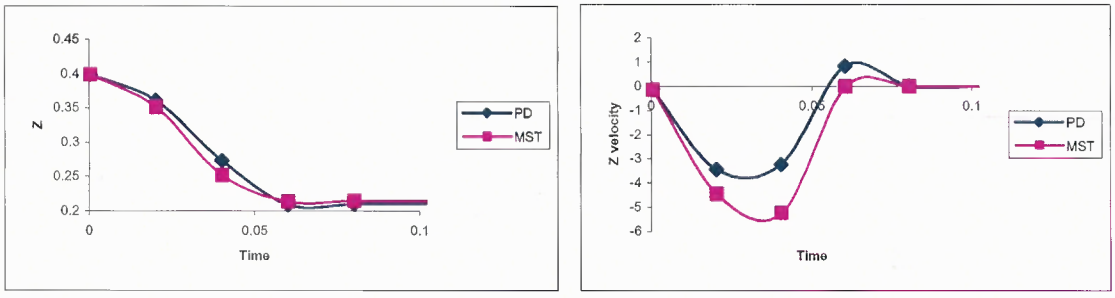

Figure 2.12 The z-component of particle position computed using the PD and MST methods for a = 0.2 and ε_p=5.0. The initial particle position is (0.35, 0.25, 0.40). (a) z-coordinate, (b) z-velocity

2.4.3 Motion of Two Particles

(a) Variation with ε_p

Now, the results are for transient motion of two particles with ε_p=0.5, which at t=0 are released at (0.2, 0.25, 0.45) and (0.8, 0.25, 0.55). Since $\varepsilon_p < \varepsilon_c$=1, this case corresponds to negative dielectrophoresis, and thus the particles eventually move to the domain center where the electric field strength is locally minimum (see Figure 2.13). Their final relative arrangements at the device center given by the PD and MST methods are different. For the PD method, they come close to each other and then rotate about the y-axis so that the line joining their centers becomes parallel to the z-direction. For the MST method, the

particles come close to each other, but then they rotate so that the line joining their centers becomes parallel to the y-direction. Similar results were obtained when the initial positions of the two particles were different showing that the final arrangement at the domain center is independent of their initial positions in the domain (see Figure 2.14).

Here make a note that a comparison between the MST and PD methods is done to determine the parameter values for which the error in the latter method is significant. This is important because, in the past, the point dipole approach has been used to study the formation of chains and columns in electrorheological suspensions even though the particles of chains and column close each other and the PD model is likely to give inaccurate results. The results describe above show that for some conditions even the qualitative arrangement predicted by the two methods is different.

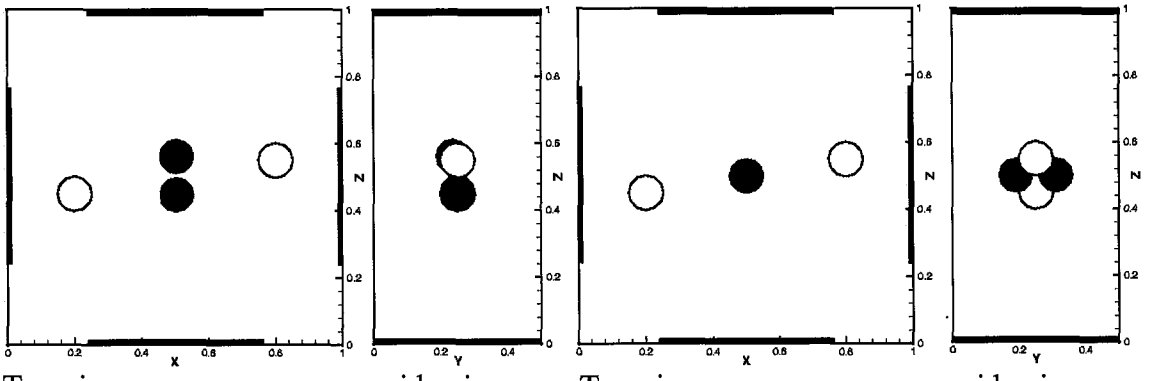

Figure 2.13 Top and side views of particles for ε_p=0.5 at t = 0 and 0.70. The initial positions of the particles (shown as white circles) are (0.2, 0.25, 0.45) and (0.8, 0.2, 0.55). Their final positions are shown by black cirlces. (i) PD, (ii) MST.

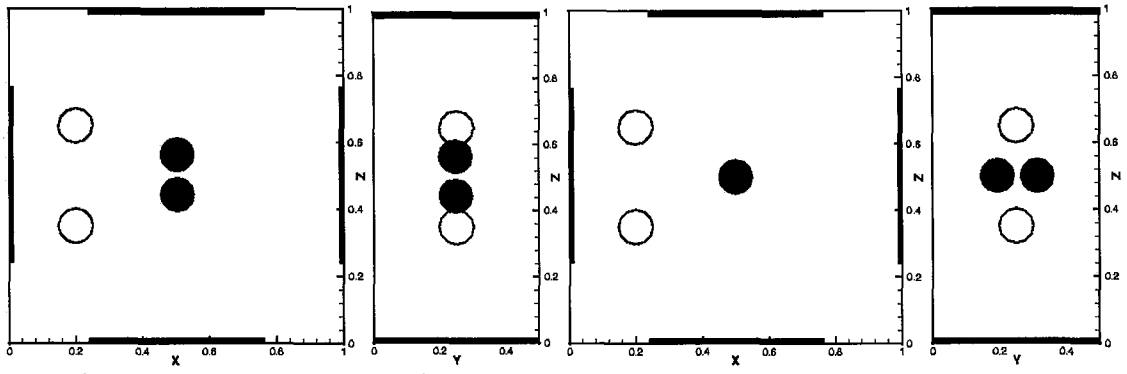

Figure 2.14 Top and side views of particles for ε_p=0.5 at t = 0 and 0.70. The initial positions of the particles (shown as white circles) are (0.2, 0.25, 0.35), and (0.2, 0.25, 0.65). Their final positions are shown by black circles. (i) PD, (ii) MST.

For ε_p=1.5, which corresponds to the case of positive dielectrophoresis, the particles are attracted to the nearby electrode edge and captured there (see Figures 2.15 and 2.16). The initial positions of the particles are the same as in Figures 2.13 and 2.14. The final positions of the captured particles at the electrodes edges given by the MST and PD methods are slightly different. This again is due to the fact that the presence of particle modifies the electric field. Clearly, the particle-particle interactions are not important in this case as the particles remained away from each other. Furthermore, since the dielectric constant of particles is not significantly different from that of the suspending fluid which is one, both methods give similar results.

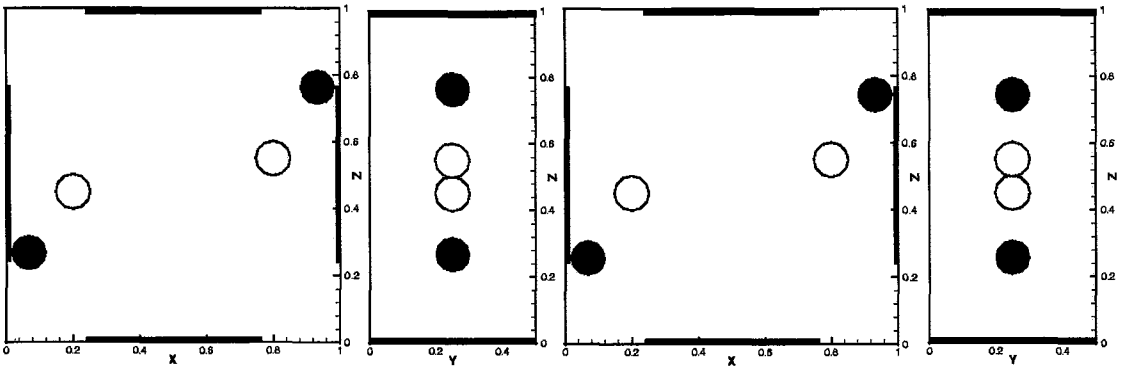

Figure 2.15 Top and side views of particles for ε_p=1.5 at t = 0 and 0.20. The initial positions of the particles (shown as white circles) are (0.2, 0.25, 0.45), and (0.8, 0.25, 0.55). The final positions are shown by black circles. (i) PD, (ii) MST.

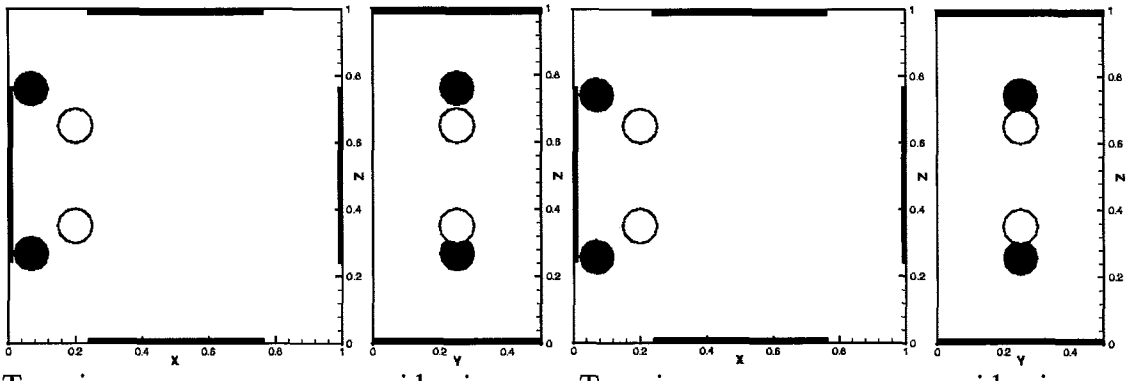

Figure 2.16 Top and side views of particles for ε_p=1.5 at t = 0 and 0.20. The initial positions of the particles (shown as white circles) are (0.2, 0.25, 0.35) and (0.2, 0.25, 0.65). The final positions are shown by black circles. (i) PD, (ii) MST.

The differences between the PD and MST methods as expected, are greater when ε_p= 5.0. Figures 2.17 and 2.18 show that for both methods the particles are captured at the electrode. Their final positions, including the orientation of the line joining their centers, however, are different. Specifically, for the MST method, the particles come closer to the electrode surface and the line joining their centers makes a smaller angle with the electrode surface. For ε_p= 0.2 in both cases, as shown in Figures 2.19 and 2.20,

the particles are captured at the domain center. However, as before, the orientation of the line joining their centers for the PD method is parallel to the y-axis, and for the MST method it is parallel to the z-axis.

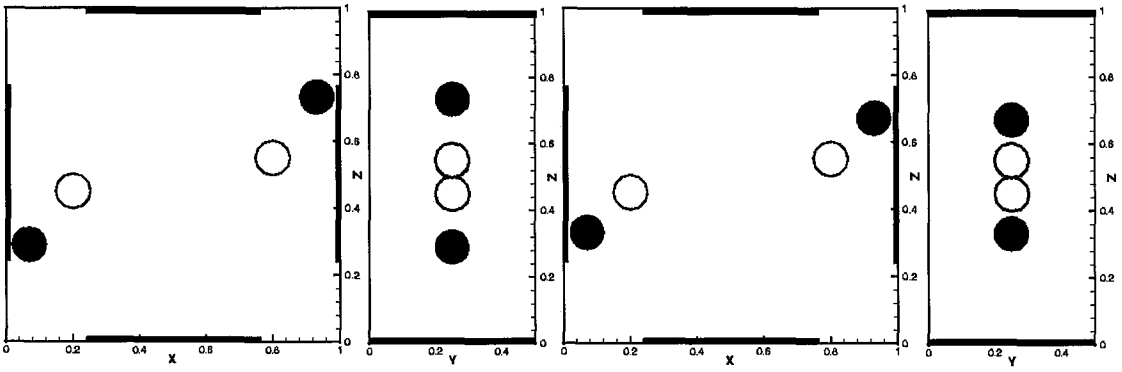

Figure 2.17 Top and side views of particles for ε_p=5.0 at t = 0 and 0.15. The initial positions of the particles (shown as white circles) are (0.2, 0.25, 0.45), and (0.8, 0.25, 0.55). The final positions are shown by black circles. (i) PD, (ii) MST.

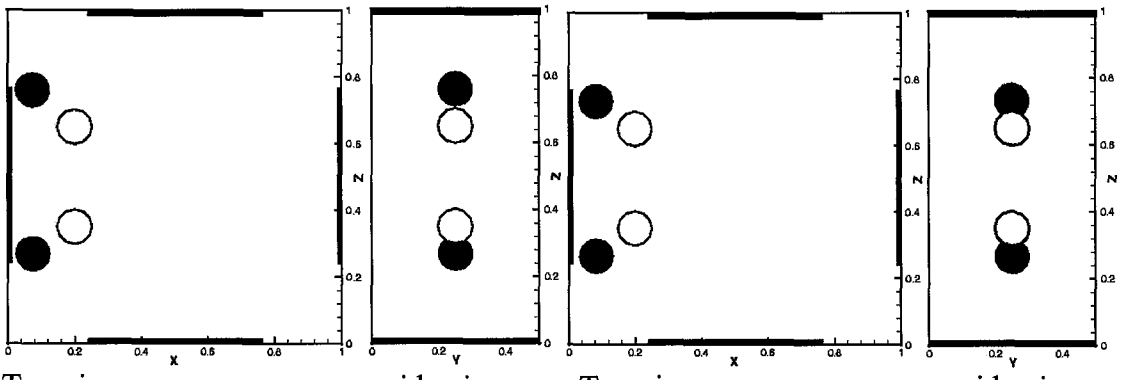

Figure 2.18 Top and side views of particles for ε_p=0.2 at t = 0 and 0.15. The initial positions of the particles (shown as white circles) are (0.2, 0.25, 0.35) and (0.2, 0.25, 0.65). The final positions are shown by black circles. (i) PD, (ii) MST.

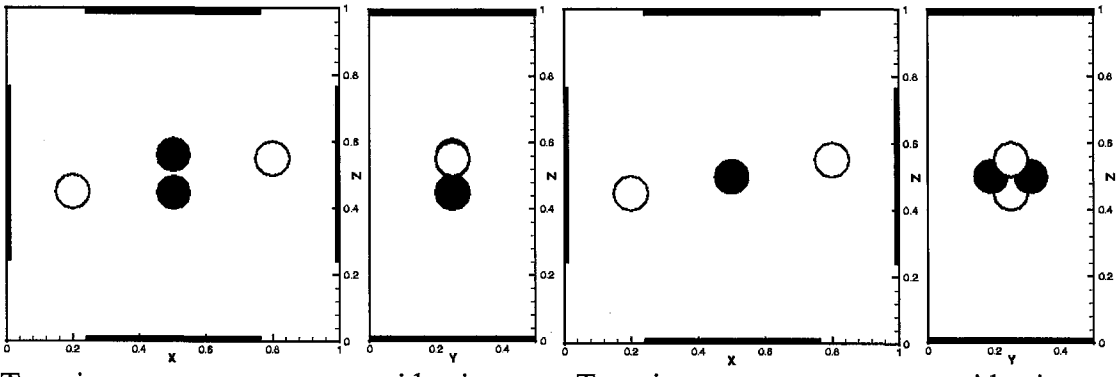

Figure 2.19 Top and side views of particles for ε_p=0.2 at t = 0 and 0.20. The initial positions of the particles (shown as white circles) are (0.2, 0.25, 0.45) and (0.8, 0.25, 0.55). The final positions are shown by black circles. (i) PD, (ii) MST.

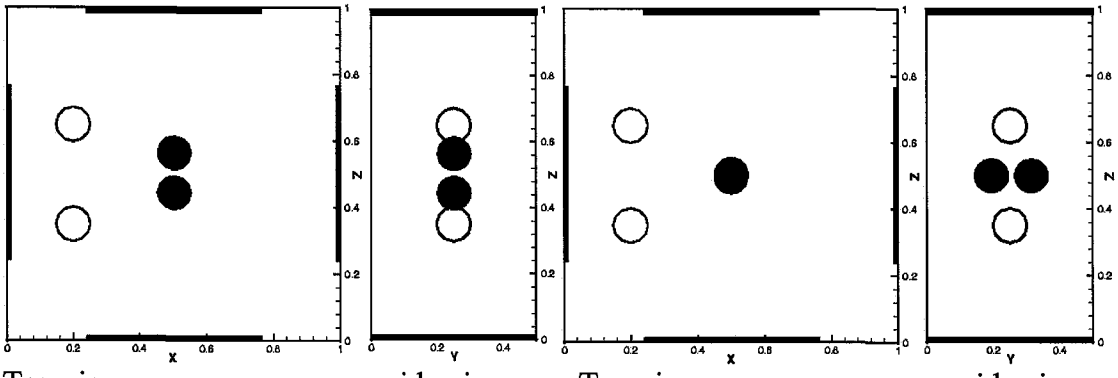

Figure 2.20 Top and side views of particles for ε_p=0.2 at t = 0 and 0.20. The initial positions of the particles (shown as white circles) are (0.2, 0.25, 0.35) and (0.2, 0.25, 0.65). The final positions are shown by black circles. (i) PD, (ii) MST.

(b) Variation with *a*

(i) Negative Dielectrophoresis

Here, the objective is to study the influence of the particle radius on the trajectories of particles. Figure 2.21, shows that particles experience negative dielectrophoresis and due to the presence of particles in domain center electric field is modified. Particles align parallel to z axis in PD approximation and for MST method particles align parallel to y

axis (as shown in Figure 2.21a). When the size of particle is increased in both cases particles align parallel to y axis (as shown in Figure 2.21b).

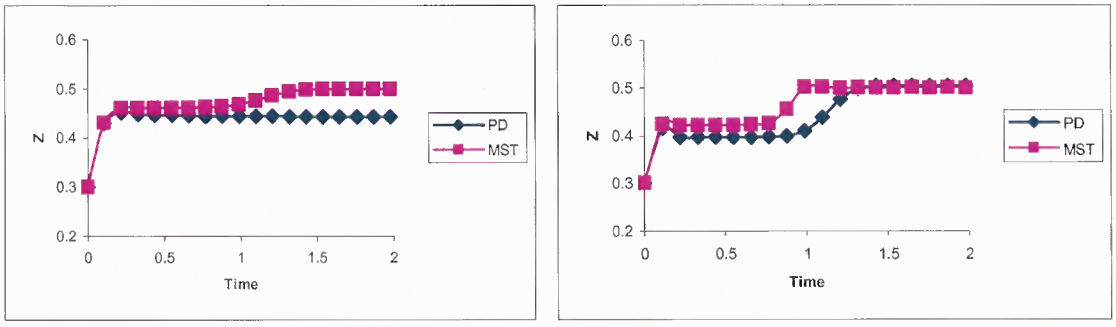

Figure 2.21 The z-component of particle position computed using the PD and MST methods for a = 0.05, 0.1 and ε_p=0.2. The initial position of particles are (0.26, 0.25, 0.30) and (0.74, 0.25, 0.7). (a) z-coordinate for a = 0.05 (b) z-coordinate for a = 0.1.

(ii) Positive Dielectrophoresis

Particles that experience positive DEP gather at electrode edges. Particles initial positions are chosen in such a way that they go to different electrodes. The final position of particle at one electrode obtained by two methods is different (as shown in Figure 2.22). When the size of the particles is increased, the particles do the same thing and the final position in z axis obtained by MST method is smaller in comparison to PD method (as shown in Figure 2.22).

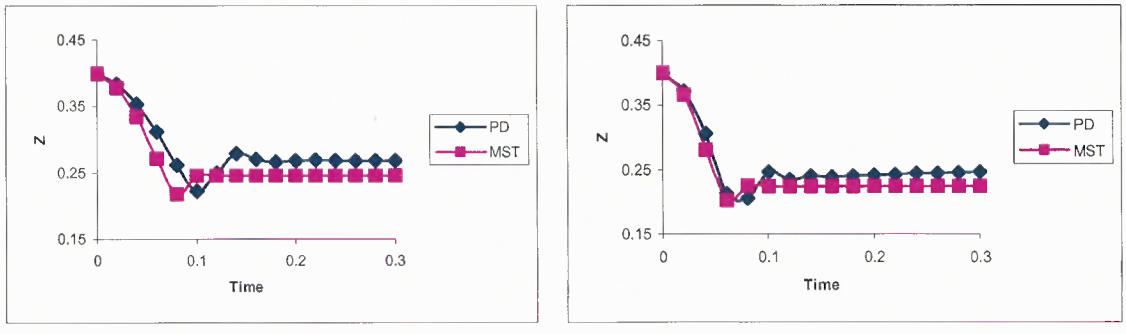

Figure 2.22 The z-component of particle position computed using the PD and MST methods for a = 0.05, 0.1 and ε_p=5.0. The initial position of particles are (0.32, 0.25, 0.40) and (0.62, 0.25, 0.6). (a) z-coordinate for a = 0.05 (b) z-coordinate for a = 0.1.

When particles initial positions are chosen, in such a way that they gather at same electrode. The final positions obtained by two methods are different, as electric field is modified due to the presence of other particle (as shown in Figure 2.23).

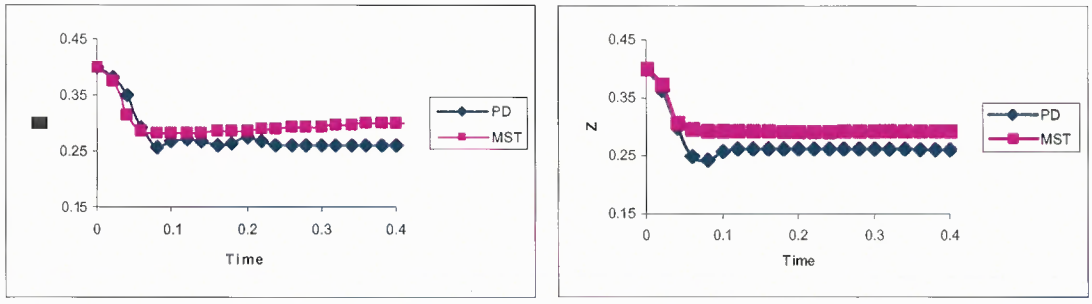

Figure 2.23 The z-component of particle position computed using the PD and MST methods for a = 0.05, 0.1 and ε_p=5.0. The initial position of particles are (0.25, 0.25, 0.40) and (0.46, 0.25, 0.48) (a) z-coordinate for a = 0.05 (b) z-coordinate for a = 0.1.

2.5 Discussion

A numerical scheme based on the distributed Lagrange multiplier method is used to study the dynamical behavior of particles in a dielectrophoretic cage. The Maxwell stress tensor method is used for computing the electric forces on the particles. The study concludes that the error in the point dipole method increases as the distance between the particles decreases. Also, the error is relatively large when the particle radius is comparable to the cage size, which determines the length scale over which the electric field varies. The error also increases as the difference between the dielectric constants of the particles and the fluid increases. The final steady positions of the particles, including the orientations of the line joining their centers, for the MST method are different from those for the point dipole method.

CHAPTER 3

MICRO AND NANO PARTICLES SELF ASSEMBLY FOR VIRTUALLY DEFECT FREE MONOLAYERS

3.1 Overview

In recent years much effort has been directed to understand the behavior of particles trapped at fluid-fluid interfaces because of its importance in a wide range of applications, e.g., the self-assembly of particles at fluid-fluid interfaces resulting in novel nano-structured materials, micro/nano manufacturing, the stabilization of emulsions, etc. [78-84].

Particles get trapped at fluid-fluid interface due to surface tension. A popular means used to assemble particles is based on the phenomenon of capillarity. A common example of capillarity-driven self-assembly is the clustering of cereal flakes floating on the surface of milk. The floating cereal particles experience attractive capillary forces due to the fact that when two such particles are close to each other, the deformed interface around them is not symmetric as the interface height between the particles is lowered due to the interfacial tension. This lowering of the interface between the particles gives rise to lateral forces that cause them to move toward one another and cluster [84-87].

This naturally-occurring phenomenon, however, leads to the uncontrollable clustering of particles, as capillary forces are attractive and increase with decreasing distance between the particles. As a result it produces monolayers that display many defects, lack order (both short and long ranged) and whose distance between the particles cannot be controlled. In addition, such a phenomenon does not manifest itself on particles

smaller than ~10 um. These drawbacks seriously limit the range of applications one can target using this technique.

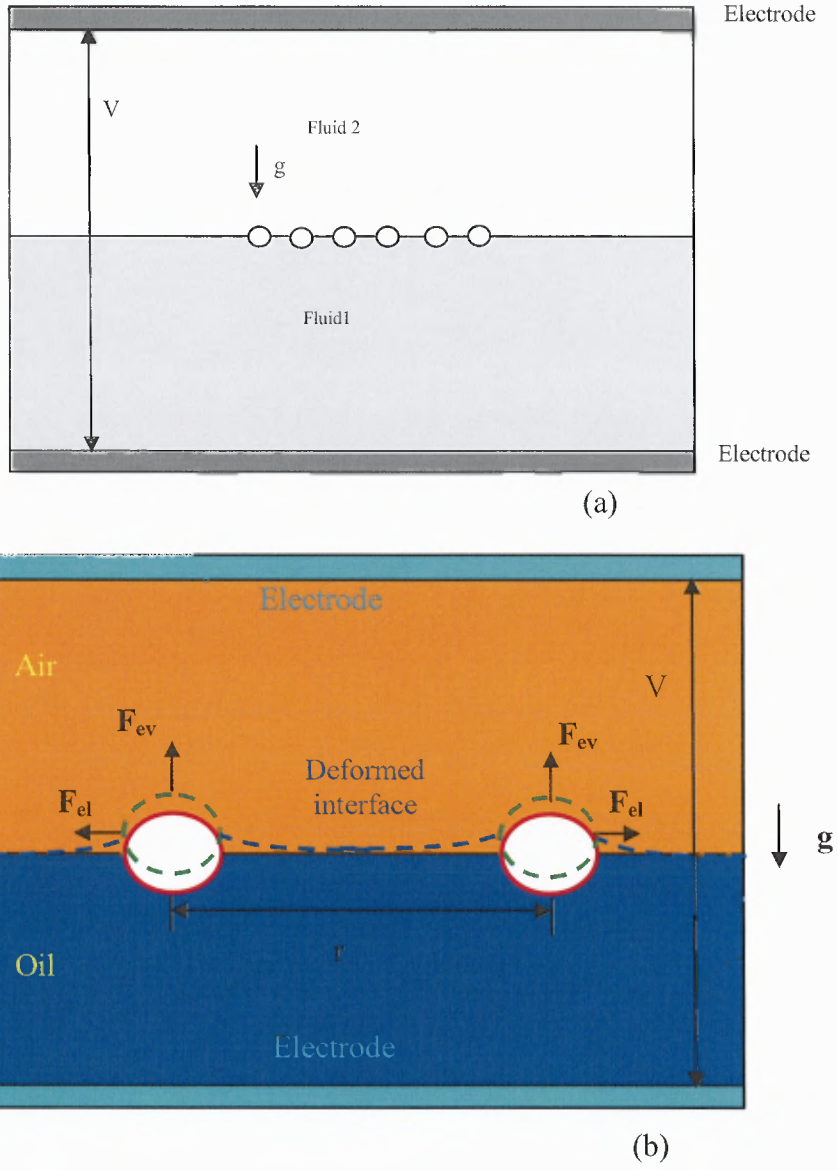

Figure 3.1 (a) Schematic of the experimental setup used to control the self-assembly of particles on a fluid-fluid interface. The distance between neighboring particles is controlled by adjusting the applied voltage; **(b)** Forces acting on particles in the presence of applied electrical field.

The technique described in refs. [88-90] overcomes all these shortcomings (see Figure 3.1) by applying an external electric field normal to the interface. The electric field causes spherical particles trapped at the interface to experience an electrostatic force

normal to the interface and since the particles become polarized they also repel each other due to the dipole-dipole interactions. The former is a new phenomenon in which the electrostatic force arises because of the jump in the dielectric properties across the interface, and not because the applied electric field is non-uniform. In fact, an isolated uncharged particle subjected to a uniform electric field and suspended in a single fluid does not experience any electrostatic force. An interesting property of interfacial phenomenon is that the electrostatic force generated varies as a^2, where a is the particle radius, and not as a^3, which is the case of the well-known dielectrophoretic force [3,4] acting on particles suspended in a bulk liquid and under the influence of a non-uniform electric field. It follows that the new interfacial electrostatic force is stronger on small particles than the classic dielectrophoretic force. In addition, the resulting self-assembly process into two-dimensional arrays is capable of controlling the lattice spacing statically or dynamically, forming virtually defect-free monolayers of monodispersed spherical particles, and manipulating a broad range of particle sizes and types including nano-particles and electrically neutral particles. Indeed, the electric field causes particles to experience electrostatic and capillary forces, the magnitudes of which can be adjusted to control the lattice spacing of the formed monolayer.

In this study, it is demonstrated that for a fluid-fluid interface the electric field applied normal to interface produces a repulsive force on particles and the lattice spacing can be controlled by changing the magnitude of electric field.

3.2 Governing Equations

The domain containing the two fluids and spherical particles (of identical radii and properties) is denoted by Ω, the interior of the ith particle and its surface by $P_i(t)$ and $\partial P_i(t)$, respectively, and the domain boundary by Γ. To calculate the electric field **E**, the electric potential problem for ϕ in Ω is solved first, namely $\nabla\cdot(\varepsilon\nabla\phi)=0$ as subjected to the boundary conditions on the particle surfaces and the two-fluid interface. On the particle surface $\partial P_i(t)$, the conditions are $\phi_1=\phi_2$, $\varepsilon_c\frac{\partial\phi_1}{\partial n}=\varepsilon_p\frac{\partial\phi_2}{\partial n}$, where ϕ_1 and ϕ_2 are the electric potentials in the liquid and particle, and ε_c and ε_p are the dielectric constants of the fluid and particle. A similar boundary condition is applied at the two-fluid interface. The electric potential is prescribed on the electrodes as constant values and the normal derivative of the potential is taken to be zero on the remaining domain boundary. The electric field is then deduced from the equation $\mathbf{E}=-\nabla\phi$. The Maxwell stress tensor $\boldsymbol{\sigma}_M$ is given by $\boldsymbol{\sigma}_M=\varepsilon\mathbf{E}\mathbf{E}-\frac{1}{2}\varepsilon(\mathbf{E}\bullet\mathbf{E})\mathbf{I}$, where **I** is the identity tensor and the electrostatic force acting on the ith particle is then obtained by integrating $\boldsymbol{\sigma}_M$ over its surface, i.e., $\mathbf{F}_{DEP}=\int_{\partial P_i(t)}\boldsymbol{\sigma}_M\cdot\mathbf{n}\,d\mathbf{s}$, where **n** is the unit outer normal on the surface of the ith particle.

Even though the applied electric field away from the interface is uniform, a particle within the interface experiences an electrostatic force normal to the interface due to a jump in dielectric constants across the interface. If the interface does not contain any particles, the electric field is normal to the interface and its intensity in the lower and

upper fluids is constant, while changing discontinuously at the interface according to the boundary condition stated above.

The vertical component of the electrostatic force in a DC field (or time averaged force in an AC field) acting on a particle can be written as:

$$F_{ev} = a^2 \varepsilon_0 \varepsilon_a \left(\frac{\varepsilon_L}{\varepsilon_a} - 1 \right) E^2 \, f_v\left(\frac{\varepsilon_L}{\varepsilon_a}, \frac{\varepsilon_p}{\varepsilon_a}, \theta_c, \frac{h_2}{a}\right) \tag{3.1}$$

Here a is the particle radius, $E = V_0/L$ is the average electric field strength away from the particle (or the RMS value of the electric field in an AC field), ε_p, ε_a and ε_L are the dielectric constants of the particle, the upper fluid and the lower fluid, respectively, and $\varepsilon_0 = 8.8542 \times 10^{-12}$ F/m is the permittivity of free space. L is the distance between the electrodes, V_0 is the voltage difference applied to the electrodes, and $f_v\left(\frac{\varepsilon_L}{\varepsilon_a}, \frac{\varepsilon_p}{\varepsilon_a}, \theta_c, \frac{h_2}{a}\right)$ is a dimensionless function of the included arguments (θ_c and h_2 being defined in Figure 3.2).

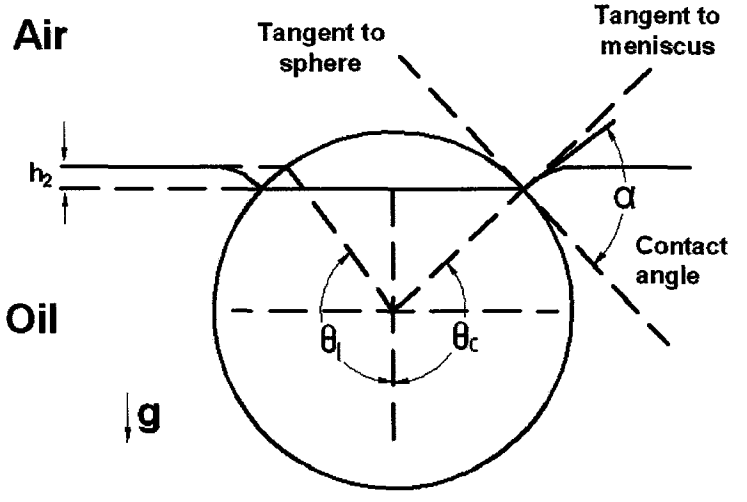

Figure 3.2 is a schematic of a heavier than liquid hydrophilic (wetting) sphere of radius a hanging on the contact line at θ_c.

The dipole-dipole interaction force between two dielectric spheres immersed in a fluid with the dielectric constant ε_a and subjected to a uniform electric field, in the point-dipole limit, is given by the following well-known expression in spherical coordinates:

$$\mathbf{F}_D(r,\theta) = f_0\left(\frac{a}{r}\right)^4\left(\left(3\cos^2\theta - 1\right)\mathbf{e}_r + \sin 2\theta\,\mathbf{e}_\theta\right) \tag{3.2}$$

where $f_0 = 12\pi\varepsilon_0\varepsilon_a a^2\beta^2E^2$ (E being the magnitude of the uniform electric field along the z-axis), θ denotes the angle between the z-axis and the vector $\mathbf{r}$ joining the centers of the two particles, $r=|\mathbf{r}|$, $\beta = \dfrac{\varepsilon_p - \varepsilon_a}{\varepsilon_p + 2\varepsilon_a}$ is the Clausius-Mossotti factor, and ε_p is the dielectric constant of the particle.

However, the above expression is not applicable to particles floating in a two-fluid interface between two fluids with different dielectric constants, as the fluid's dielectric constant changes discontinuously across the interface. The modified expression for the lateral interaction force can be written as

$$\mathrm{F}_D(r) = \varepsilon_0\varepsilon_a\left(\frac{\varepsilon_L}{\varepsilon_a}+1\right)a^2E^2\left(\frac{a}{r}\right)^4 f_D\left(\frac{\varepsilon_L}{\varepsilon_a},\frac{\varepsilon_p}{\varepsilon_a},\theta_c,\frac{h_2}{a}\right) \tag{3.3}$$

where f_D is a dimensionless function of the included arguments, with the force depending upon the sixth power of the particle radius a and on the fourth power of the inverse of the distance between the particles

The repulsive interaction energy W_D between two particles can be obtained by integrating (Equation 3.3) with respect to r, which gives

$$W_D(r) = -\frac{1}{3}\varepsilon_0\varepsilon_a\left(\frac{\varepsilon_L}{\varepsilon_a}+1\right)a^2E^2\left(\frac{a^4}{r^3}\right)f_D\left(\frac{\varepsilon_L}{\varepsilon_a},\frac{\varepsilon_p}{\varepsilon_a},\theta_c,\frac{h_2}{a}\right) \tag{3.4}$$

Now, assume that $\varepsilon_a = 2.0$, $\varepsilon_L = 4.0$, $E = 3\text{x}10^6$ volt/m, $f_D = 3.1$, and $r = 2a$. For these parameter values, the interaction energy is shown as a function of the particle radius in Figure 3.3. For $a = 1$ μm, $W_D(r) = \sim 1.67\text{x}10^4\ kT$ and for $a = 100$ nm, $W_D(r) = \sim 16.7\ kT$, where k is the Boltzman constant and T is the temperature, indicating that the repulsive electrostatic force is larger than the random Brownian force acting on the particles. This shows that the electrostatic repulsive force (Equation 3.3) can be used to manipulate nanoparticles within a two-fluid interface.

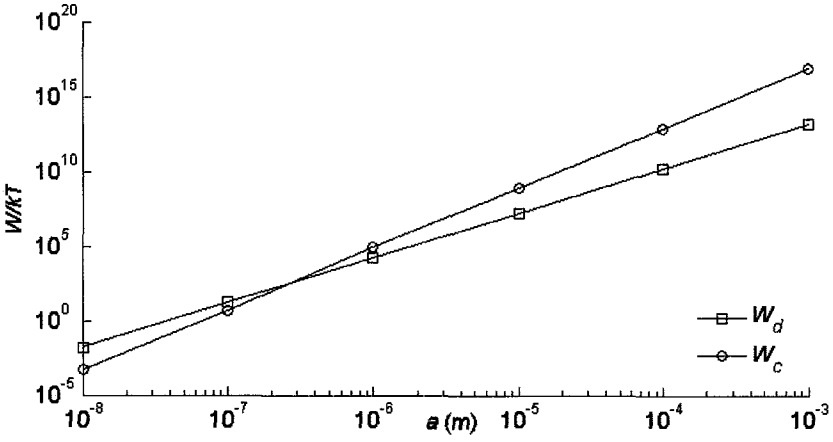

Figure 3.3 Energies of capillary attraction (W_c) and dipole-dipole repulsion (W_d).

3.2.1 Vertical Force Balance in Equilibrium

Next consider the vertical force balance for a spherical particle floating within the interface between two immiscible fluids. The buoyant weight F_b of the particle is balanced by the capillary force F_c and the electrostatic force F_{ev}, such as

$$F_c + F_{ev} + F_b = 0. \tag{3.5}$$

The buoyant weight is given by $F_b = -g\rho_L a^3 f_b(\frac{\rho_a}{\rho_L}, \frac{\rho_p}{\rho_L}, \theta_c, \frac{h_2}{a})$, where g is the acceleration due to gravity, ρ_p is the particle density, ρ_a and ρ_L are the densities of the upper and lower fluids, θ_c and h_2 are defined in Figure 3.2, and f_b is a function of $\frac{\rho_a}{\rho_L}$, $\frac{\rho_p}{\rho_L}$, θ_c and $\frac{h_2}{a}$. It can be deduced from Figure 3.2 that the capillary force F_c takes the expression $F_c = -2\pi\gamma a \sin\theta_c \sin(\theta_c + \alpha)$, where α is the contact angle. Therefore, (Equation 3.5) can be rewritten as

$$F_c = -2\pi\gamma a \sin\theta_c \sin(\theta_c + \alpha) =$$

$$g\rho_L a^3 f_b(\frac{\rho_a}{\rho_L}, \frac{\rho_p}{\rho_L}, \theta_c, \frac{h_2}{a}) - a^2 \varepsilon_0 \varepsilon_a \left(\frac{\varepsilon_L}{\varepsilon_a} - 1\right) E^2 f_v(\frac{\varepsilon_a}{\varepsilon_L}, \frac{\varepsilon_p}{\varepsilon_L}, \theta_c, \frac{h_2}{a}) \qquad (3.6)$$

In dimensionless form, the previous equation has the form

$$2\pi \sin\theta_c \sin(\theta_c + \alpha) = -\mathrm{B}\ f_b(\frac{\rho_a}{\rho_L}, \frac{\rho_p}{\rho_L}, \theta_c, \frac{h_2}{a}) + \mathrm{W}_E \left(\frac{\varepsilon_L}{\varepsilon_a} - 1\right) f_v(\frac{\varepsilon_a}{\varepsilon_L}, \frac{\varepsilon_p}{\varepsilon_L}, \theta_c, \frac{h_2}{a}) \qquad (3.6')$$

Here $\mathrm{B} = \rho_L a^2 g/\gamma$ is the Bond number and $\mathrm{W}_E = \varepsilon_0 \varepsilon_a \frac{aE^2}{\gamma}$ is the electric Weber number.

As the particle radius a approaches zero, the Bond number $\mathrm{B} = \rho_L a^2 g/\gamma \to 0$. In this limit, in the absence of an electrostatic force, the right hand side of equation (3.6') is zero and thus $\sin(\alpha + \theta_C) \approx 0$ or $\theta_C \approx \pi - \alpha$ (see Figure 3.2). This means that a small particle floats so that the interfacial deformation is insignificant. Hence, the lateral capillary force, which arises from the interfacial deformation, in this limit, is also insignificant. As noted earlier, for particles floating on water, this limit is reached when the particles radius is approximately 10 μm.

Another important limit is the case for which the Bond number approaches zero, but W_E does not. This situation arises, for instance, for small particles when the magnitude of the electric field is sufficiently large. The equilibrium position of a particle within the interface in this case is determined by the balance of the interfacial and electrostatic forces alone. The interface is then deformed by the particle, and so the lateral (electric field induced) capillary forces are present and can cause particles within the interface to cluster.

3.2.2 Interfacial Deformation and Lateral Capillary Force

In equilibrium, the external vertical force acting on a particle is balanced by the vertical component of the capillary force which, as noted earlier, arises because of the deformation of the interface. The profile of the deformed interface around a particle can be obtained by integrating Laplace's equation and using the boundary conditions that (i) the interface far away from the particle is flat and (ii) the angle between the interface and the horizontal at the particle surface is known in terms of the total external force acting on the particle. It can be shown that the interface height $\eta(r)$ at a distance r from a spherical particle is given by:

$$\eta(r) = a \sin(\theta_c + \alpha)\, K_0(qr) \tag{3.7}$$

where $K_0(qr)$ is the modified Bessel function of zeroth order and $q = \sqrt{\frac{(\rho_L - \rho_a)g}{\gamma}}$. In obtaining the above expression the influence of the electrostatic stress on the interface, including the stress that arises due to the presence of the particle has been ignored, and it is assumed that the interfacial deformation is small.

Now consider a second particle at a distance r from the first particle. The height of the second particle is lowered because of the interfacial deformation caused by the first particle, and thus the work done by the electrostatic force and gravity (buoyant weight) is

$$W_c = -\eta(r)\,(F_{ev} + F_b)\,. \tag{3.8}$$

Notice that the electrostatic force is due to a field that is external to the fluid-particle system, as is the gravitational field, and therefore the work done by both fields is treated in a similar manner. In this analysis, work done by the electrostatic stress that acts on the two-fluid interface will be ignored. In addition, this analysis of the behavior of two particles does not account for the multi body interactions (which could be accounted for by summing the forces exerted by all other particles on one given particle). Using Equations (3.6) and (3.7), Equation (3.8) can be rewritten as

$$W_c = -\frac{(F_{ev} + F_b)^2}{2\pi\gamma} K_0(qr) = -\left(-\varepsilon_0\varepsilon_a\left(\frac{\varepsilon_L}{\varepsilon_a} - 1\right)a^2E^2 f_v + \frac{4}{3}\pi a^3 \rho_p g\, f_b\right)^2 \frac{1}{2\pi\gamma} K_0(qr) \tag{3.9}$$

Figure 3.3 illustrates energies of capillary attraction (W_c) and dipole-dipole repulsion (W_d), in kT units, plotted against the particle radius. For $W/(kT) > 1$, the capillary attraction and the dipole-dipole repulsion are stronger than the Brownian force for all particles sizes down to a radius of approximately 100 nm. The parameters are $\varepsilon_a = 2.0$, $\varepsilon_L = 4.0$, $E = 3\text{x}10^6$ volt/m, $f_v = 1$, $f_D = 1$, $\gamma = 0.01$, $\rho_a = 1$ kg/m^3, $\rho_L = 1000$, $\rho_p = 3000$ kg/m^3 and $r = 2a$.

In Figure 3.3, the interaction energy W_c due to the lateral capillary force is plotted as a function of the particle radius. The parameter values are $\varepsilon_a = 2.0$, $\varepsilon_L = 4.0$, $E = 3\text{x}10^6$ volt/m, $f_v = 1$, $\gamma = 0.01$, $\rho_a = 1$ kg/m^3, $\rho_L = 1000$, $\rho_p = 3000$ kg/m^3 and $r = 2a$. The

figure shows that for these parameter values, the interaction energy (Equation 3.9) is significant for nano sized particles.

The lateral capillary force between two particles is therefore given by

$$F_{lc} = -\frac{dW_c}{dr} = \left(-\varepsilon_0 \varepsilon_a \left(\frac{\varepsilon_L}{\varepsilon_a} - 1\right) a^2 E^2 f_v + \frac{4}{3}\pi a^3 \rho_p g f_b\right)^2 \frac{qK_1(qr)}{2\pi\gamma} \tag{3.10}$$

where $K_1(qr)$ is the modified Bessel function of first order. When the two particles are far away from each other, the above reduces to

$$F_{lc} = -\left(-\varepsilon_0 \varepsilon_a \left(\frac{\varepsilon_L}{\varepsilon_a} - 1\right) a^2 E^2 f_v + \frac{4}{3}\pi a^3 \rho_p g f_b\right)^2 \frac{1}{2\pi\gamma r} \tag{3.11}$$

Notice that the lateral capillary force depends on the net vertical force acting on the particle, which includes its buoyant weight and the vertical electrostatic force. The force varies as the fourth power of the applied electric field, and if the electrostatic force and the buoyant weight are in the same direction, the electric field enhances the lateral capillary forces among the particles.

However, the vertical electrostatic force may not be in the same direction as the buoyant weight, and if this is the case there is a critical value of the electric field strength for which the net vertical force acting on the particle is zero. The lateral capillary force among the particles under these conditions would also be zero; this suggests that the electric field can be used to decrease, or even eliminate, capillarity induced attraction among the particles. If the electric field strength is increased further, the particles move upward in the interface and the capillary forces arise again but the interface near the particles would be curved downwards. The capillary force can cause particles to interact with each other only when the associated interaction energy is greater than kT, and

therefore, when the net external vertical force acting on the particles is small the latter are not likely to cluster as their motion would be governed by thermal fluctuations.

The lateral electric for due to particle-particle interactions can be written as

$$F_{el}(r) = \varepsilon_0 \varepsilon_a \left(\frac{\varepsilon_L}{\varepsilon_a} + 1 \right) a^2 E^2 \left(\frac{a}{r} \right)^4 f_l \left(\frac{\varepsilon_L}{\varepsilon_a}, \frac{\varepsilon_p}{\varepsilon_a}, \theta_c, \frac{h_2}{a} \right) \tag{3.12}$$

where r is the distance between the particles and f_l is an O(1) dimensionless function of the included arguments. The lateral electric force is repulsive and causes particles to move away from each other.

3.3 Results

3.3.1 Spheres at a Liquid-Air Interface

An electric field is applied perpendicular to the interface (shown in Figure 3.1) which allows to manipulate the clustering of particles floating at an interface to form well-controlled, and even active monolayers (i.e., capable of changing in time) (see the schematic in Figure 3.4). The technique is capable of not only expanding an already assembled monolayer but also tuning the lattice spacing by changing the voltage as shown later in Figure 3.7. It is interesting to point out that the particle arrangements are very different before turning on the electric field (Figure 3.4a) and after turning on the electric field and decreasing it to zero (Figure 3.4c). As previously mentioned, defects are present in absence of an electric field. However, when the electric field is turned on and slowly decreased to zero (Figure 3.4c), the particles gain a well-ordered, triangular (hexagonal) lattice arrangement and maintain it as the lattice distance decreases until the particles touch each other. Therefore, the interstices in between the particles (i.e., the pores of the ultra-fine porous membrane) in this new state are also regular - the only

irregularities remaining being due to the variation in the size of the particles themselves. The same phenomenon is illustrated in Figures 3.5 and 3.6 for bigger (55 μm of radius) and smaller sized particles (12 μm of radius). In all cases, the new states display long-range order, which is highlighted in Figure 3.2c by drawing straight lines joining the particles centers; notice that the lines are oriented at an angle of 120° of one another, a value characteristic of a hexagonal lattice

The lateral capillary forces (Equation 3.11) dominate when the distance between the particles is larger than a critical value (these forces decay as r^{-1}). On the other hand, the repulsive forces due to the inter-particles electrostatic interactions decay relatively faster (Equation 3.12) with the distance between the particles (these forces decay as r^{-4}) [91-95]. Since the repulsive force decays faster than the attractive capillary force, there is an equilibrium distance at which the two curves intersect and the total lateral force acting on the particles is zero. The value of this equilibrium distance can be controlled by adjusting the electric field strength. Since the electric field intensity can be varied with time, the control can be exerted in a dynamic fashion to form dynamic monolayers with adaptable characteristics and properties.

The equilibrium separation between two particles is estimated as

$$\frac{r_{eq}}{2a}=\frac{1}{2}\left(\frac{2\pi\varepsilon_0\varepsilon_a\left(\frac{\varepsilon_L}{\varepsilon_a}+1\right)\gamma E^2 f_l}{a\left(-\varepsilon_0\varepsilon_a\left(\frac{\varepsilon_L}{\varepsilon_a}-1\right)E^2 f_v+\frac{4}{3}\pi a\rho_p g f_b\right)^2}\right)^{\frac{1}{3}} \quad \text{for } r_{eq}/(2a)>1. \tag{3.12}$$

Notice that $r_{eq}/(2a)$ decreases with increasing particle radius a. In addition, although the equation itself allows values $r_{eq}/(2a)<1$, those values are not physically possible and should therefore be excluded because once particles come in contact of one

another the distance between them cannot decrease any further. Also note that since for large particles the buoyant weight is much larger than the vertical electric force, as $r_{eq}/(2a)$ increases with increasing electric field strength as $E^{\frac{2}{3}}$. The attractive capillary forces for such particles are primarily generated by the interfacial deformation due to their buoyant weight. In the intermediate size range, $r_{eq}/(2a)$ varies as E^{β}, with β being between 2/3 and –2/3, and decreases with decreasing particle radius and increasing electric field strength. These results are in excellent agreement with our experimental data for particles of radius a = 37 μm (Figure 3.7). For submicron sized particles (a=1 μm or smaller) for which the buoyant weight is negligible, $r_{eq}/(2a)$ decreases as $E^{-2/3}$ with increasing electric field strength. This behavior will be checked experimentally in the future.

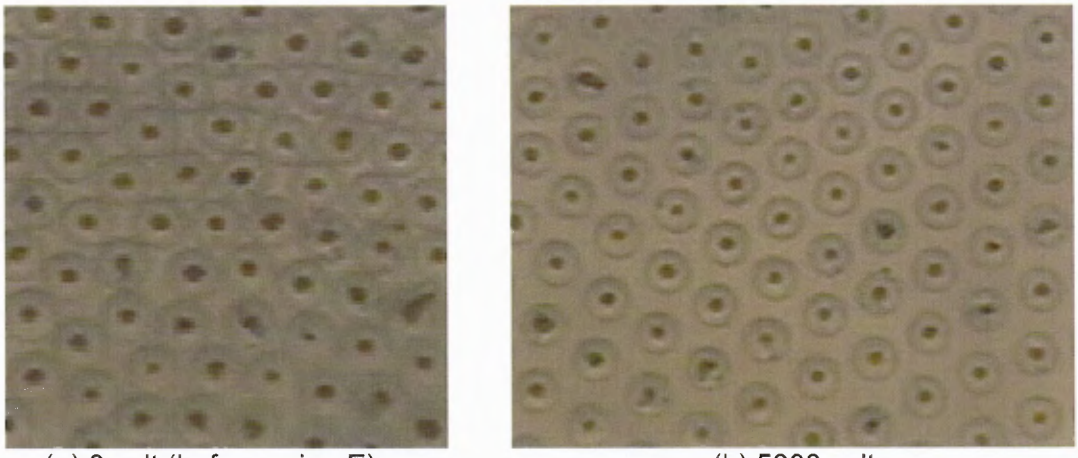

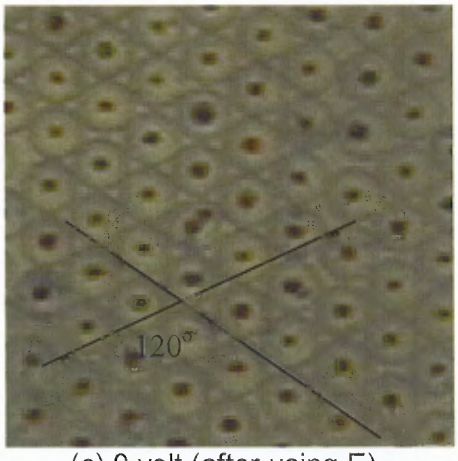

Figure 3.4 Assembly of glass particles floating at the air-oil interface. The average radius of particles is 37 μm. (a) Particles self-assemble under the action of the lateral capillary forces alone. The lattice is approximately triangular, but lacks long range order and contains many defects. (b) When a voltage V=5000 volts is applied, particles move away from each other and form a defect-free triangular lattice in which the distance between the particles is approximately 2.7 times the particle radius. (c) The applied voltage is slowly decreased to 0 volt. Particles touch each other in a well organized triangular (hexagonal) lattice and the lattice exhibits long range order which is indicated by the straight lines passing through their centers. Notice that the number of lattice defects is considerably reduced compared to that in (a) where the monolayer was assembled under the action of capillary forces alone.

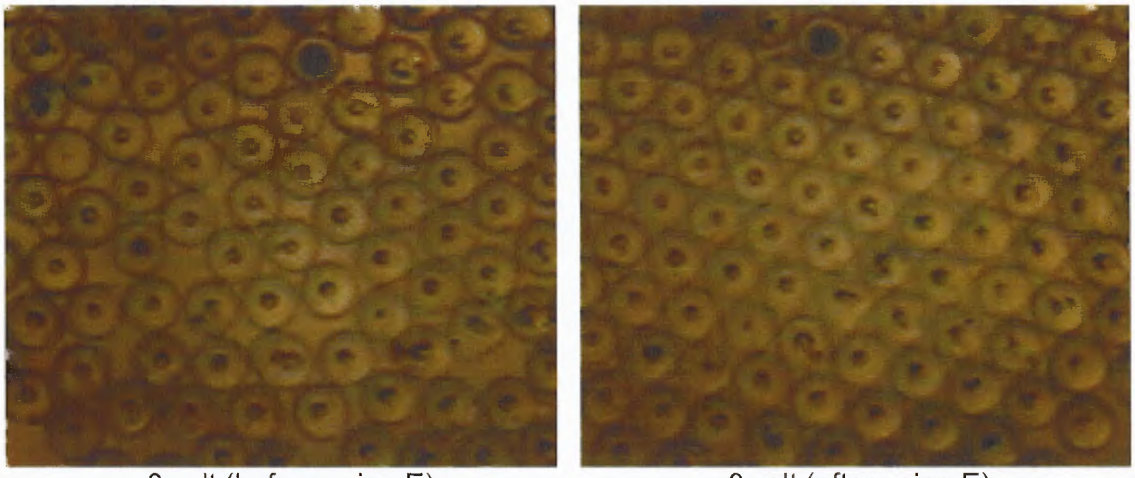

Figure 3.5 Assembled glass particles monolayers for particles with an average radius of 55 μm. The monolayer on the left was assembled under the action of capillary forces alone, and that on the right was formed by turning on the electric field and decreasing it to zero. Monolayer is highly organized as particles are mono-dispersed.

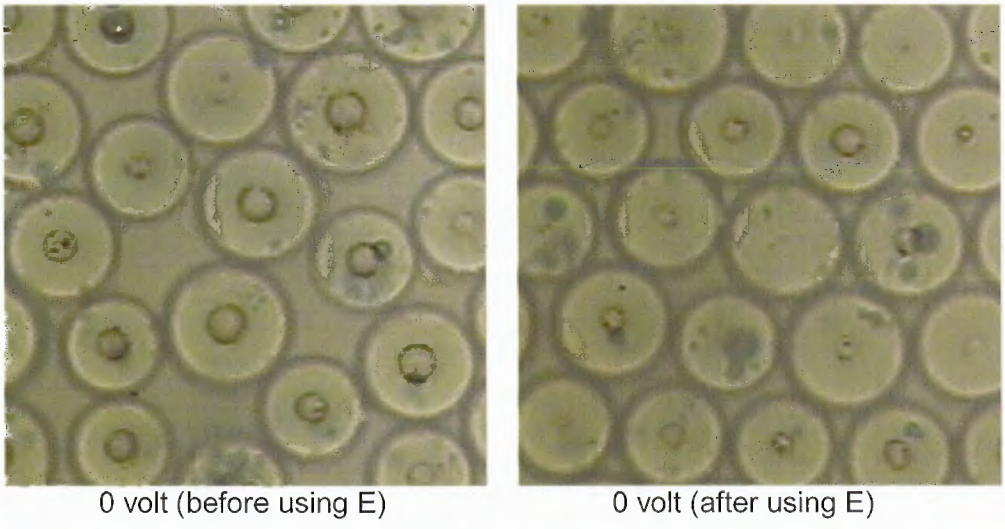

Figure 3.6 Assembled glass particles monolayers for particles with an average radius of 12 μm. The monolayer on the left was assembled under the action of capillary forces alone, and that on the right was formed by turning on the electric field and decreasing it to zero. Notice that the monolayer is relatively less organized than in Figure 3.4 as the size variation of the particles is quite significant.

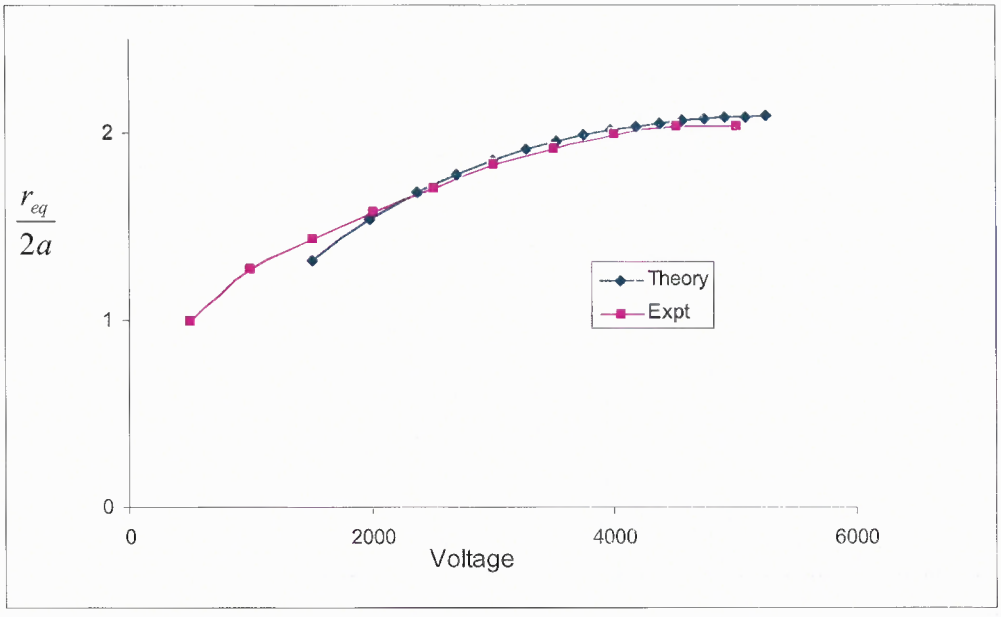

Figure 3.7 The equilibrium separation between two particles of radius a = 37 μm, as given by equation (3.12) for the experiment described in Figure 3.4, and the actual measured value are shown as functions of the voltage applied to the device. The electric force coefficients were numerically estimated (using the numerical technique of reference[7]) to be f_v=0.27, f_l=0.019, and f_b=0.64. From the experimental photographs we estimated θ_c=76.5 degrees. The agreement between the theory and the experimental data is very good, especially when the distance between the particles is more than 2.5a, considering that there are no adjustable parameters.

3.3.2 Spheres at a Liquid-Liquid Interface

In these experiments a hollow circular shaped device is used to self assemble particles on liquid-liquid interface. Diameter of the circular device is 137 mm and height is 12 mm. A mixture of corn oil (brand name Mazola) of density 0.924 g/cm^3 and castor oil of density 0.957 g/cm^3 was used with silicone oil of density 0.932 g/cm^3 to create an interface. The corn and castor oil are miscible and used in fixed proportion, so that the density of mixture is 0.942 g/cm^3. Silicon oil is immiscible with this mixture of corn and castor, and thus stays on top. 40 ml of each liquid is inserted in the circular device. The dielectric constant of corn oil is 2.87 and castor oil is 4.7. Silicone oil has a dielectric constant of

2.4. Approximately mono-dispersed soda lime glass particles of 24 microns were used. The density of glass particles is 1.3 g/cm^3.To remove any moisture that the particles may contain they were dried in oven for more than 3 hours at a temperature of 120^o C.

The electric field is generated by two electrodes, one electrode was mounted at the bottom of the circular device and a transparent electrode was placed at the top as shown in Figure 3.1. The electrodes are carefully mounted so that they are parallel to each other as well as to the liquid-liquid interface. AC voltage was used to energize the electrodes. The magnitude of voltage is adjusted to control the electric field strength in the device. A frequency of 100 hertz was used to eliminate any charge effect.

The experiments were started by simply sprinkling dried soda lime particles on the silicone oil. Soda lime particles sink in silicone oil and become trapped at the interface between two liquids. The particles experienced a vertical interfacial force that ensured that the particles would stay afloat at the interface. Figure 3.8 shows the top view of self-assembled particles for different values of electric field strength as well as the distributions before the electric field was switched on and after the electric field strength was reduced to zero. The self-assembled microstructure, however, contains many defects as the particles physically block each other from forming a perfect lattice. The problem is magnified, because particles used in this study were not perfectly mono dispersed or spherical. Fig 3.8a shows the self assembly of particles. Figure 3.8b shows that when 5000 volts are applied, the particles expand and arrange them in a nice uniform structure. The distance between the particles can be controlled with electric field strength. After the electric field strength is reduced below a critical value the particles again touch each

other. The lattice formed in Figure 3.8f by decreasing the voltage has a much nicer structure to it compared to the original lattice in Figure 3.8a.

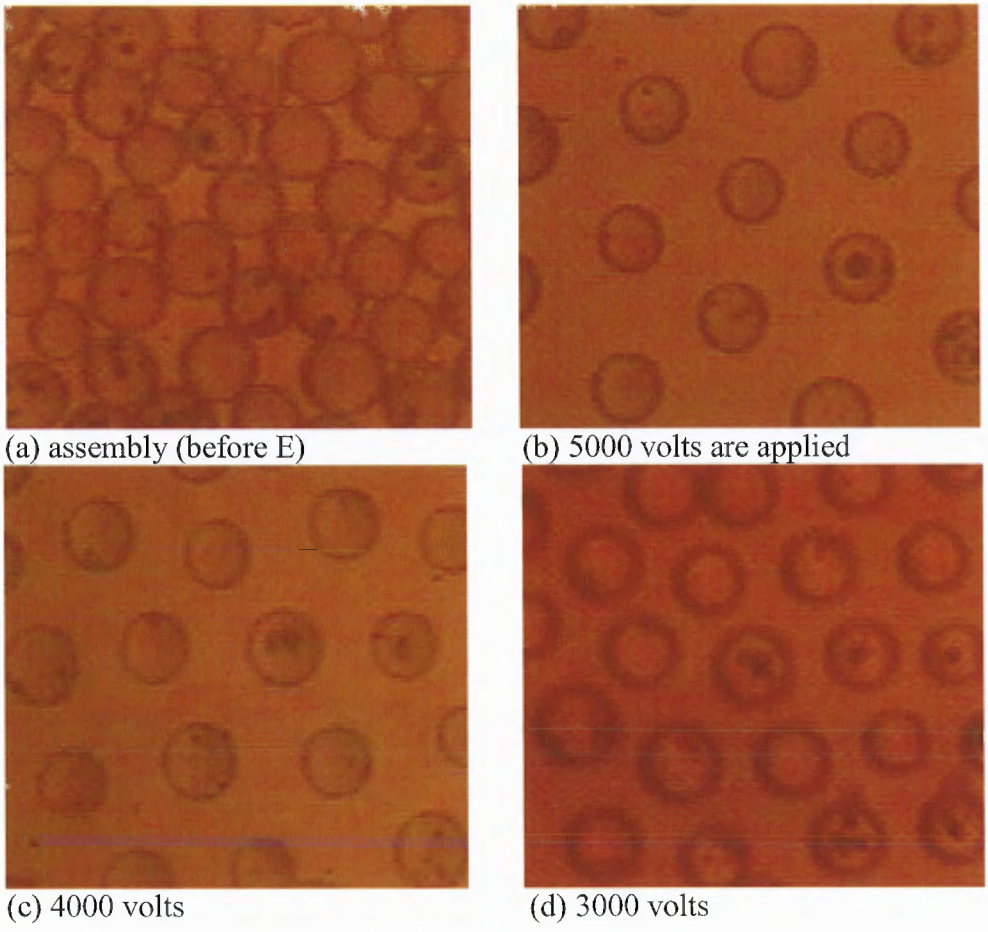

Figure 3.8. Self assembly of glass particles floating on the liquid-liquid interface. The diameter of particles is 24 μm. (a) Particles self assemble under the action of lateral capillary forces alone to form a triangular lattice. The lattice however contains many defects. (b) For V = 5000 volts, particles move away from each other and forma a highly organized lattice. (c-d) notice that as the voltage applied to the device is decreased, the distance between particles decreases.

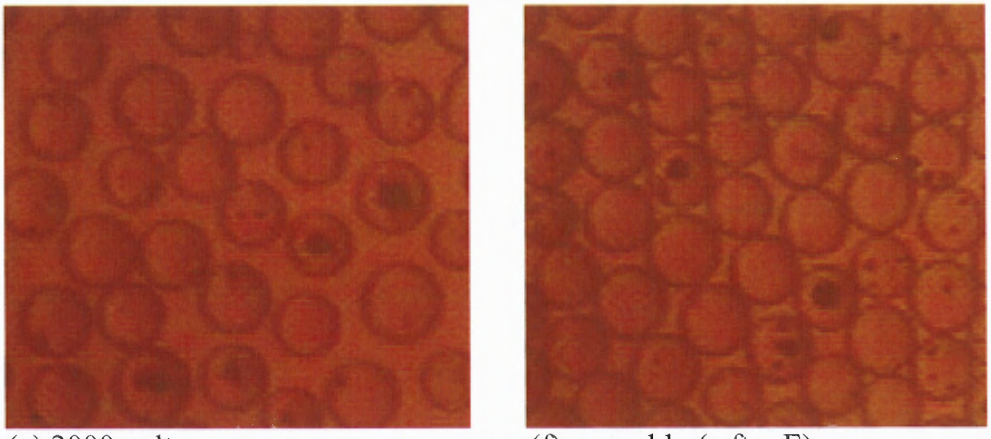

(e) 2000 volts (f) assembly (after E)

Figure 3.8. Self assembly of glass particles floating on the liquid-liquid interface. The diameter of particles is 24 μm. (e) Notice that as the voltage applied to the device is decreased, the distance between particles decreases. They begin to touch each other when the voltage is 2000 volts. (f) For V = 0 volts, particles touch each other in a relatively well organized triangular lattice. Notice that the number of lattice defects is considerably reduced compared to that in (a), where the monolayer was assembled under the action of capillary forces alone (continued).

3.4 Discussion

Experiments performed using glass particles, with radii between 2 and 80 μm, showed that such particles sprinkled at a fluid/fluid interface in an electric field normal to the interface are subjected to electrostatic forces which, when combined with capillary forces, lead the particles to self-assembly and thus lattices whose spacing can be adjusted by varying the electric field strength. Such self-assembly finds its root in the presence of a vertical electrostatic force, which, contrarily to the case of a neutral particle suspended in a bulk fluid in a uniform electric field, is non-zero. This force leads to a vertical capillary force and the deformation of the interface. An (attractive) capillary force is then also generated which, at equilibrium, balances the (repulsive) electrostatic particle-particle interaction force. The latter (including its scaling) is also different from the

electrostatic particle-particle interaction force known in the case of particles suspended in a bulk fluid.

The new particle assembling technique offers various advantages compared to capillarity-induced self-assembly based on the particles' buoyant weight alone. First, the technique is applicable to both large and small particles. Although we performed experiments using particles of size 2 μm or larger, we have also predicted (using force analysis) that the technique is also applicable to smaller, submicron sized, floating particles. In particular, it was shown that the lateral forces generated with the new technique can overcome Brownian forces present in the case of nanoparticles.

Second, the lattice spacing of the assembled monolayers can be adjusted by varying the intensity of the electric field, and thus the properties of a monolayer. Since the electric field can be varied in time, such properties can be changed dynamically.

Third, the assembled monolayers display long range order and, for particles of uniform size, shape and electrical properties, should be inherently low in defects or even defect-free. This order is achieved when particles are away from each other and thus do not block each other. For lattices in which particles touch each other, this is achieved by applying an electric field sufficiently large to bring particles away from each other into a an hexagonal pattern and then by decreasing the electric field to zero. The technique thus eliminates defects related to the initial positions of the particles but not those due to a possible non-uniformity in the particles' size, shape or electrical properties.

CHAPTER 4

ELECTRIC FIELD INDUCED ALIGNMENT AND SELF-ASSEMBLY OF RODS AND ELLIPSOIDSON FLUID-FLUID INTERFACES

4.1 Overview

In this section we show that an external electric field normal to a fluid-fluid interface can align rods floating on the interface as well as adjust the lattice spacing of a monolayer of rods. The method consists of sprinkling rods onto a fluid interface, with the fluids contained in a chamber subjected to a vertical electric field. The rods are attracted to one another and cluster under the action of capillary forces. A rod floating on the fluid interface experiences both a lateral force and a torque normal to the interface due to capillarity, and in the presence of an electric field, it is also subjected to an electric force and torque. While the electric force affects the rods' approach velocity, the torque aligns the rods parallel to each other. In the absence of an electric field, two rods that are initially more than one rod length away from each other come in contact so that they are either perpendicular or parallel to the line joining their centers, depending on their initial orientations. In the latter case, their ends are touching. These experiments show that in an electric field of sufficiently large strength, only the latter arrangement is stable. Experiments also show that in this case the electric field causes the rods of the monolayer to align parallel to one another and that the lattice spacing of a self-assembled monolayer of rods increases. The alignment, however, is not complete since the rods physically block one another and the direction of the alignment is arbitrary in the sense that it only depends on the initial orientations of the rods.

4.2 Results

Here are some experimental results for the clustering behavior of borosilicate glass rods floating on the surface of corn oil. Experiments were conducted in a device for which the distance between the electrodes is 8 mm and the cross-section is circular with the diameter of 48 mm (see Figure 3.1). The depth of the corn oil layer was 5 mm.

First result is for two rods floating on the surface of corn oil. The rods were made by cutting borosilicate fibers. The diameter of the rods is 39.8 μm, and the length of one rod is 255.2 μm and of the second 260 μm. The dielectric constant of corn oil is 2.87, its conductivity is 32.0 pSm^{-1} and its density is 0.922 g/cm^3. The density of the borosilicate glass rods is 2.5 g/cm^3 and their dielectric constant is 5.8. A variable frequency AC signal generator (BK Precision Model 4010A) was used along a high voltage amplifier (Trek Model 5/80) to apply a voltage to the electrodes at a frequency of 1 kHz. The applied voltage was 5000 V P/P (peak-to-peak). The motion of the rods was recorded using a digital color camera connected to a Nikon Metallurgical MEC600 microscope. The use of an AC electric field ensures that the motion of the rods is not due a coulomb force even if the rods acquire an electrostatic charge.

As already noted, in experiments, rods float such that their axes are parallel to the interface. In this configuration, the interfacial deformation at the contact line on the curved surfaces is different from that at the flat ends. Thus, as discussed below, the lateral attraction due to capillarity is not the same along all radial directions. Notice that although the contact-angle condition is satisfied at both the curved and flat surfaces, the direction of the normal at the two surfaces is different, and as a result, the interfacial

deformation at these surfaces is different. Experiments show that the attractive force in the direction perpendicular to the rod's axis is greater than in the parallel direction.

Three different initial configurations for the two rods were considered. In the first, the rods were parallel to one another and oriented perpendicular to the line joining their centers, in the second they were parallel to one another and parallel to the line joining their centers, and in the third they were perpendicular to each other. The initial distance between the rods was about 1.5 times their length. Next, discussion is about the behavior of the rods without and with the electric field. In the former case, the rods come together under the action of the force and torque due to capillarity, and in the latter case it is shown how this dynamics can be altered due to the additional presence of the electric force and torque.

4.2.1 Alignment of Two Rods in the Absence of an Electric Field

Experiments described below show that in the absence of electric field, the rods arrange themselves into one of the two stable configurations. In the first stable configuration, the rods are parallel to each other with their long sides touching, and in the second they are parallel to each other with their ends touching. The initial configuration of the rods determines which one of these stable configurations they evolve to. In the presence of an electric field of sufficiently large strength only the latter configuration is stable.

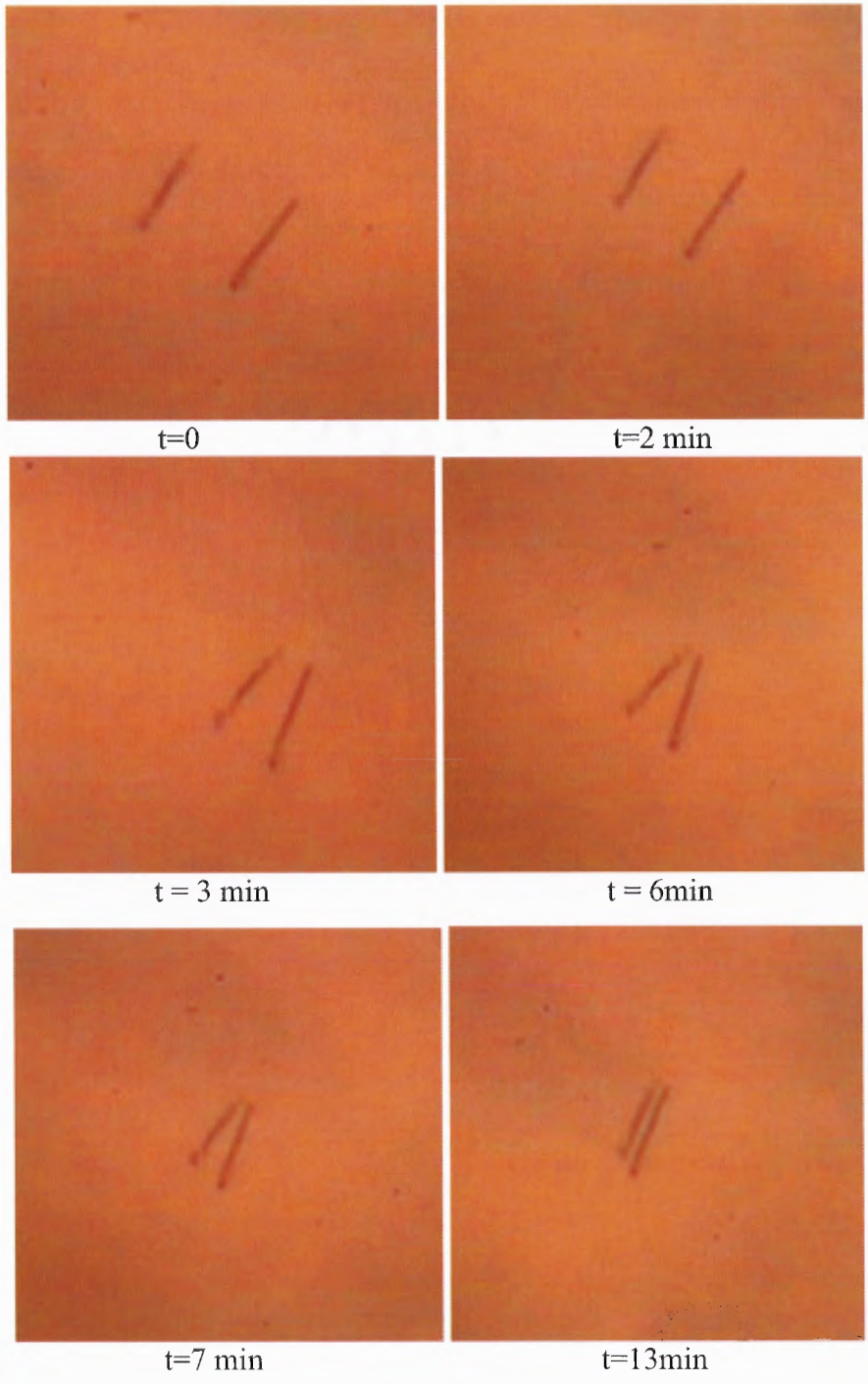

Figure 4.1 Transient positions of two rods floating on the surface of corn oil. The electric field is turned off. The rods diameter is 39.8 μm and the length of the left rod is 255.2 μm and the right rod is 260 μm. Initially, the rods are approximately parallel. However, as they come closer to one another under the action of the lateral capillary force, they rotate so that their upper ends come in contact at t=5 min 31sec. After coming in contact, the rods become approximately parallel again. Initial distance between rods is 240.5 μm at t =0 min.

Figure 4.1 shows the case in which the two rods are initially approximately parallel to each other and the line joining their centers is perpendicular to the rods. The rods maintain this approximate orientation as they come closer. However, when the distance between them is approximately one half of their length, they rotate so that the upper ends of the rods come closer faster. This indicates that the attractive capillary force between the upper ends is larger than between the lower ends, and thus the rods are subjected to a net torque causing them to rotate so that the upper ends come closer faster. This becomes even more clear in the photograph taken at t=5 min. The rods continue to come closer and rotate with the rate of approach increasing as the distance between them decreases. The upper ends of the rods touch at t=5 min 31sec, and the lower ends touch at t=13 min. In this final configuration, the rods are again parallel to each other. It is noteworthy that the final orientation of the rods is arbitrary in the sense that it only depends on their initial orientations.

Furthermore, notice that the upper ends of the rods are closer than the lower ends which again is the result of the larger attractive force between these ends. For the case described above, the attractive capillary force between the upper ends is larger than between the lower ends because for the rods used in our experiments the geometry of the end planes varies, i.e., the angle between the normal to the rods' end planes and the rod's axis varies. In this case, the geometry is such that the attractive capillary force between the upper ends is larger than between the lower ends. Also note that the torque due to this asymmetry becomes significant only when the distance between the rods is about one-half of their length causing them to rotate, and that when the distance between the rods is larger they remain approximately parallel to each other.

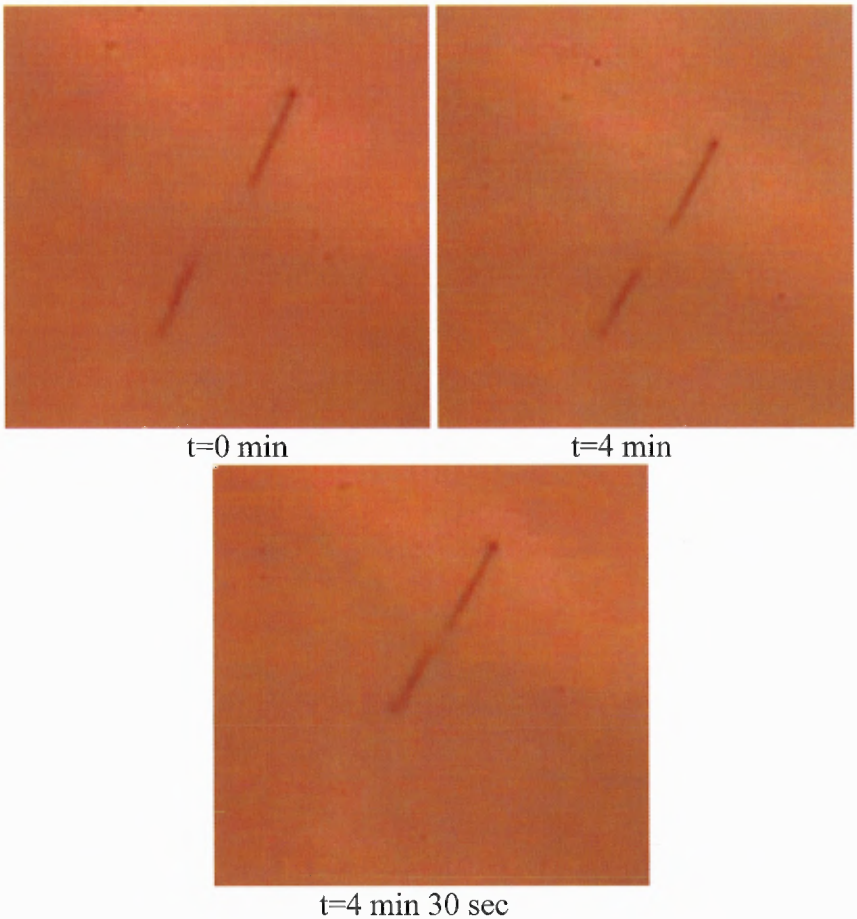

Figure 4.2 Attraction between two floating rods. The parameters are the same as in Figure 4.1. The electric field is still turned off. Initially, the rods are approximately parallel to the line joining their centers. As they come closer, they align so that they are approximately parallel to the line joining their centers. In their final equilibrium position, the rods maintain this orientation and touch each other at t=4 min 27sec. Initial distance between rods is 141 μm at t =0 min.

Next consider the case for which the two rods are initially approximately parallel to the line joining their centers (see Figure 4.2). As before, the rods come closer under the action of the attractive capillary force while approximately maintaining their initial orientations. The approach velocity increases with decreasing distance between the rods. The approach velocity in Figure 4.2 is smaller than for the case described in Figure 4.1. Notice that the elapsed time in Figure 4.2 is smaller because the initial separation between the rods was smaller. This indicates that the lateral capillary force for this

orientation of the rods is weaker. Notice that when the rods come in contact at t=270 s they are approximately parallel to the line joining their centers. This shows that this orientation of the rods is also stable and that if the rods are initially parallel to the line joining their centers they are likely to come together maintaining this orientation. The final orientation attained is stable.

In Figure 4.3, the case is presented where initially the rods are approximately perpendicular to each other. They rotate under the action of the capillary torque (acting normal to the interface) to become parallel to each other, and afterwards their behavior is similar to that for the case described in Figure 4.1 (not shown).

This shows that the preferred arrangement for the two rods (with a larger basin of attraction) is to align parallel to each other with their broad sides touching. Also, as noted above, the lateral capillary attraction between the rods for this configuration is greater as the approach velocity is larger. However, if the rods are initially approximately parallel to the line joining their centers, they maintain this orientation while coming closer. After joining, they remain parallel with their ends touching.

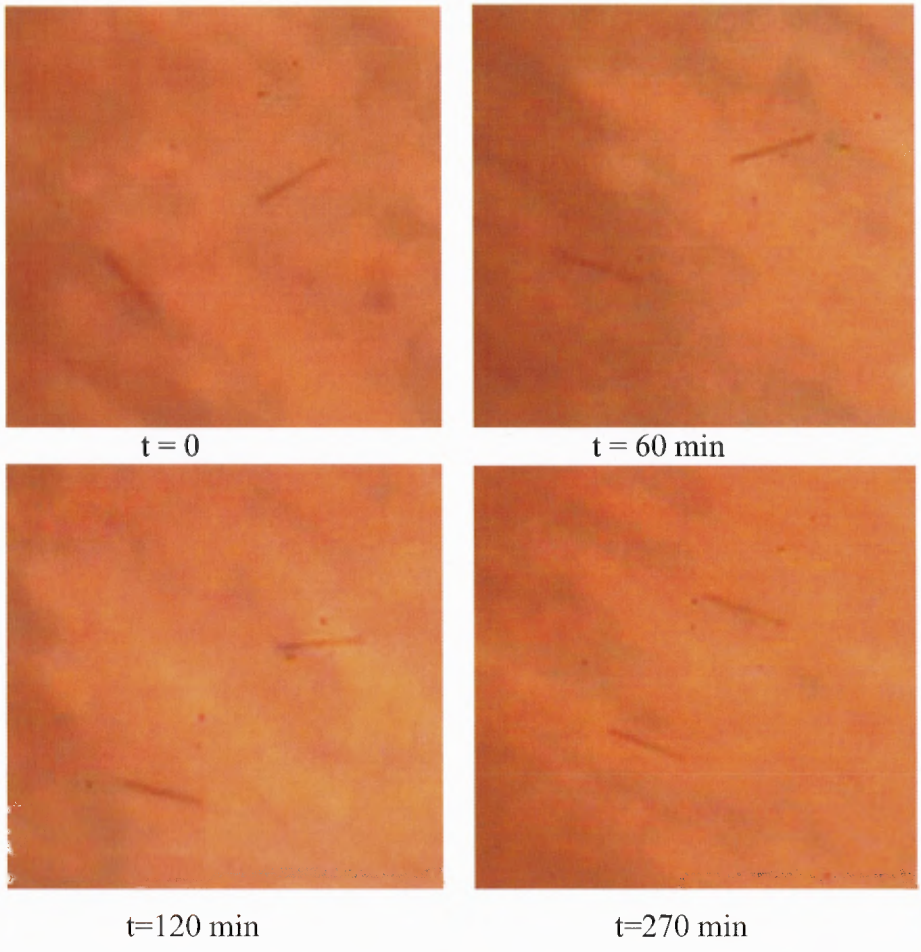

Figure 4.3 Attraction between two floating rods. The parameters are the same as in figure 2, except that initially the rods are approximately perpendicular to each other. The electric field is still turned off. The rods rotate to become approximately parallel to one another at t=270 min. Their motion after that point is similar to that in Figure 4.1, and is thus not shown in this Figure.

4.2.2 Alignment of Two Rods in the Presence of an Electric Field

Next, look at the influence of an electric field normal to the interface on the motion and orientation of the rods as they come closer under the combined action of the electric and capillary forces. In Figure 4.4, the initial configuration which is similar to that in Figure 4.2 is considered. The two rods are attracted to one another because of the attractive capillary forces, and their approach velocity increases with decreasing distance. As the rods come closer, they align along the line joining their centers. They touch at t=4 min 30

s. The approach velocity is approximately the same as for the case without electric field (see Figure 4.5). This indicates that for this orientation of the rods the repulsive dipole-dipole force between the rods is relatively small, and does not significantly influence the rods' motion.

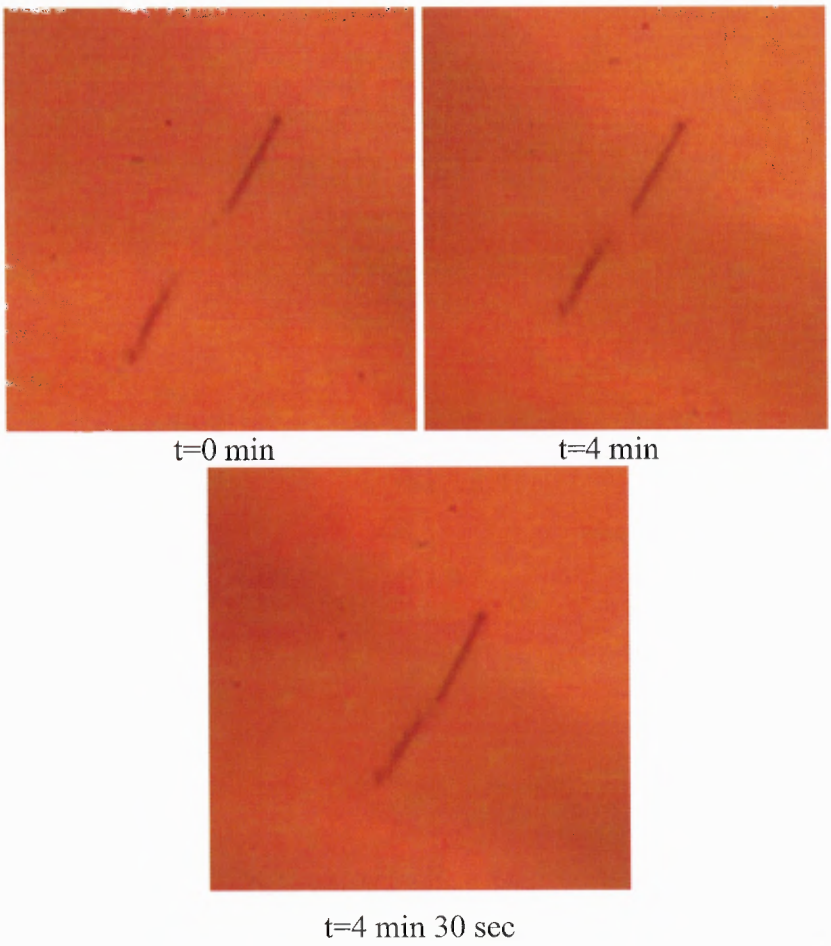

Figure 4.4 Attraction between two floating rods in the presence of the electric field. As the rods come closer, they align along the line joining their centers and touch at t =4min 30 sec. They maintain this orientation until touching.

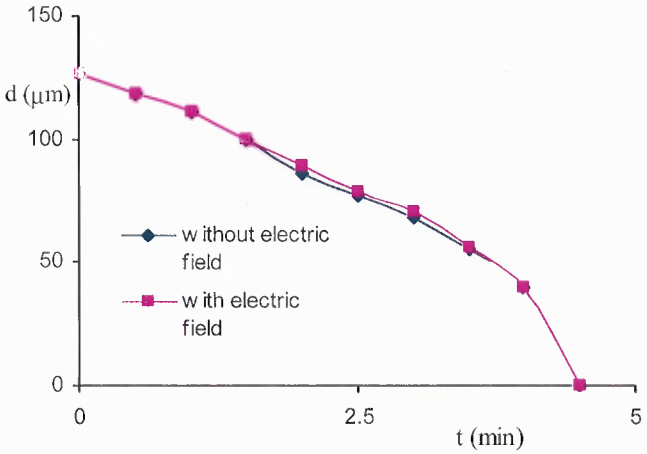

Figure 4.5. The distance between the rods' tips is plotted as a function of time for the experiments shown in Figures 4.2 and 4.4 (with and without electric field). The rods are aligned parallel to the line joining their centers. Notice that the trajectories for the cases with and without the electric field are approximately the same. The voltage applied to the device is 5000 V.

Figure 4.6 Attraction between two floating rods in presence of an electric field. The voltage applied is 5000 V. The other parameters are the same as in figure 4.1. Initially, the rods are approximately parallel, but when they are closer, they rotate so that the lower ends come in contact first at t =7min 40sec. After coming in contact, the rods rotate so that the angle between them increases with time. In the final configuration, the rods align parallel to the line joining their centers with their ends touching.

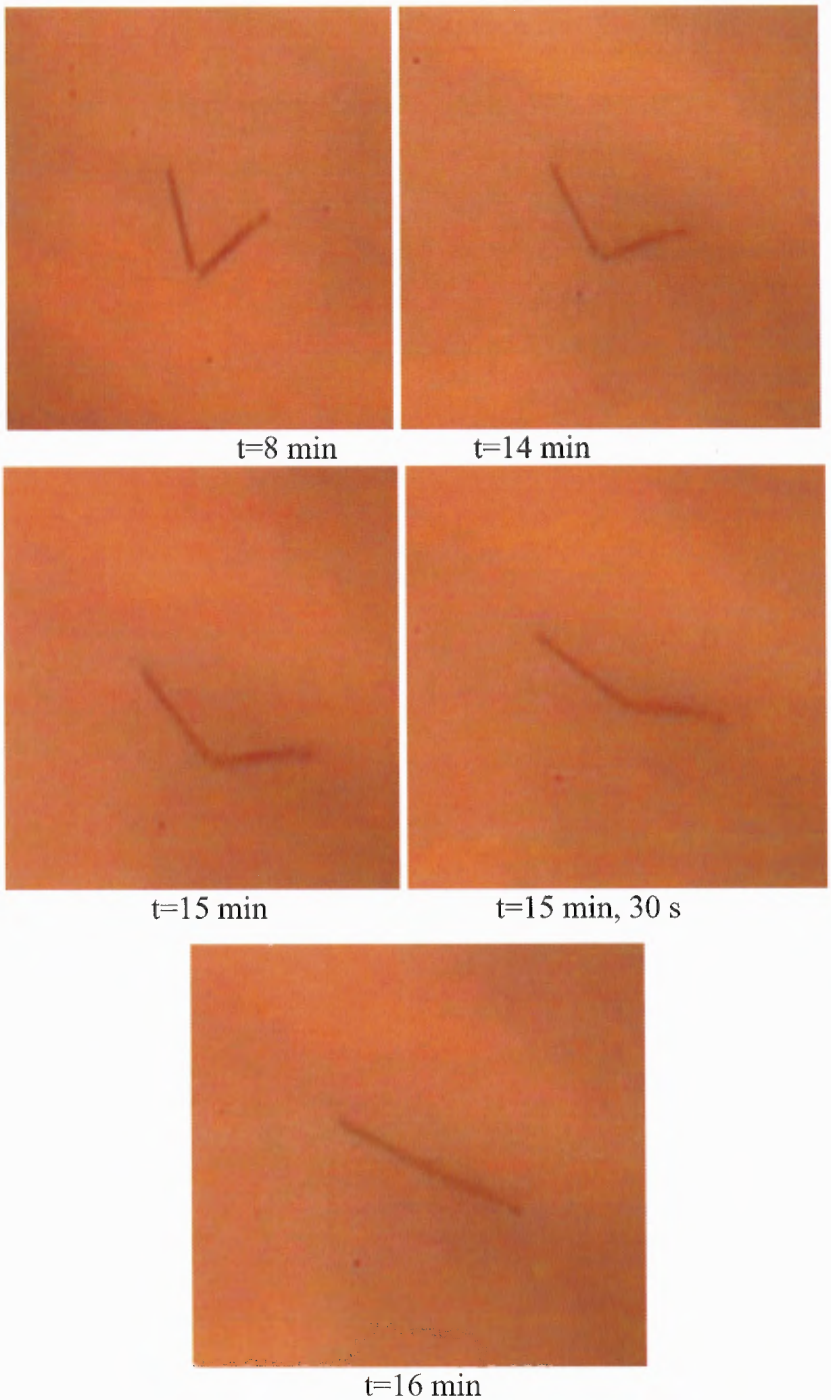

Figure 4.6 Attraction between two floating rods in presence of an electric field. The voltage applied is 5000 V. The other parameters are the same as in figure 4.1. Initially, the rods are approximately parallel, but when they are closer, they rotate so that the lower ends come in contact first at t =7min 40sec. After coming in contact, the rods rotate so that the angle between them increases with time. In the final configuration, the rods align parallel to the line joining their centers with their ends touching. (continued)

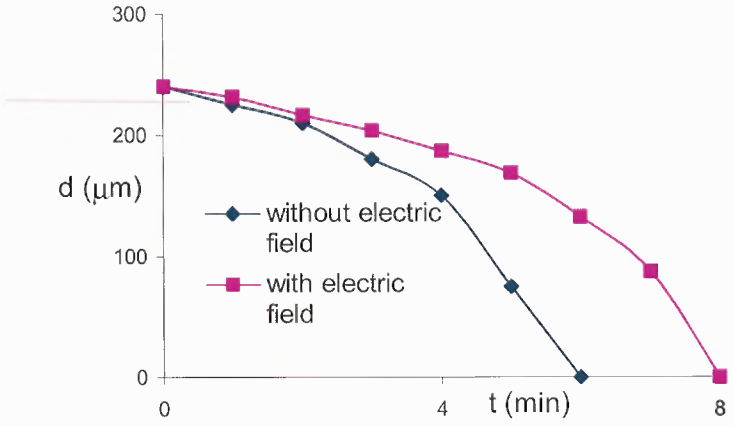

Figure 4.7 Distance between the rods' closest ends shown as a function of time in presence of an electric field, for the experiments shown in Figures 4.1 and 4.6. Initially, the rods are approximately perpendicular to the line joining their centers. The approach velocity is reduced in the presence of the electric field. The voltage applied is 5000 V.

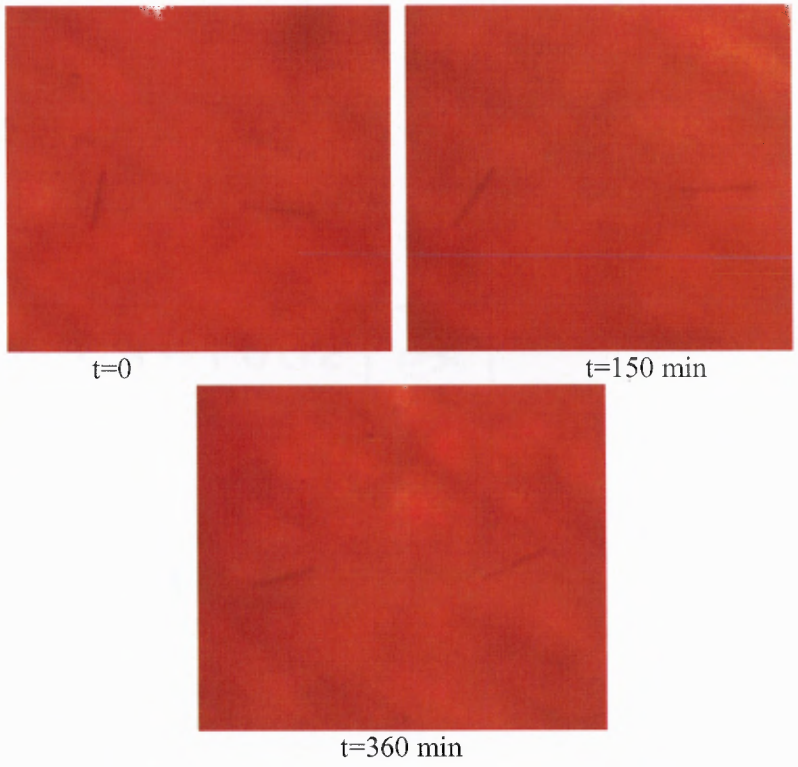

Figure 4.8. Attraction between two floating rods in presence of an electric field. The voltage applied is 5000 V. The remaining parameters are the same as in Figure 4.1. Initially, the rods are approximately perpendicular to each other. However, they rotate to become approximately parallel to the line joining their centers. The rods' behavior being the same as in Figure 4.2 after t=360 min, the dynamics after that time is not reproduced.

In Figure 4.6, the influence of the electric field on the attraction of two rods initially parallel and aligned approximately perpendicular to the line joining their centers is considered. The rods come closer as time increases, with an average approach velocity about 1.4 times smaller than without the electric field, the latter case being described in Figure 4.1. This decrease in the approach velocity is due to the repulsive dipole-dipole force between the rods. When the distance between the rods is greater than the rod length they remain approximately parallel, but when the distance is smaller than about one half of the rod length they rotate and the lower ends first come in contact. This was also the case in Figure 4.1 without the electric field (although the upper ends came in contact first). Once the rods touch, they begin to rotate so that the angle between them increases. This is the opposite of what took place in Figure 4.1, where the angle between the rods decreased. Here, in contrast the angle between the rods continues to increase until it becomes 180 degrees. The influence of the electric field is thus to align the rods so that in their equilibrium position they are parallel to the line joining their centers with their ends touching. It is postulated that this rotation is due to an electric torque which arises because of the dipole-dipole interaction between the rods. From symmetry, the electric torque must be zero when the rods are parallel or perpendicular to each other.

To further verify that the influence of the electric field is indeed to align the rods along a common line. Consider the initial configuration in which the two rods are approximately perpendicular to each other (see Figure 4.8). The rods rotate to become parallel to the line joining their centers, and afterwards their behavior is similar to that described in Figure 4.6 (not shown in Figure 4.8). Therefore, it is concluded that the preferred stable arrangement of two rods in the presence of electric field is to align

parallel to the line joining their centers, with their ends touching. Just to remind that the lateral capillary attraction between the rods makes them align perpendicular to the line joining their centers. This indicates that for the case shown in Figure 4.8 the torque due to the electric field was sufficiently strong to overcome the torque due to capillarity.

The influence of the electric field on two rods that are initially in contact, with their long sides touching is also considered. The dipole-dipole repulsion causes the rods to move away from each other to a distance of about one rod diameter. The rods stop moving when this separation is reached. In some cases, two ends of the rods separate while the other two ends remain joined, thus resulting in the rods forming a "V" shape (see Figure 4.9). The angle between the rods increases with increasing electric field strength and is larger for longer rods. After the electric field is turned off, the angle between the rods decreases and the rods return to their original equilibrium configuration. In some cases, the angle increases to 180 degrees and the rods become parallel. In these cases, even after the electric field is removed, the rods remain parallel to the line joining their centers with their ends touching.

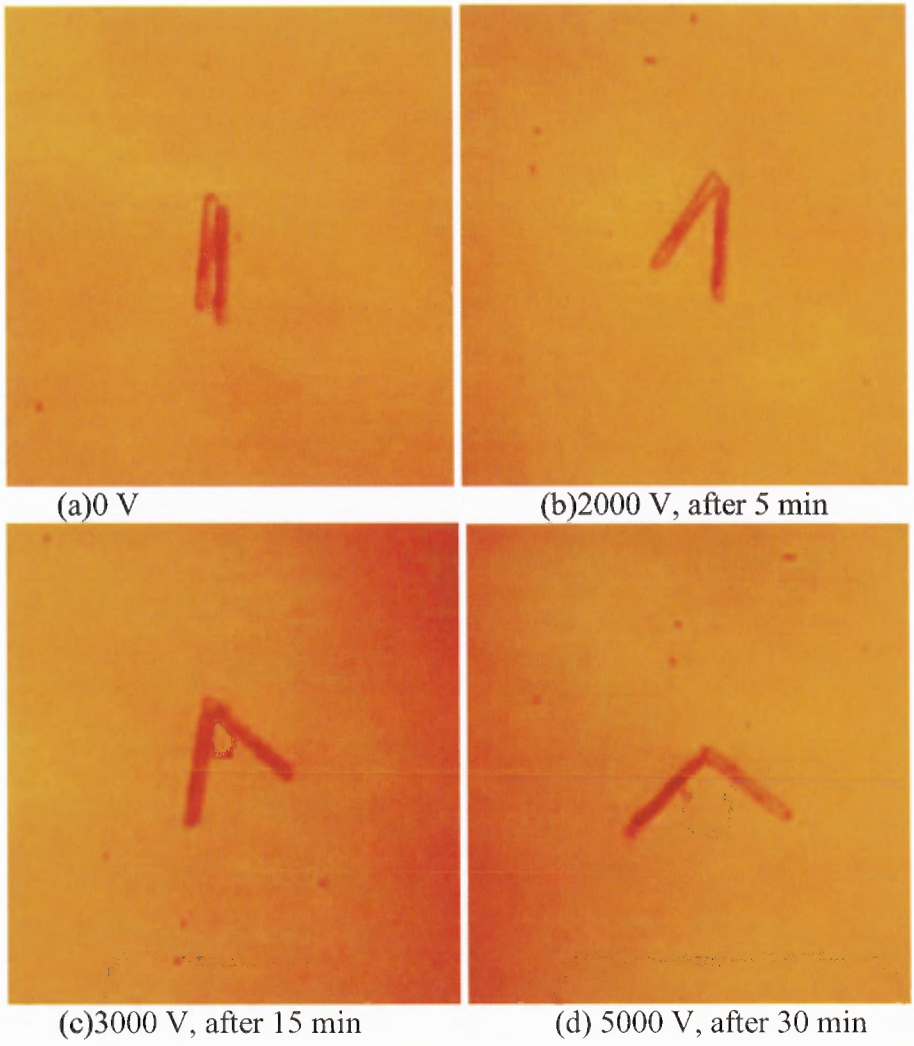

Figure 4.9 Repulsion between two rods with their long side touching when a voltage is applied to the device. The rods assume a shape which looks like the letter "V". The angle between the rods increases with increasing voltage.

4.2.3 Monolayers of Rods

Next consider the case in which many rods are sprinkled onto the corn oil surface in a random fashion. The length of the rods used in this experiment varied significantly. As shown in figure 4.10a, in the absence of electric field rods cluster under the action of capillary forces. The arrangement of rods appears to be random with no overall pattern. Nearby rods are, however, more likely to be parallel with their long sides touching. This

happens because as the rods come closer they physically block each other and thus prevent an overall pattern from developing.

The monolayer of rods is observed to expand when a voltage of 5000 V is applied to the device (see Figure 4.10). The electric field also causes the rods to align parallel to each other. Figure 4.10c shows a section of the monolayer in which rods form lines with their tips approximately touching. The alignment is not complete, as some individual rods seem trapped oriented in other directions. Furthermore, there are local regions in which the rods are aligned parallel to each other. The alignment of the rods, however, is not global as it may vary from region to region. It is postulated that this is due to both the presence of neighboring rods which can physically prevent a particular rod from aligning and the relatively large variation in the rods' lengths. Also, in these experiments the extent of alignment was found to improve with increasing electric field strength. The maximum voltage available was 5000 V.

(a) 0 V

(b) 5000 V, 5 min

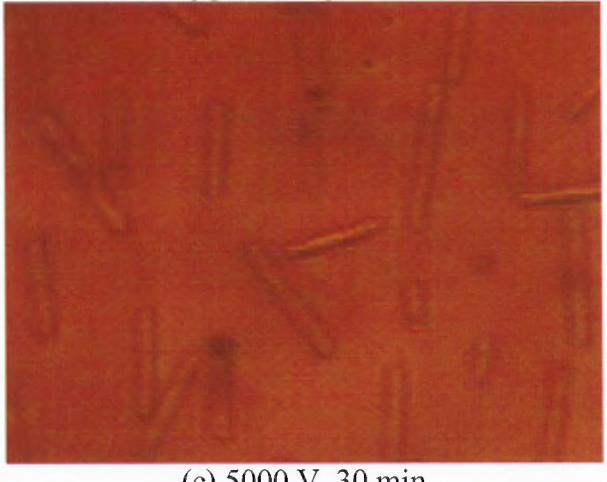

(c) 5000 V, 30 min

Figure 4.10 Self assembly of rods floating on the surface of corn oil. (a) In the absence of electric field the rods cluster together. (b) When a voltage of 5000 V is applied to the device, the distance between rods increases (c) After 30 minutes under the influence of the electric field the rods align approximately parallel to each other.

4.2.4 Alignment of Two Ellipsoids in the Absence of an Electric Field

Experiments described below show that in the absence of electric field, two ellipsoids arrange themselves in only one stable configuration. The stable configuration is when two major axes of ellipsoids are parallel and their long sides touch each other. Two initial configurations are considered when the major axes of two ellipsoids are parallel (shown in Figure 4.11) and when the major axes are inline (shown in Figure 4.12). The case where major axis are parallel, ellipsoids approach each other because of capillary forces and just before touching they rotate due to the hydrodynamic torque acting on them. The final orientation obtained is shown in Figure 4.11. In the other case, ellipsoids approach with their major axes inline, they start to rotate even before touching and after touching the angle between the two major axis start to reduce and they end up being parallel with long sides touching each other as shown in Figure 4.12.

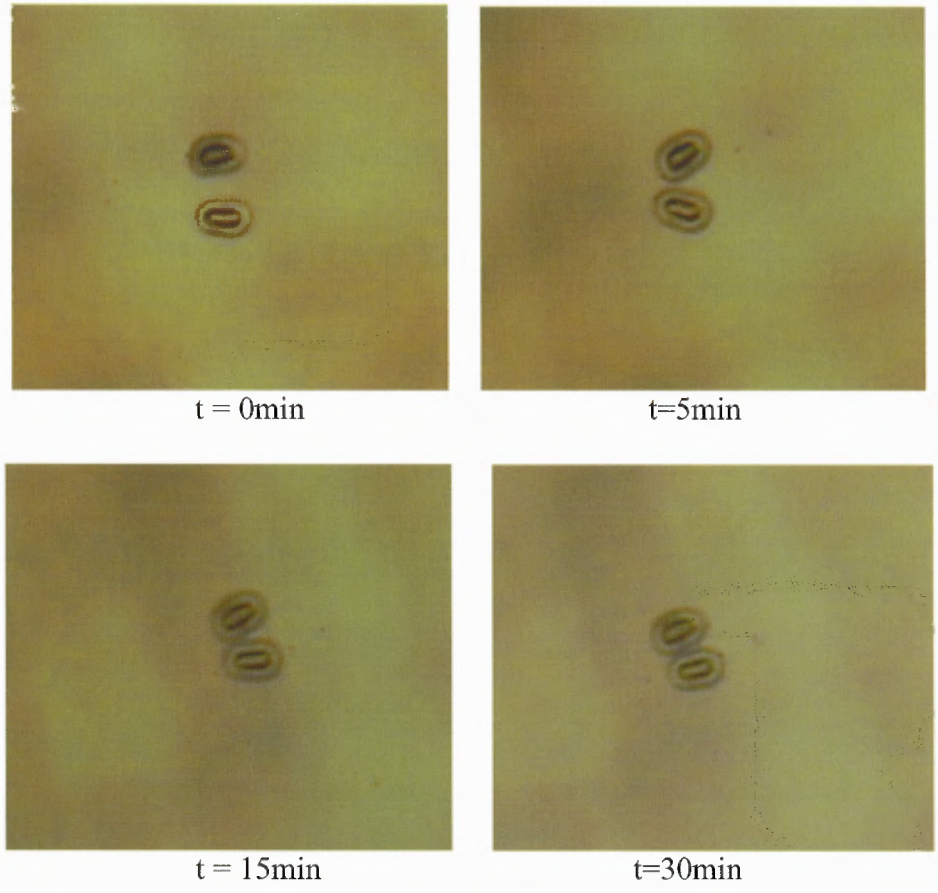

Figure 4.11 Transient positions of two ellipsoids floating on the surface of corn oil. The electric field is turned off. The top ellipsoid major and minor diameters are 150 μm and 80 μm respectively, and the bottom ellipsoid major and minor diameters are 145 μm and 75 μm. Initially, the ellipsoids are approximately parallel. However, as they come closer to one another under the action of the lateral capillary force, they rotate so that their ends come in contact at t=5 min. After coming in contact, the ellipsoids become approximately parallel again with their long sides touching.

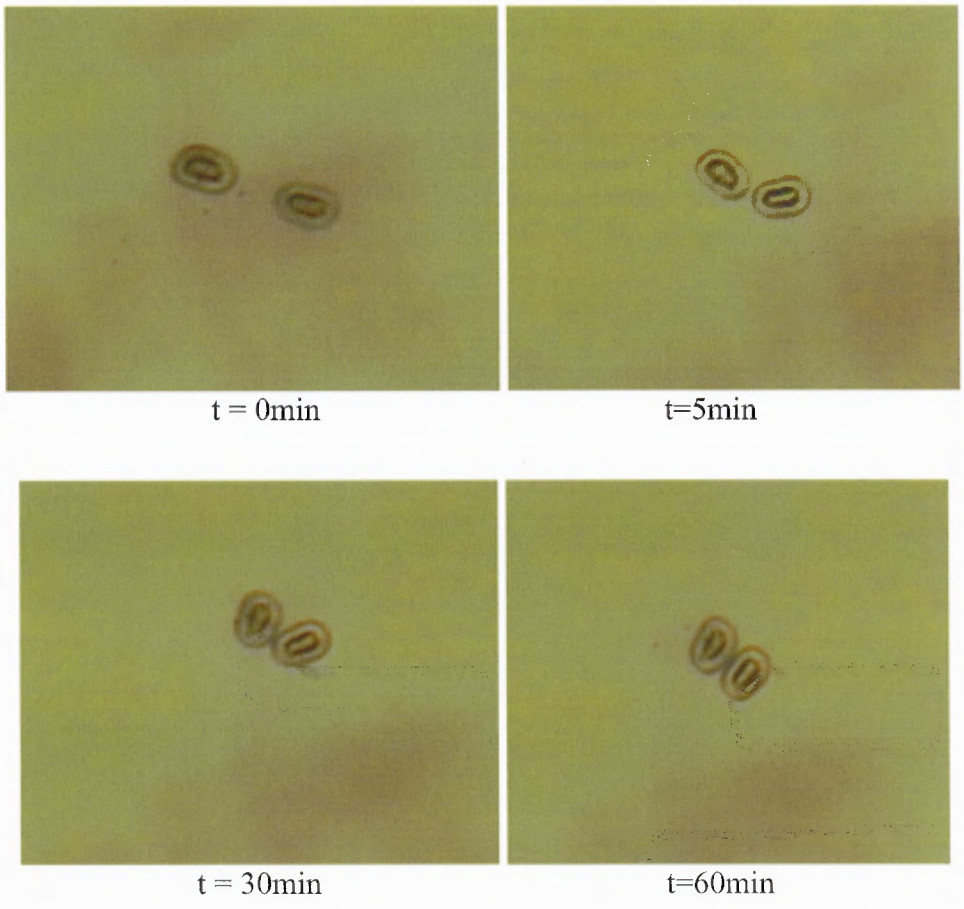

Figure 4.12 Transient positions of two ellipsoids floating on the surface of corn oil. The electric field is turned off. The top ellipsoid major and minor diameters are 150 μm and 80 μm respectively, and the bottom ellipsoid major and minor diameters are 145 μm and 75 μm. Initially, the ellipsoids are approximately inline with respect to their major axes. However, as they come closer to one another under the action of the lateral capillary force, they rotate so that their ends come in contact at t=5 min. After coming in contact, the ellipsoids become approximately parallel again with their long sides touching.

4.2.5 Alignment of Two Ellipsoids in the Presence of an Electric Field

Next, look at the influence of an electric field applied normal to the interface on the orientation of the ellipsoids as they come closer under the combined action of the electric and capillary forces. In Figure 4.13, the initial configuration which is similar to that in Figure 4.11 is considered. The two ellipsoids are attracted to one another because of the

attractive capillary forces. As the ellipsoids come closer, they align parallel with their major axes but the line joining their centers makes a small angle with their major axes.

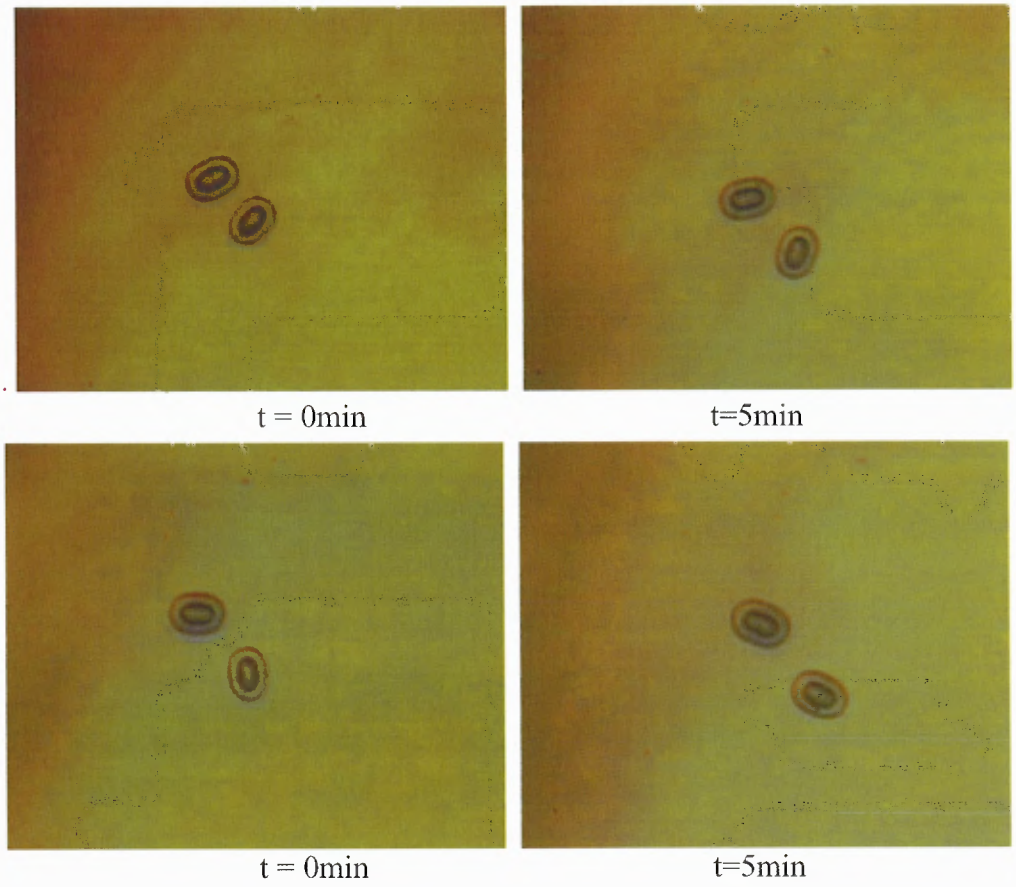

Figure 4.13 Attraction between two floating ellipsoids in presence of an electric field. The voltage applied is 3000 V. The other parameters are the same as in Figure 4.11. Initially, the ellipsoids are approximately parallel with respect to their major axes. The ellipsoids rotate so that the angle between the major axes increases with time. In the final configuration, the ellipsoids align parallel with their major axes but the line joining their centers makes a small angle with their major axes.

In Figure 4.14, the influence of the electric field on the attraction of two ellipsoids whose major axes are initially in-line is considered. The ellipsoids align parallel with their major axes but the line joining their centers makes a small angle with their major axes.

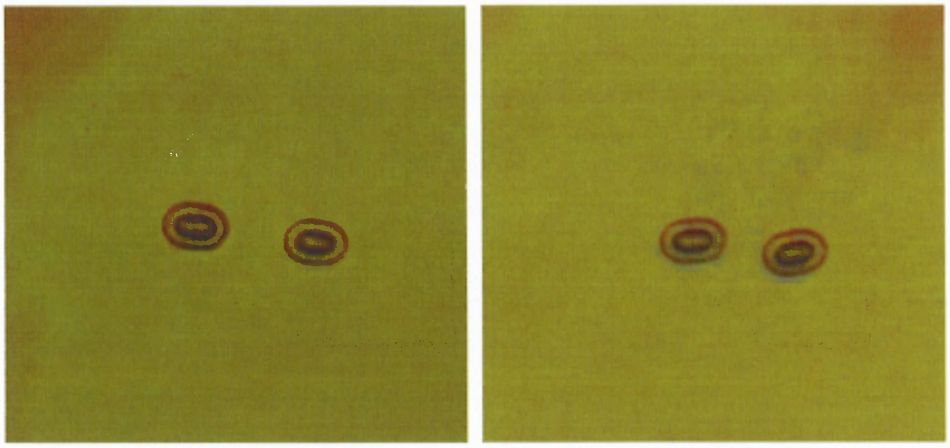

t = 0min t=30min

Figure 4.14 Attraction between two floating ellipsoids in presence of an electric field. The voltage applied is 3000 V. The other parameters are the same as in Figure 4.12. Initially, the ellipsoids are inline with respect to their major axes. In the final configuration, the ellipsoids align parallel with their major axes but the line joining their centers makes a small angle with their major axes.

4.2.6 Monolayers of Ellipsoids

Next consider the case in which many ellipsoids are sprinkled onto the corn oil surface in a random fashion. The ellipsoids have different sizes and there is some variation in their shapes too. As shown in Figure 4.15a, in the absence of electric field ellipsoids cluster under the action of capillary forces. The arrangement of ellipsoids appears to be random with no overall pattern. This happens because as the ellipsoids come closer they physically block each other and thus prevent an overall pattern from developing.

The monolayer of ellipsoids expands when a voltage of 5000 V is applied to the device (see Figure 4.15b). The electric field also causes the ellipsoids to align parallel to their major axes. Figure 4.10c shows the final picture when electric field is switched off. The alignment is not complete, as some individual ellipsoids seem trapped oriented in other directions. It is postulated that this is due to both the presence of neighboring

ellipsoids which can physically prevent a particular ellipsoid from aligning and the relatively large variation in the ellipsoids shapes and sizes.

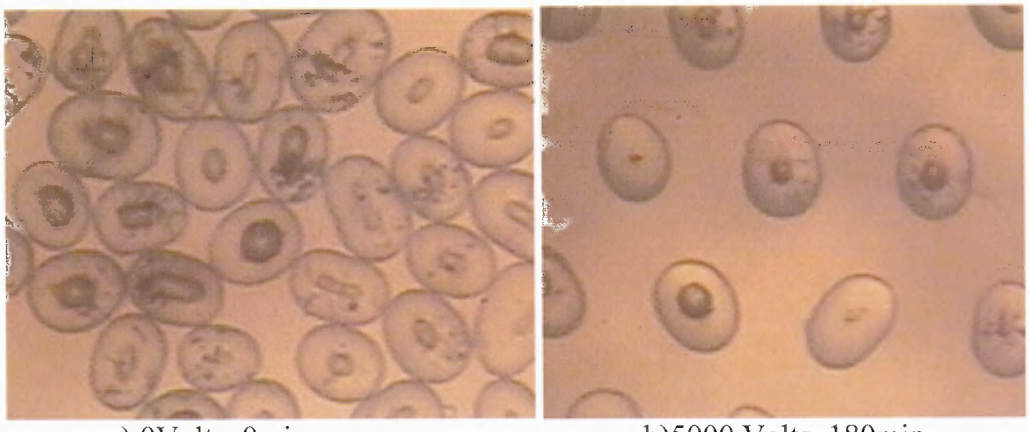

a) 0Volts, 0min b)5000 Volts, 180min

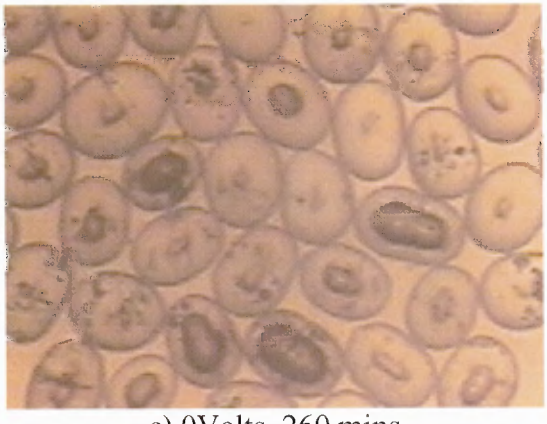

c) 0Volts, 260 mins

Figure 4.10 Self-assembly of rods floating on the surface of corn oil. (a) In the absence of electric field the rods cluster together. (b) When a voltage of 5000 V is applied to the device, the distance between rods increases (c) After 30 minutes under the influence of the electric field the rods align approximately parallel to each other.

4.3 Discussion

Experiments show that two or more glass rods floating on the surface of corn oil cluster under the action of lateral capillary forces that arise because of the deformation of the interface. Since rods are also subjected to a torque due to capillarity, they come together either with their long sides touching or with their ends touching. In both cases they are

parallel to each other. The alignment of rods in a monolayer assembled under the action of capillary forces appears to be random as the rods physically block each other and prevent any pattern from developing.

In the presence of an electric field of sufficiently large magnitude, two rods released about one and half rod lengths away from each other arrange themselves to form a single line, i.e., they become parallel to the line joining their centers and come in contact so that their ends touch. This equilibrium arrangement is independent of their initial orientation. The electric field causes a rod on the interface to experience an electrostatic force normal to the interface. In addition, in an electric field the rods become polarized and interact with each other via dipole-dipole interactions. This results in a repulsive force and a torque. Furthermore, although the electric field causes rods to align parallel to each other, the direction of the alignment is not determined by the electric field which is normal to the interface. In experiments, the final direction of alignment depends on the rods' initial orientations.

It is also shown that a monolayer of rods can be expanded and its rods aligned approximately parallel to each other by applying an electric field normal to the interface. The distance between the rods is determined by the balance of the attractive capillary forces and the repulsive dipole-dipole forces. It is also shown that the lattice spacing of a self-assembled monolayer of rods can be increased by applying an electric field. The alignment, however, is not complete since the rods physically block each other.

The same analysis is done for ellipsoids. For the case of two ellipsoids, without the presence of electric field, it is demonstrated that ellipsoids only achieve one stable configurations with their major axes parallel and their larger sides touching. When

electric field is applied, the stable orientation is that their major axes are parallel but the line joining their centers makes a small angle with their major axes.

It is also shown that a monolayer of ellipsoids can be expanded and major axes of ellipsoids align approximately parallel to each other when an electric field normal to the interface is present. The distance between the ellipsoids is determined by the balance of the attractive capillary forces and the repulsive dipole-dipole forces. The alignment, however, is not complete since the ellipsoids physically block each other and ellipsoids vary in size and shape.

CHAPTER 5

SELF ASSEMBLY OF PRISMATIC PARTICLES

5.1 Overview

It is worth noting that the deformed interface around an isolated spherical particle is symmetric about the vertical passing through its center, and thus the lateral capillary force that arises due to this deformation is independent of the radial direction. The deformed interface around prismatic and non spherical particles, however, is not symmetric, and consequently their clustering behavior is more complex.

In general, for non-spherical and prismatic particles deformed interface is such that the interface slope at the contact line on the particle's surface varies, as the direction of the normal to the surface varies. In fact, on a part of the contact line the slope of the interface can be in the upward direction, and for the remaining part it can be in the downward direction. Notice that the slope of the interface determines the direction of the capillary force which acts on the particle. Thus, the magnitude of the vertical component of capillary force varies along the contact line, and its direction on a portion of the contact can be in the downward direction. As a result, although the total vertical capillary force is still equal to the buoyant weight, the contribution of some sections of the contact line to the vertical capillary force can be negative and for some positive.

The above implies that two particles can attract or repel depending on the interface deformation between them, i.e., if both particles cause upward or downward interface deformation of the interface, they attract; otherwise they repel. Depending on the form of the asymmetric deformation around them, such particles can assemble into several different periodic arrangements, e.g., hexagonal or cubic. In addition, rods and

prismatic particles experience a torque normal to the interface that causes them to rotate making them align in certain preferred orientations.

5.2 Results

Figure 5.1 shows that a cubical particle floats such that the contact line is pinned at its top sharp edges. The floating behavior of prismatic particles is therefore different from that of a spherical particle (shown in Figure 3.2) because in case of spherical particle, the contact line moves to meet the contact angle requirement while in case of cube, contact line moves to meet the weight requirement.

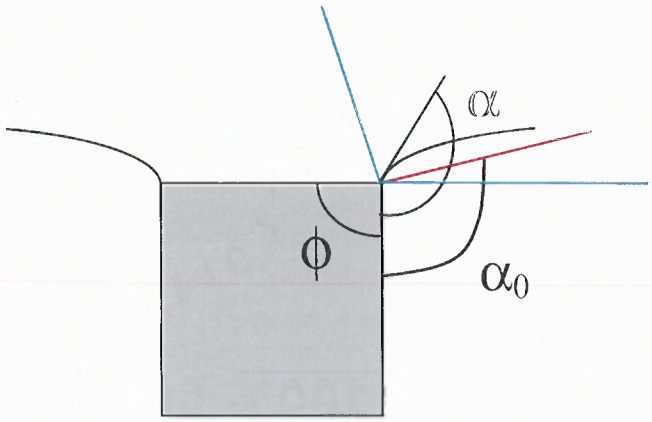

Figure 5.1 is a schematic of floating cube. The interface is pinned at the sharp edge. α is the contact angle, ϕ is the wedge angle and α_o is the equilibrium contact angle.

Contact line [95], remain pinned even when an electric field normal to the interface is applied. This is shown in Figure 5.2 for the case of two cubes which cluster under the action of capillary forces when the electric field is not applied. After the electric field of sufficiently large magnitude is applied, the cubes separate and the distance between them increases with increasing electric field strength (see Figure 5.3).

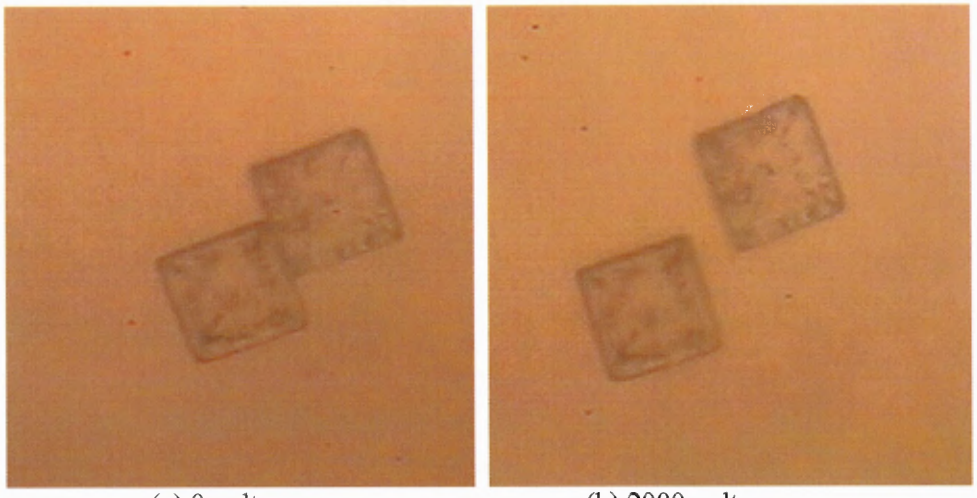

(a) 0 volts, (b) 2000 volts,

(c) 4000 volts

Figure 5.2 The floating behavior of two cubes (size ~ 150 um) is shown. The lattice distance between the cubes increases with electric field strength. The contact line is pinned at the upper edge of the cubes, and remains pinned even when the electric field is present.

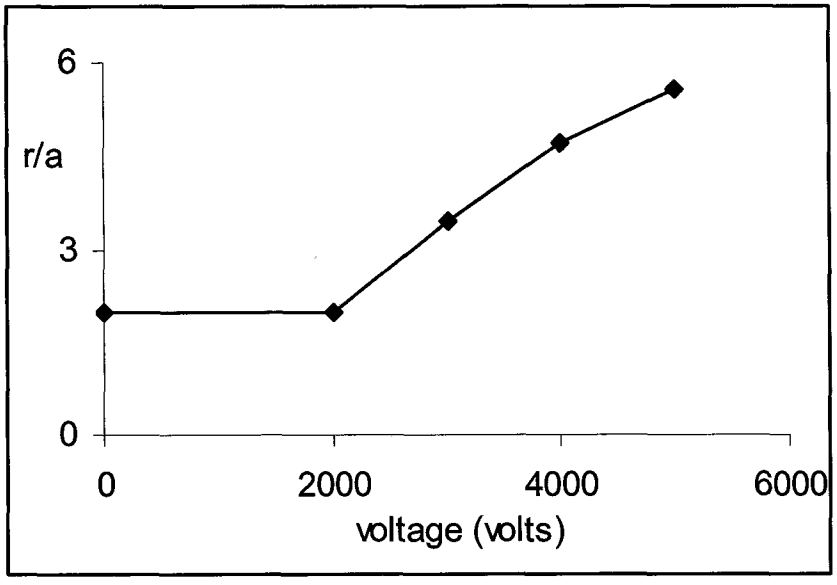

Figure 5.3 The dimensionless distance between two cubes is plotted as a function of the applied voltage. Notice that there a critical voltage at which the two cubes separate.

Also, since the interfacial deformation caused by a cube is asymmetric, they arrange in certain preferred orientations. Figure 5.4 shows that in the absence of an externally applied electric field cubes cluster, but when an electric field of sufficiently large magnitude is applied the cluster is broken. The Figure 5.4 also shows that spacing of the monolayer can be controlled by changing the electric field strength. Since the contact line remains pinned at the sharp edge, the electro-wetting effect is not present [96] (the contact angle, however, can change because the vertical electrostatic force on the particle [88, 89 and 90]).

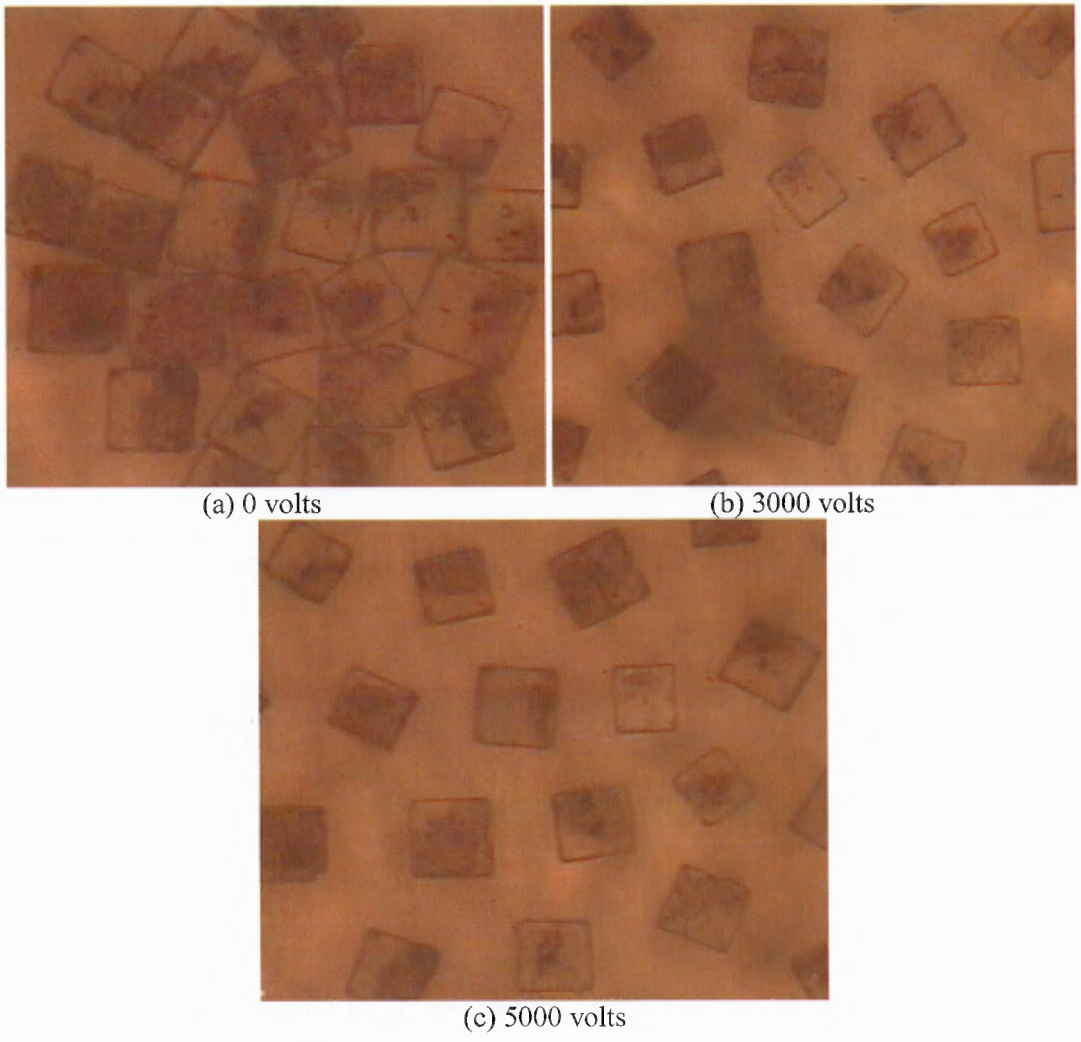

(a) 0 volts (b) 3000 volts

(c) 5000 volts

Figure 5.4 An assembled monolayer of cubes. In the absence of the electric field cubes cluster. When an electric field normal to the interface is applied the lattice spacing increases with increasing electric field strength. The contact line is pinned at the upper edge of the cubes, and remains pinned even when the electric field is present.

5.3 Discussion

Experiments show that two or more cubical particles floating on the surface of corn oil cluster under the action of lateral capillary forces that arise because of the deformation of the interface. The cubical particles physically block each other and prevent any pattern from developing.

It is also shown that a monolayer of cubes can be expanded. The distance between the cubes is determined by the balance of the attractive capillary forces and the repulsive dipole-dipole forces. It is also shown that the lattice spacing of a self-assembled monolayer of cubes can be increased by applying an electric field.

CHAPTER 6

CONCLUSIONS

The two main objectives of this work was to numerically study the motion of particles subjected to non-uniform electric fields, and also to investigate the process of self assembly of particles at a fluid-fluid interface under the influence of a uniform electric field normal to the interface.

In the first case, the direct numerical simulations (DNS) used for studying the fluid-particle system are based on the distributed Lagrange multiplier method. In this approach the fluid equations are solved both inside and outside the particle boundaries and rigid body motion is enforced inside the particle boundaries by using the distributed Lagrange multiplier. In the direct numerical scheme the governing equations for the fluid and particles are solved exactly without using any models. The electric forces acting on the particles were computed using the Maxwell Stress Tensor (MST) method.

The numerical scheme was tested to ensure that the results converge in both time and space. DNS results were compared with results obtained by point-dipole approximation. The MST method is more accurate for larger particles and when the dielectric mismatch between the particle and fluid is larger.

The second part of the research studied the electrostatic and capillary forces acting on a particle within a two-fluid interface in the presence of both an externally applied electric field and other particles. The electrostatic force was found to contain components both normal and tangential to the interface. The former arises because the dielectric constants of the two fluids involved are different (and is thus zero for two fluids

of identical dielectric constants) and the latter is due to the dipole-dipole interactions among the particles.

In equilibrium, the net vertical force acting on a particle at the interface, which includes the electrostatic force and the buoyant weight, is balanced by the vertical capillary force which arises because of the deformation of the interface. The deformation of the interface, in turn, gives rise to lateral capillary forces which cause particles at the interface to cluster. More specifically, the magnitude of these lateral forces is determined by the square of the net vertical force acting on the particle which includes both the buoyant weight and the vertical electrostatic force. The lateral capillary forces are long ranged and depend on the fourth power of the electric field intensity. The buoyant weight and the vertical electrostatic force, however, may not be in the same direction, and when this is the case the electric field, in fact, reduces lateral capillary forces. If the electrostatic force and buoyant weight are in the same direction, the electric field enhances lateral capillary forces. This is an important result, especially for micron and sub micron sized particles for which the buoyant weight is negligible, because it shows that the clustering behavior of particles, including that of small particles, can be controlled using an externally-applied electric field.

The equilibrium distance between two particles was obtained by equating the attractive capillary and repulsive electrostatic forces. Equilibrium is possible because the attractive capillary force between the particles is long ranged (decays as r^{-1}) and dominates the electrostatic repulsive force which is short ranged (decays as r^{-4}) when the distance between the particles is large. The opposite is true when the distance between

the particles is small. The equilibrium distance was shown to depend on the particle radius, the electric field intensity, the buoyant weight, and the dielectric constants.

Experiments show that two or more glass rods floating on the surface of corn oil cluster under the action of lateral capillary forces that arise because of the deformation of the interface. Since rods are also subjected to a torque due to capillarity, they come together either with their long sides touching or with their ends touching. In both cases they are parallel to each other. The alignment of rods in a monolayer assembled under the action of capillary forces appears to be random as the rods physically block each other and prevent any pattern from developing.

In the presence of an electric field of sufficiently large magnitude, two rods released about one and half rod lengths away from each other arrange themselves to form a single line, i.e., they become parallel to the line joining their centers and come in contact so that their ends touch. This equilibrium arrangement is independent of their initial orientation. The electric field causes a rod on the interface to experience an electrostatic force normal to the interface. In addition, in an electric field the rods become polarized and interact with each other via dipole-dipole interactions. This results in a repulsive force and a torque. Furthermore, although the electric field causes rods to align parallel to each other, the direction of the alignment is not determined by the electric field which is normal to the interface. In experiments, the final direction of alignment depends on the rods' initial orientations.

It is also shown that a monolayer of rods can be expanded and its rods aligned approximately parallel to each other by applying an electric field normal to the interface. The distance between the rods is determined by the balance of the attractive capillary

forces and the repulsive dipole-dipole forces. It is also shown that the lattice spacing of a self-assembled monolayer of rods can be increased by applying an electric field. The alignment, however, is not complete since the rods physically block each other.

Similar experiments are performed for ellipsoids. It is shown that for two ellipsoids floating on a fluid-fluid interface. Only one orientation is stable when the electric field is not present. The particles preferred orientation is when their major axes are parallel and their major sides are touching. When electric field is present the preferred orientation for ellipsoids is to align parallel to their major axes but the line joining their centers makes a small angle with their major axes. It is also shown the lattice spacing of self-assembled monolayer of ellipsoids can be increased by applying an electric field.

Experiments performed using spheres, rod-like, ellipsoids and cubic particles show that the distance between them and their relative orientations can be controlled by applying an electric field normal to the interface. The electric field causes particles on the fluid/fluid interface to experience an electrostatic force normal to the interface. In addition, particles become polarized and interact with each other via dipole-dipole interactions, which for the particles trapped on the interface is repulsive. The distance between the particles is determined by the balance of the attractive capillary forces and the repulsive dipole-dipole forces. In the presence of the electric field, the preferred orientation for rod-like particles is to align parallel to each other, and form lines with their ends touching. Ellipsoids also align parallel to each other in the presence of electric field but line joining their centers make a small angle with their major axes.

For future work, ellipsoids with different aspect ratios can be used to better understand the physics as to why ellipsoids make an angle with line joining their centers

with their major axes when electric field is present and the effect of aspect ratio on this angle.

For sharp edged particles, interface is pinned at the edges. Contact angle will change to meet the weight requirement when the electric field is applied. By mapping out the surface profile close to sharp edge, the effect of electrostatic force can be separated out.

Different type of particles by shape and dielectric constants can be used to see what structures can be obtained. The idea of dielectrophoresis along with self-assembly of particles can be employed to manipulate particles on the surface of drops.

The objective of future studies will be to control the self-assembly process and this can be useful in micro-fabrication and controllable filters.

REFERENCES

1. Winslow, M. W. (1949). Induced fibration of suspensions. Journal of Applied Physics, 20, 1137-1140.

2. Bonnecaze, R.T., & Brady, J.F. (1992). Dynamic simulation of an electrorheological fluid. Journal of Chemical Physics, 96, 2183-2202.

3. Jones, T. B. (1995). Electromechanics of particles, Cambridge University Press, New York City, NY.

4. Pohl, H. A. (1978). Dielectrophoresis, Cambridge University press, Cambridge.

5. Shih Chen, C., & Pohl, H. A. (1974). Biological dielectrophoresis: The behavior of lone cells in a nonuniform electric field. Annals of the New York Academy of Sciences, 238, 176-185.

6. Gvozdyak, P. I., & Chekhovskaya, T. P. (1976). Electro-retention of microorganisms. Mikrobiologiya, 45(5), 901-905.

7. Glaser, R., Pescheck Ch., & Krause, G. (1979). Dielectro phoresis and preparative separation of cells. Zeitschrift Fur Allgemeine Mikrobiologie, 19(9), 601-607.

8. Jones, T. B., & Kallio, G. A. (1979). Dielectrophoretic levitation of spheres and shells. Journal of Electrostatics, 6(3), 207-224.

9. Jones, T. B., & Bliss, G. W. (1977). Bubble dielectrophoresis. Journal of Applied Physics, 48(4), 1412-1417.

10. Zimmermann, U., & Scheurich, P. (1981). Fusion of avena sativa mesophyll cell protoplasts by electrical breakdown. BBA - Biomembranes, 641(1), 160-161.

11. Sukharev, S. I., Bandrina, I. N., Barbul, A. I., Fedorova, L. I., Abidor, I. G., & Zelenin, A. V. (1990). Electrofusion of fibroblasts on the porous membrane. Biochimica Et Biophysica Acta - General Subjects, 1034(2), 125-131.

12. Arnold, W. M., & Zimmermann, U. (1988). Electro-rotation: Development of a technique for dielectric measurements on individual cells and particles. Journal of Electrostatics, 21(2-3), 151-191.

13. Gherardi, L., Mognaschi, E. R., & Savini, A. (1985). Dielectrophoretic motion of a lossy dielectric sphere in a liquid of a non-zero conductivity. IEEE Transactions on Electrical Insulation, EI-20(2), 385-388.

14. Mognaschi, E. R., & Savini, A. (1985). Dielectrophoresis of a lossy dielectrics. IEEE Transactions on Industry Applications, IA-21(4), 926-929.

15. Goossens, K., & Van Biesen, L. (1988). Computer-aided analysis of dielectrophoretic force calculations. 5th International Conference on Dielectric Materials, Measurements and Applications, 131-134.

16. Henry, F. S., & Ariman, T. (1986). Numerical calculation of a particle collection in electrically enhanced fibrous filters. Particulate Science and Technology, 4(4), 455-477.

17. Adamson, R. J., & Kaler, K. V. I. S. (1988). Automated stream-centred dielectrophoretic system. IEEE Transactions on Industry Applications, 24(1), 93-98.

18. Masuda, S., Washizu, M., & Nanba, T. (1989). Novel method of cell fusion in field constriction area in fluid integrated circuit. IEEE Transactions on Industry Applications, 25(4), 732-737.

19. Washizu, M., & Kurosawa, O. (1990). Electrostatic manipulation of DNA in microfabricated structures. IEEE Transactions on Industry Applications, 26(6), 1165-1172.

20. Washizu, M., Nanba, T., & Masuda, S. (1990). Handling biological cells using a fluid integrated circuit. IEEE Transactions on Industry Applications, 26(2), 352-358.

21. Pethig, R. (1984). Dielectric properties of biological materials: Biophysical and medical applications. IEEE Transactions on Electrical Insulation, EI-19(5), 453-474.

22. Gascoyne, P. R. C., Huang, Y., Pethig, R., Vykoukal, J., & Becker, F. F. (1992). Dielectrophoretic separation of mammalian cells studied by computerized image analysis, Measurement Science and Technology 3 (5), 439-445.

23. Huang, Y., & Pethig, R. (1991). Electrode design for negative dielectrophoresis. Measurement Science and Technology, 2(12), 1142-1146.

24. Price, J. A., Burt, J. P. H., & Pethig, R. (1998). Applications of a new optical technique for measuring the dielectrophoretic behavior of micro organisms, Biochimica et Biophsica acta, 964, 221-230.

25. Pethig, R., Huang, Y., Wang, X., & Burt, J. P. H. (1992). Positive and negative dielectrophoretic collection of colloidal particles using interdigitated castellated microelectrodes. Journal of Physics D: Applied Physics, 25(5), 881-888.

26. Wang, X., Huang, Y., Burt, J. P. H., Markx, G. H., & Pethig, R. (1993). Selective dielectrophoretic confinement of bioparticles in potential energy wells. Journal of Physics D: Applied Physics, 26(8), 1278-1285.

27. Wang, X-B., Huang, Y., Holzel, R., Burt, J. P. H., & Pethig R. (1993). Theoretical and experimental investigations of the interdependence of the dielectric, dielectrophoretic and electrorotational behavior of colloidal particles, Journal of Physics D: Applied Physics, 25, 905-912.

28. Huang, Y., Holzel, R., Pethig, R., & Xiao-B.Wang. (1992). Differences in the AC electrodynamics of viable and non-viable yeast cells determined through combined dielectrophoresis and electrorotation studies. Physics in Medicine and Biology, 37(7), 1499-1517.

29. Wang, X., Pethig, R., & Jones, T. B. (1992). Relationship of dielectrophoretic and electrorotational behaviour exhibited by polarized particles. Journal of Physics D: Applied Physics, 25(6), 905-912.

30. Batchelder, J. S. (1983). Dielectrophoretic manipulator, Review of Scientific Instruments, 54, 300-302.

31. Washizu, M., & Jones, T. B. (1994). Multipolar dielectrophoretic force calculation. Journal of Electrostatics, 33(2), 187-198.

32. Jones, T. B., & Washizu, M. (1996). Multipolar dielectrophoretic and electrorotation theory. Journal of Electrostatics, 37(1-2), 121-134.

33 .Washizu, M., & Jones, T. B. (1996). Generalized multipolar dielectrophoretic force and electrorotational torque calculation. Journal of Electrostatics, 38(3), 199-211.

34. Gunji, M., Washizu, M., & Jones, T. B. (2000). Dielectrophoretic microfluidic devices, Proceedings of IEJ/ESA Joint Symposium on Electrostatics, Kyoto, Japan, September,78-87.

35. Jones, T. B. (2003). Electrostatics and the lab on a chip. Conference of Institute of Physics, Edinburgh, March,1-10.

36. Jones, T. B. (2003). Influence of scale on electrostatic forces and torques in AC particulate electrokinetics. IEE Proceedings Nanobiotechnology, 150(2), 39-46.

37. Jones, T. B., Gunji, M., Washizu, M., & Feldman, M. J. (2001). Dielectrophoretic liquid actuation and nanodroplet formation. Journal of Applied Physics, 89(2), 1441-1448.

38. Gunji, M., Jones, T. B., & Washizu, M. (2001). DEP microactuation of liquids. 14th IEEE Conference on MEMS, 385-388.

39. Vella, D., & Mahadevan, L. (2005). The "cheerios effect". American Journal of Physics, 73(9), 817-825.

40. Campbell, D. J., Freidinger, E. R., Hastings, J. M., & Querns, M. K. (2002). Spontaneous assembly of soda straws. Journal of Chemical Education, 79(2), 201.

41. Gerson, D. F., Zajic, J. E., & Ouchi, M. D. (1979). Relation of surfactant properties to the extraction of bitumen from Athabasca tar sand by a solvent-aqueous-surfactant process. ACS Symposium Series, (90), 66-79.

42. Bowden, N., Choi, I. S., Grzybowski, B. A., & Whitesides, G. M. (1999). Mesoscale self-assembly of hexagonal plates using lateral capillary force: Synthesis using the 'capillary bond'. Journal of the American Chemical Society, 121(23), 5373-5391.

43. Kralchevsky, P. A., & Nagayama, K. (2000). Capillary interactions between particles bound to interfaces, liquid films and biomembranes. Advances in Colloid and Interface Science, 85(2), 145-192.

44. Saif, T. A. (2002). On the capillary interaction between solid plates forming menisci on the surface of a liquid. Journal of Fluid Mechanics, (473), 321-347.

45. Nikolaides, G., Bausch, A., Hsu, M., Dinsmore, A., Brenner, M., Gay, C., & Weitz, D. (2002). Electric field induced capillary attraction between like charged particles at liquid interfaces. Nature 420, 299-301.

46. Aveyard, R., Binks, B., Clint, J., Fletcher, P., Horozov, T., Neumann, B., & Paunov, V. (2002). Measurement of long range repulsive forces between charged particles at an oil water interface. Physical Review Letters, 88, 246102-1 - 246102-3.

47. Hosokawa, K., Shimoyama, I., & Miura, H. (1996). Two-dimensional micro-self-assembly using the surface tension of water. Sensors and Actuators, 57, 117-125.

48. Golosovsky, M., Saado, Y., & Davidov, D. (1999). Self-assembly of floating magnetic particles into ordered structures: A promising route for the fabrication of tunable photonic band gap materials.Applied Physics Letters, 75(26), 4168-4170.

49. Ismagilov, R., Schwarz, A., Bowden, N., & Whitesides, G. (2002). Autonomous Movement and Self Assembly. Angewandte Chemie International Edition, 41, 652-654.

50. Grzybowski, B., Stone, H., & Whitesides, G.M. (2002). Dynamic Self Assembly of Magnetized, Millimeter-Sized Objects Rotating at a Liquid Air Interface. Nature, 405, 1033-1036.

51. Grzybowski, B., Jiang, X., Stone, H., & Whitesides, G.M. (2001). Dynamic, Self Assembled Aggregates of Magnetized, Millimeter-Sized Objects Rotating at the Liquid Air Interface: Macroscopic, Two-Dimensional Classical Artificial Atoms and Molecules. Physical Review E, 64, 011603.

52. Grzybowski, B., Stone, H., & Whitesides, G.M. (2002). Dynamics of Self Assembly of Magnetized Disks Rotating at the Liquid Air Interface, Prcoceeding of National Academy of Sciences, 99, 4147-4151.

53. Grzybowski, B., Radkowski, M., Campbell, C., Ng Lee, J., & Whitesides, G.M. (2004). Self Assembling Fluidic Machines, Applied. Physics Letters, 84, 1798-1800.

54. Washizu, M., Kurosawa, O., Arai, I., Suzuki, S., & Shimamoto, N. (1995). Applications of electrostatic stretch-and -positioning of DNA. IEEE Transactions on Industrial Applications, 30, 835-843.

55. Hughes, M. P., Morgan, H., & Rixon, F. J. (2002). Measuring the dielectric properties of herpes simplex virus type 1 virions with dielectrophoresis. Biochimica Et Biophysica Acta - General Subjects, 1571(1), 1-8.

56. Becker, F. F., Wang, X., Huang, Y., Pethig, R., Vykoukal, J., & Gascoyne, P. R. C. (1994). Removal of human leukaemia cells from blood using interdigitated microelectrodes. Journal of Physics D: Applied Physics, 27(12), 2659-2662.

57. Becker, F. F., Wang, X. -., Huang, Y., Pethig, R., Vykoukal, J., & Gascoyne, P. R. C. (1995). Separation of human breast cancer cells from blood by differential dielectric affinity. Proceedings of the National Academy of Sciences of the United States of America, 92(3), 860-864.

58. Markx, G. H., Dyda, P. A., & Pethig, R. (1996). Dielectrophoretic separation of bacteria using a conductivity gradient. Journal of Biotechnology, 51(2), 175-180.

59. Hughes, M. P., & Morgan, H. (1998). Dielectrophoretic trapping of single sub-micrometre scale bioparticles. Journal of Physics D: Applied Physics, 31(17), 2205-2210.

60. Voldman, J., Braff, R. A., Toner, M., Gray, M. L., & Schmidt, M. A. (2001). Holding forces of single-particle dielectrophoretic traps. Biophysical Journal, 80(1), 531-541.

61. Voldman, J., Toner, M., Gray, M. L., & Schmidt, M. A. (2003). Design and analysis of extruded quadrupolar dielectrophoretic traps. Journal of Electrostatics, 57(1), 69-90.

62. Pethig, R., Huang, Y., Wang, X., & Burt, J. P. H. (1992). Positive and negative dielectrophoretic collection of colloidal particles using interdigitated castellated microelectrodes. Journal of Physics D: Applied Physics, 25(5), 881-888.

63. Hughes, M. P., & Morgan, H. (1999). Measurement of bacterial flagellar thrust by negative dielectrophoresis. Biotechnology Progress, 15(2), 245-249.

64. Nedelcu, S., & Watson, J. H. P. (2004). Size separation of DNA molecules by pulsed electric field dielectrophoresis. Journal of Physics D: Applied Physics, 37(15), 2197-2204.

65. Bonnecaze, R. T., & Brady, J. F. (1992). Dynamic simulation of an electrorheological fluid. Journal of Chemical Physics, 96(3), 2183-2202.

66. Washizu, M., & Jones, T. B. (1996). Generalized multipolar dielectrophoretic force and electrorotational torque calculation. Journal of Electrostatics, 38(3), 199-211.

67. Wang, X., Wang, X., & Gascoyne, P. R. C. (1997). General expressions for dielectrophoretic force and electrorotational torque derived using the maxwell stress tensor method. Journal of Electrostatics, 39(4), 277-295.

68. Singh, P., & Aubry, N. (2004). Particle separation using dielectrophoresis. Proceedings of ASME Annual Meeting.

69. Aubry, N., & Singh, P. (2006). Control of electrostatic particle-particle interactions in dielectrophoresis. Europhysics Letters, 74(4), 623-629.

70. Kadaksham, J., Singh, P., & Aubry, N. (2004). Dynamics of electrorheological suspensions subjected to spatially nonuniform electric fields. Journal of Fluids Engineering, Transactions of the ASME, 126(2), 170-179.

71. Kadaksham, A. T. J., Singh, P., & Aubry, N. (2004). Dielectrophoresis of nanoparticles. Electrophoresis, 25(21-22), 3625-3632.

72. Kadaksham, J., Singh, P., & Aubry, N. (2005). Dielectrophoresis induced clustering regimes of viable yeast cells. Electrophoresis, 26(19), 3738-3744.

73. Kadaksham, J., Singh, P., & Aubry, N. (2006). Manipulation of particles using dielectrophoresis. Mechanics Research Communications, 33(1), 108-122.

74. Glowinski, R., Pan, T. Hesla, T. I., & Joseph, D. D. (1999). A distributed lagrange multiplier/fictitious domain method for particulate flows. International Journal of Multiphase Flow, 25(5), 755-794.

75. Singh, P., Joseph, D. D., Hesla, T. I., Glowinski, R., & Pan, T. (2000). A distributed lagrange multiplier/fictitious domain method for viscoelastic particulate flows. Journal of Non-Newtonian Fluid Mechanics, 91(2-3), 165-188.

76. Glowinski, R., Pan, T., Hesla, T. I., & Joseph, D. D. (1999). A distributed lagrange multiplier/fictitious domain method for particulate flows. International Journal of Multiphase Flow, 25(5), 755-794.

77. Patankar, N. A., Singh, P., Joseph, D. D., Glowinski, R., & Pan, T. (2000). A new formulation of the distributed lagrange multiplier/fictitious domain method for particulate flows. International Journal of Multiphase Flow, 26(9), 1509-1524.

78. Murray, B., Kagan, R., & Bawendi, G.. (2000). Synthesis and characterization of monodisperse nanocrystals and close-packed nanocrystal assemblies. Annual Review of Material Science, 30, 545-610.

79. Tang, Z., Zhang, Z., Wang, Y., Glotzer, S., & Kotov, N. (2006). Self-Assembly of CdTe Nanocrystals into Free-Floating Sheets. Science, 314,274-278.

80. Bowden, N., Choi, I., Grzybowski, A., & Whitesides, G. (1999). Mesoscale self-assembly of hexagonal plates using lateral capillary forces: synthesis using the "capillary bond". Journal of American Chemical Society, 121, 5373-5391.

81. Bowden, N., Terfort, A., Carbeck, J., & Whitesides, G. (1997). Self-assembly of mesoscale objects into ordered two-dimensional arrays. Science, 276, 233-235.

82. Grzybowski, A., Bowden, N., Arias, F., Yang, H., & Whitesides, G. (2001). Modeling of menisci and capillary forces from the millimeter to the micrometer size range. Journal of Physical Chemistry B, 105,404-412.

83. Wasielewski, R. (1992). Photoinduced electron transfer in supramolecular systems for artificial photosynthesis. Chemical Reviews, 92, 435-461.

84. Balzani, V., Venturi, M., & Credi, A. (2003). Molecular devices and Machines.Wiley VCH, Weinheim.

85. Chan, D., Henry J., & White, L. (1981). The interaction of colloidal particles collected at the fluid interface. Journal of Colloid Interface Science, 79, 410-418.

86. Fortes, M. A. (1982). Attraction and repulsion of floating particles. Canadian Journal of Chemistry, 60, 2889-2895.

87. Kralchevsky, P., & Nagayama, K. (2000). Capillary interactions between particles bound to interfaces, liquid films and biomembranes. Advances in Colloid and Interface Science, 85,145-192.

88. Aubry, N., Singh, P., Janjua, M., & Nudurupati. S. (2008). Assembly of defect-free particle monolayers with dynamically adjustable lattice spacing. Proceedings of the National Academy of Sciences, 105, 3711-3714.

89. Aubry, N., & Singh, P. (2008). Physics underlying the controlled self-assembly of micro and nanoparticles at a two-fluid interface using an electric field. Physical Review E, 77, 056302.

90. Aubry, N., & Singh, P., (2007). Electrostatic forces on particles floating within the interface between two immiscible fluids. Paper IMECE2007-44095, Proceedings of 2007 ASME International Mechanical Engineering Congress and Exhibition.

91. Chan, D. Y. C., Henry, J. D., & White, L. R. (1981). The interaction of colloidal particles collected at the fluid interface. Journal of Colloid and Interface Science, 79, 410-418.

92. Aubry, N., & Singh, P. (2006). Control of Electrostatic Particle-Particle Interactions in Dielectrophoresis. Euro Physics Letters, 74, 623–629.

93. Lucassen, J. (1992). Capillary forces between solid particles in fluid interfaces. Colloids and Surfaces, 65, 131-137.

94. Klingenberg, D. J., Van, S., Zukoski, C. F. (1989). Simulation of electrorheological suspensions. Journal of Chemical Physics, 91, 7888-7895.

95. Singh, P., & Joseph, D.D. (2005). Fluid dynamics of Floating particles. Journal of Fluid Mechanics, 530, 31-80.

96. Mugele, F., & Baret, J. (2005). Electrowetting: from basics to applications. Journal of Physical Condensate Matter, 17, 705-774.